OUTPUT FEEDBACK CONTROL IN THE PRESENCE OF UNCERTAINTIES: USING EXTENDED HIGH-GAIN OBSERVERS WITH DYNAMIC INVERSION

By

Joonho Lee

A DISSERTATION

Submitted to Michigan State University in partial fulfillment of the requirements for the degree of

Mechanical Engineering – Doctor of Philosophy

2014

Abstract

OUTPUT FEEDBACK CONTROL IN THE PRESENCE OF UNCERTAINTIES: USING EXTENDED HIGH-GAIN OBSERVERS WITH DYNAMIC INVERSION

By

Joonho Lee

Control design for uncertain nonlinear systems is an important issue. Uncertainties always reside in nonlinear systems due to incomplete mathematical model description or intended approximation factors in system models, e.g. linearization for system models. Furthermore, unexpected external disturbances and unmeasured system states increase the uncertainties in the systems.

In this dissertation, we consider an uncertain nonlinear systems that takes the form of a chain of integrators and introduce control design methodologies based on output feedback control: using extended high-gain observers and dynamic inversion.

The proposed output feedback controller results in a closed-loop system with a three-time-scale structure; an extended high-gain observer estimates unmeasured states and uncertainties in the fastest time scale and dynamic inversion is used to deal with nonaffine control inputs or input uncertainties in the intermediate time scale whereas the plant dynamics evolves in the slowest time scale. The dynamic inversion algorithm, based on sector conditions, results in fast convergence into inputs under state feedback control. Together with the extended high-gain observer, dynamic inversion results in performance recovery of a target system.

The time-scale-separation approach is well-suited to underactuated mechanical systems to overcome the lack of the number of inputs. Since the time separation is created between subsystems in plant dynamics, subsystem dynamics are viewed as virtual inputs for the other subsystems. In this dissertation, we apply the time-scale separation strategy to two

examples of underactuated mechanical systems in the presence of uncertainties, the inverted pendulum on a cart and the autonomous helicopter.

Copyright by JOONHO LEE 2014

ACKNOWLEDGMENTS

I would like to express my deepest and sincere gratitude to my two advisors, Professor Hassan Khalil and Professor Ranjan Mukherjee for their invaluable advice, guidance, constant support and encouragement. Without their help and support, this dissertation would not have been possible. I am especially thankful to my principle advisor, Dr. Khalil, for his wisdom, endless patience, and boundless knowledge on control theory. I have learned from him not only scholarly knowledge but also wisdom how to live as a good researcher.

I would like to thank the members of my Ph.D. committee, Professor Guoming Zhu and Professor Brian Feeny for their willingness to serve on the committee as well as for their assistance and valuable input.

To my wife, S.M., my two children, Ryan Lee and Isla Lee, my father, and mother, from the bottom of my heart, I appreciate their endless support. Especially, to my lovely wife, I would like to appreciate her endless support and patience. About her support, I cannot put into words. At every moment, she was with me bringing joy, love, happiness, and hope.

TABLE OF CONTENTS

LIST OF TABLES	viii
LIST OF FIGURES	ix
Chapter 1 Introduction	1
1.1 Motivation	$\overline{2}$
1.2 Dynamic Inversion	4
1.3 High-Gain Observers and Extended High-Gain Observers	5
1.3.1 High-Gain Observers	7
1.3.2 Extended High-Gain Observers	8
Chapter 2 Output Feedback Performance Recovery in the Presence of Un-	
certainties	10
2.1 Introduction	10
2.2 Problem Statements	12
2.3 Control Design	16
2.4 Main Result	19
2.5 Simulations	26
2.5.1 Example 1	27
2.5.2 Example 2	28
2.6 Conclusions	32
Chapter 3 Output Feedback Stabilization of Inverted Pendulum on a Cart in the Presence of Uncertainties	34 34
3.2 Stabilization in the Absence of Uncertainties	37
3.2.1 Dynamics of an inverted pendulum on a cart	37
3.2.2 Control Design	39
3.2.3 Closed-loop system	40
3.2.4 Analysis using singular perturbations	41
3.3 Stabilization in the Presence of Uncertainties	44
3.3.1 Dynamic inversion	45
3.3.2 Extended High-Gain Observers (EHGOs)	46
3.3.3 Output feedback control	47
3.3.4 Stability analysis in the presence of uncertainties	48
3.4 Simulation and Experiment	56
3.4.1 Simulation results	56
3.4.2 Experimental results	59
3.5 Conclusion	63
Chapter 4 Output Feedback Control for an Autonomous Helicopter in the	66

4.1 Introduction	66
4.2 Dynamics of a Helicopter	69
	71
	73
	74
4.3.1 State feedback control	75
4.3.2 Stability analysis	78
4.4 Stability Analysis in the Presence of Disturbances	84
4.4.1 Design of Extend High-Gain Observers (EHGOs)	85
4.4.2 Output feedback control	86
	87
4.5 Simulation Results	95
4.6 Conclusions	99
Chapter 5 Conclusions and Future Works)7
5.1 Concluding Remarks	07
5.1.1 Main contributions	08
5.2 Future Works	09
APPENDICES	11
	12
	20
BIBLIOGRAPHY	25

LIST OF TABLES

Table 4.1	Parameters in a helicopter		 											7	0

LIST OF FIGURES

Figure 2.1	The trajectory starting from $(e_0, z_0, s_0) \in \Omega_a$ and $\eta_0 \notin \{V_{\eta} \leq b_3(\varepsilon/\mu)^2\}$ converges into $(e, z, s, \eta) \in \Omega_b \times \{V_{\eta} \leq b_3(\varepsilon/\mu)^2\}$	22
Figure 2.2	The solid and dashed lines represent trajectories x_i for $i = 1, 2$ driven by the proposed controller in (2.53) and reference trajectories x_{ri} for $i = 1, 2$ in (2.52), respectively	28
Figure 2.3	Input trajectories u_1 and u_2 in (2.53) are shown and both u_1 and u_2 cross the values $u_1 = 2, 3$ and $u_2 = 2, 3$ which make the Jacobian matrix $(\partial f/\partial u)$ singular	29
Figure 2.4	The solid and dotted lines represent the system states x_1 and x_2 , and estimates \hat{x}_1 and \hat{x}_2 , respectively	31
Figure 2.5	The solid and dotted lines represent the system states \dot{x}_1 and \dot{x}_2 , and estimates $\hat{\sigma}_1$ and $\hat{\sigma}_2$, respectively	32
Figure 2.6	The solid, dashed, and dotted lines represent the inputs $u_r = R_m^{-1} x$, u with $\mu = 0.02$ and $\varepsilon/\mu = 0.01$, and u with $\mu = 0.2$ and $\varepsilon/\mu = 0.01$, respectively	33
Figure 3.1	Inverted pendulum on a cart	37
Figure 3.2	The two-time-scale structure of the inverted pendulum on a cart system	44
Figure 3.3	Multi-time-scale structure for the closed-loop system	48
Figure 3.4	Trajectories of x_1 and x_2 for state feedback (solid line), output feedback with $(\varepsilon_2, \varepsilon_3) = (0.02, 0.002)$ (dotted line), and output feedback with $(\varepsilon_2, \varepsilon_3) = (0.01, 0.0001)$ (dashed line)	59
Figure 3.5	Trajectories of α_1 and α_2 for state feedback (solid line), output feedback with $(\varepsilon_2, \varepsilon_3) = (0.02, 0.002)$ (dotted line), and output feedback with $(\varepsilon_2, \varepsilon_3) = (0.01, 0.0001)$ (dashed line)	60
Figure 3.6	Trajectories of x_1 and α_1 (solid lines), and x_2 and α_2 (dashed lines) are shown in the top and middle subfigures. In the bottom subfigure, a trajectory of the input F in (3.26) is shown.	61
Figure 3.7	Experimental testbed for the inverted pendulum on a cart - a product of Quanser [1]	62
Figure 3.8	Trajectories of x_1 and its estimate \hat{x}_1 , and α_1 and its estimate $\hat{\alpha}_1$ are shown. The estimated values are indistinguishable from their true (measured) values	63

Figure 3.9	Trajectories of x_1 and α_1 are shown with different control schemes. Solid lines driven by our control scheme, converge into the origin. Dotted lines generated by a LQR controller, have ultimate boundedness. Dash-dot lines provided by the control algorithm in [63] have the biggest ultimate boundedness.	64
Figure 3.10	Trajectories of inputs F in (3.26) (the top subfigure), LQR (the middle subfigure), and [63] (the bottom subfigure) are shown	65
Figure 4.1	Side and top view of the helicopter	71
Figure 4.2	The block diagram is shown for rotational dynamics (inner-loop) and translational dynamics (outer-loop) control structure via two time-scale separation. The blocks P_R , P_T are rotational dynamics and translational dynamics, respectively. The blocks C_R , C_T are controllers for rotational and translational dynamics, respectively. χ is the position of the helicopter and χ_r and Θ_r are reference trajectories for the translational and rotational dynamics, respectively	72
Figure 4.3	Trajectories x_1 , y_1 , and z_1 (solid-lines) under the state feedback in the presence of disturbances and reference states x_r , y_r , and z_r (dished-lines)	97
Figure 4.4	Trajectories of x_1 , y_1 , and z_1 (solid-lines) under the output feedback in (4.53) in the presence of disturbances, and references x_r , y_r , and z_r (dashed-lines) for $r_x(t) = 5 \sin t$, $r_y(t) = 5 \cos t$, and $r_z(t) = 5 \sin t$ in (4.14)	98
Figure 4.5	Trajectories ϕ_d , θ_d , and ψ_r (dashed-lines) are references for the states ϕ_1 , θ_1 , ψ_1 of the rotational dynamics in the presence of disturbances	99
Figure 4.6	Trajectories x_1 , y_1 and z_1 (solid-lines) and the estimates \hat{x}_1 , \hat{y}_1 , and \hat{z}_1 (dashed-lines) by the EHGO	100
Figure 4.7	Trajectories x_2 , y_2 and z_2 (solid-lines) and the estimates \hat{x}_2 , \hat{y}_2 , and \hat{z}_2 (dashed-lines) by the EHGO	101
Figure 4.8	Trajectories ϕ_1 , θ_1 and ψ_1 (solid-lines) and the estimates $\hat{\phi}_1$, $\hat{\theta}_1$, and $\hat{\psi}_1$ (dashed-lines) by the EHGO	102
Figure 4.9	Trajectories ϕ_2 , θ_2 and ψ_2 (solid-lines) and the estimates $\hat{\phi}_2$, $\hat{\theta}_2$, and $\hat{\psi}_2$ (dashed-lines) by the EHGO	103
Figure 4.10	Plots for sum of the actual terms of acceleration (without approximation in model, F_p in (4.7)) and external disturbances σ_{Θ} : dashed-lines and plots for sum of nominal terms of acceleration (i.e., F_O in (4.11)) the estimate of external disturbances σ_{χ} by the EHGO: solid-lines	104
Figure 4.11	Plots for the external disturbances σ_{Θ} (solid-lines) and plots for the estimates $\hat{\sigma}_{\Theta}$ (dashed-lines)	105

Figure 4.12	Plots for the helicopter actual control inputs, T_M , T_T , a_{1s} , and b_{1s} under	
	the output feedback	106

Chapter 1

Introduction

Control design of uncertain nonlinear systems has been a challenging problem. Mathematical models cannot capture entire features of system dynamics or unexpected external disturbances. Even if system dynamics were precise, nonaffine control inputs add difficulties to the design. Furthermore, systems states are not always measurable. All these factors make control design a challenging task.

In this dissertation, we consider a class of nonlinear systems in the presence of uncertainties, which takes the form of a chain of integrators, e.g., a single-input-single-output nonlinear system,

$$\dot{x}_i = x_{i+1}, \quad \text{for } i = 1, \dots, n-1$$

$$\dot{x}_n = f(x, z, u) + \delta(x, u, t)$$

$$\dot{z} = f_0(x, z)$$

$$y = x_1$$

$$(1.1)$$

where $x = [x_1, \ldots, x_n]^T \in \mathbf{R}^n$ and $z \in \mathbf{R}^m$ are the system states, $u \in \mathbf{R}$ is the control input, $\delta(x, u, t) \in \mathbf{R}$ is the uncertainty, and $y \in \mathbf{R}$ is the measured output. The chain of integrators is commonly used to describe dynamics of mechanical systems. If f(x, z, u) in (1.1) has affine control, i.e., $f(x, z, u) = f_n(x, z) + g(x)u$, the system of (1.1) become a standard

normal form [30], [33]. This dissertation provide a way to deal with a class of uncertain nonlinear systems using extended high-gain observers and dynamic inversion. The extended high-gain observer is used to estimate both unmeasured states and uncertainties and the dynamic inversion deals with the nonaffine control or input uncertainties. In other words, using the extended high-gain observers and the dynamic inversion, a control design problem for uncertain nonlinear systems with the nonaffine control input, is viewed as the control design for the standard normal form in the absence of uncertainties.

The dissertation is organized as follows. In Chapter 1, motivation examples, the dynamic inversion, high-gain observers, and the extended high-gain observers are introduced. Chapter 2 presents the performance recovery in the presence of uncertainties using the extended high-gain observer and dynamic inversion. In Chapter 3, the stabilization problem is introduced for the inverted pendulum on a cart in the presence of uncertainties. In Chapter 4, the output feedback control is designed for an autonomous helicopter in the presence of external disturbances. Lastly, conclusions and future works are provided in Chapter 5.

1.1 Motivation

First, we consider the example of translational dynamics for x-direction in a helicopter with bounded uncertainty $\delta(t)$, i.e., an uncertain nonlinear system with nonaffine

$$\dot{x}_1 = x_2$$

$$\dot{x}_2 = -\frac{1}{m} (\cos \phi_1 \sin \theta_1 \cos \psi_1 + \sin \phi_1 \sin \psi_1) T_M + \delta(t)$$
(1.2)

where x_1 and x_2 are a position and velocity respectively, ϕ_1 is viewed as an input given appropriate values of θ_1 , ψ_1 , and T_M . One approach to deal with the nonaffine control in (1.2), is to introduce an additional integrator into the state space equation for the control

variable ϕ_1 , i.e., $x_3 = \phi_1$, and $\dot{x}_3 = \nu = \dot{\phi}_1$. We obtain the new system equation

$$\dot{x}_1 = x_2$$

$$\dot{x}_2 = -\frac{1}{m}(\cos x_3 \sin \theta_1 \cos \psi_1 + \sin x_3 \sin \psi_1)T_M + \delta(t)$$

$$\dot{x}_3 = \nu$$
(1.3)

However, this approach changes the matched uncertainty in (1.2) into the unmatched uncertainty $\delta(x_1, t)$ in (1.3). The matching condition plays an important role in robust nonlinear control design as in Sections 14.1 and 14.2 of [33]. The uncertainty is matched when it enters the system equation at the same point as the control input.

As the second motivation, we will consider uncertainties in the system. Consider the example of the inverted pendulum on a cart,

$$\dot{x}_1 = x_2$$

$$\dot{x}_2 = \delta_1(\alpha_1) - \delta_2(\alpha_1)u$$

$$\dot{\alpha}_1 = \alpha_2$$

$$\dot{\alpha}_2 = u$$

$$y = [x_1, \alpha_1]^T$$
(1.4)

where $x = [x_1, x_2]^T \in \mathbf{R}^2$ and $\alpha = [\alpha_1, \alpha_2]^T \in \mathbf{R}^2$ are the system states; $y \in \mathbf{R}^2$ is the measured output; the domain of α_1 is $-\pi/2 < \alpha_1 < \pi/2$; δ_1 and δ_2 are uncertainties; and we assume that $\delta_2 > 0$ and the sign of δ_2 is known. The control objective is to stabilize the system at x = 0 and $\alpha = 0$.

In this dissertation, using the extended high-gain observer and the dynamic inversion, we will deal with the control design for the two cases: one is for control design for stabilization of the inverted pendulum on a cart at the upper equilibrium in Chapter 3 and the other is for control design for an autonomous helicopter with nonaffine control input in Chapter 4.

1.2 Dynamic Inversion

In this section, we introduce a control algorithm to find approximate solutions for nonlinear maps, which is called dynamic inversion. In [52,53], observers were used to invert nonlinear maps. In [25], two dynamic inversion algorithms were introduced: one is based on a Newton method and the other uses a gradient-decent algorithm. In [28,29], using a two-time-scale approach together with a gradient decent algorithm, a dynamic inversion scheme was generated. In [64], a second-order sliding mode controller with saturation for a single-input-single-output nonaffine systems was used to deal with uncertainties and nonaffine input forms. In [24], neural-networks and the mean value theorem were used to produce a dynamic inversion algorithm. Hovakimyan et al [27] also used neural-networks with a two-time-scale approach to deal with a single-input-single-output uncertain nonaffine system.

To briefly explain the principle of dynamic inversion, the example in (1.2) is reconsidered. Now, it is assumed that $\delta(x,t)$ in (1.2) is known. For the stabilization of the system in (1.2), a controller form of the dynamic inversion is given by

$$\varepsilon \dot{\phi}_1 = -K(x, \phi_1) \left\{ -\frac{1}{m} (\cos \phi_1 \sin \theta_1 \cos \psi_1 + \sin \phi_1 \sin \psi_1) T_M - u_c \right\}$$
 (1.5)

where $u_c \in \mathbf{R}$ is a reference input (e.g. $u_c = -k_p x_1 - k_v x_2 + r_x(t)$ with $k_p, k_v > 0$), $r_x(t)$ is a reference trajectory, $K(x, \phi_1) \in \mathbf{R}$ is satisfies $K(x, \phi_1) \geq k_0 > 0$ with the positive constant k_0 , over the domain of interest. With a sufficiently small positive $\varepsilon \simeq 0$ in (1.5), we obtain the quasi steady-state equation

$$-K(x,\phi_1)\left\{-\frac{1}{m}(\cos\phi_1\sin\theta_1\cos\psi_1+\sin\phi_1\sin\psi_1)T_M-u_c\right\}=0$$
(1.6)

Using the assumption that $K(x, \phi_1) \ge k_0 > 0$, we have

$$-\frac{1}{m}(\cos\phi_1\sin\theta_1\cos\psi_1 + \sin\phi_1\sin\psi_1)T_M = u_c = -k_p x_1 - k_v x_2 + r_x(t)$$
 (1.7)

Since in view of a multi-time-scale approach, the system of (1.5) is fast and the system of (1.2) is slow, the fast system of (1.5) reaches the quasi-steady state while the variable x in the slow system is almost frozen. This means that $-\frac{1}{m}(\cos\phi_1\sin\theta_1\cos\psi_1+\sin\phi_1\sin\psi_1)T_M$ is replaced with $-k_px_1-k_vx_2+r_x(t)$ and then we obtain

$$\dot{x}_1 = x_2$$

$$\dot{x}_2 = -k_p x_1 - k_v x_2 + r_x(t)$$
(1.8)

With a reference system

$$\dot{x}_{r_1} = x_{r_2}
\dot{x}_{r_2} = -k_p x_{r_1} - k_v x_{r_2} + r_x(t)$$
(1.9)

and error variables $e_1 = x_1 - x_{r_1}$ and $e_2 = x_2 - x_{r_2}$, the error dynamics are

$$\dot{e}_1 = e_2
\dot{e}_2 = -k_p e_1 - k_v e_2$$
(1.10)

which means that x_1 and x_2 track asymptotically the reference system in (1.9).

In the next section, to realize the controller in (1.5) for the case of the unknown $\delta(x,t)$ and unmeasured states, the extended high-gain observers will be introduced. We start by introducing high-gain observers.

1.3 High-Gain Observers and Extended High-Gain Observers

High-gain observers started from the earlier work in [21]. In [21], a fully linearizable nonlinear system was dealt with, which is a special case of the normal form. It was shown that the high-gain observers recovered the performance of state feedback controllers when the

observer gain is sufficiently high and the control input is globally bounded. In [7], the performance recovery of state feedback controllers was accomplished using saturated inputs and a separation principle for nonlinear systems was shown. More recent results on high-gain observers are available in [35].

We consider a multi-input-multi-output nonlinear system with multiple chains of integral, given by

$$\dot{x} = Ax + B\phi_u(x, u, t)$$

$$y = Cx$$
(1.11)

where $x \in \mathbf{R}^{\rho}$ is system states, $y \in \mathbf{R}^{m}$ is a measured system output, $u \in \mathbf{R}^{p}$ is the control input, $\phi_{u} = [\phi_{u_{1}}, \dots, \phi_{u_{m}}]^{T}$ is assumed to be locally Lipschitz in its arguments over the domain of interest, and matrices A, B, C are

$$A = \operatorname{block} \operatorname{diag}[A_1, \dots, A_m], \quad A_i = \begin{bmatrix} 0 & 1 & \cdots & 0 \\ 0 & 0 & 1 & \cdots & 0 \\ \vdots & & & \vdots \\ 0 & \cdots & \cdots & 0 & 1 \\ 0 & \cdots & \cdots & 0 & 1 \end{bmatrix} \in \mathbf{R}^{\rho_i \times \rho_i}$$

$$B = \operatorname{block} \operatorname{diag}[B_1, \dots, B_m], \quad B_i = [0, 0, \cdots, 0, 1]^T \in \mathbf{R}^{\rho_i \times 1}$$

$$C = \operatorname{block} \operatorname{diag}[C_1, \dots, C_m], \quad C_i = [1, 0, \cdots, \cdots, 0] \in \mathbf{R}^{1 \times \rho_i}$$

$$(1.12)$$

with $1 \leq i \leq m$ and $\rho = \rho_1 + \cdots + \rho_m$. It is assumed that a state feedback controller, $u = \Gamma(x, t)$ is designed to asymptotically stabilize the system in (1.11) at the origin, where $\Gamma(x, t)$ is locally Lipschitz in its arguments over the domain of interest.

1.3.1 High-Gain Observers

We design a high-gain observer for the system in (1.3) as

$$\dot{\hat{x}} = A\hat{x} + B\phi_n(\hat{x}, u, t) + H(y - C\hat{x})$$
 (1.13)

where $\phi_n(x, u, t) = [\phi_{n_1}, \dots, \phi_{n_m}]^T$ is a nominal model of ϕ_u in (1.11) and $\phi_n(0, 0, t) = 0$, and the observer gain, H, is chosen as

$$H = \text{block diag}[H_1, \dots, H_m], \quad H_i = \begin{bmatrix} h_{i_1}/\varepsilon \\ h_{i_2}/\varepsilon^2 \\ \vdots \\ h_{i_{\rho_i-1}}/\varepsilon^{\rho_i-1} \\ h_{i_{\rho_i}}/\varepsilon^{\rho_i} \end{bmatrix}$$
(1.14)

with a small positive constant, $0 < \varepsilon \ll 1$. The components h_{i_j} of H are chosen such that the polynomials

$$\lambda^{\rho_i} + h_{i_1} \lambda^{\rho_i - 1} + \dots + h_{i_{\rho_i - 1}} \lambda + h_{i_{\rho_i}} = 0, \quad \text{for } i = 1, \dots, m$$
 (1.15)

are Hurwitz. An important phenomenon in high-gain observers is peaking [7]. The scaled error variable is defined by $\eta = [\eta_1^T, \eta_2^T, \cdots, \eta_m^T]^T$, $\eta_i = [\eta_{i_1}, \cdots, \eta_{i_{\rho_i}}]^T$,

$$\eta_{i_j} = \frac{x_{i_j} - \hat{x}_{i_j}}{\varepsilon^{\rho_i + 1 - j}}, \quad \text{for } 1 \le i \le m, \quad 1 \le j \le \rho_i$$

$$\tag{1.16}$$

To show the peaking phenomenon, a SISO second-order subsystem with i=1 and $\rho_1=2$ is considered as

$$\dot{x}_{1_1} = x_{1_2}, \quad \dot{x}_{1_2} = \phi_{1_1} \tag{1.17}$$

and the scaled error variables are

$$\eta_{1_1} = \frac{x_{1_1} - \hat{x}_{1_1}}{\varepsilon}, \quad \eta_{1_2} = x_{1_2} - \hat{x}_{1_2}$$
(1.18)

The error dynamics are

$$\varepsilon \dot{\eta}_{1_1} = -h_{1_1} \eta_{1_1} + \eta_{1_2}
\varepsilon \dot{\eta}_{1_2} = -h_{1_2} \eta_{1_1} + \varepsilon (\phi_{u,1} - \phi_{n,1})$$
(1.19)

With sufficiently small ε , the effect of the difference, $(\phi_{u,1} - \phi_{n,1})$, on the right-hand side of (1.19) is small enough that the behavior of the differential equation of (1.19) becomes a linear system. The solution of such linear systems contains a term of the form

$$\frac{a}{\varepsilon} \exp(-at/\varepsilon), \quad \text{with } a > 0$$
 (1.20)

As $\varepsilon \to 0$, peaking of a/ε degrades the system performance and may destabilize the system [7]. One approach to overcome the peaking phenomenon is to design the control as a globally bounded function of the state, which can be achieved by saturating the control inputs or the state estimates [33]. The saturations are chosen such that they are not active over the domain of interest under state feedback.

1.3.2 Extended High-Gain Observers

By adding one more integrator into the high-gain observer, an extended high-gain observer is created to estimate both unmeasured system states and uncertainties [23]. Consider a multi-input-multi-output nonlinear system in the presence of uncertainties $\sigma(x,t)$ =

 $[\sigma_1, \cdots, \sigma_m]^T \in \mathbf{R}^m$, given by

$$\dot{x} = Ax + B[\phi_n(x, u, t) + \sigma(x, t)]$$

$$y = Cx$$
(1.21)

where $x, y, \phi_u(x, u, t), A, B$ and C are given below (1.11). An extended high-gain observer is designed as

$$\dot{\hat{x}} = A\hat{x} + B[\phi_n(\hat{x}, u, t) + \hat{\sigma}(t)] + H(y - C\hat{x})$$

$$\dot{\hat{\sigma}} = H_e(y - C\hat{x})$$
(1.22)

where ϕ_n and H are same in (1.13) and H_e is

$$H_e = [h_{1_{\rho_1}}/\varepsilon^{\rho_1+1}, \cdots, h_{m_{\rho_m}}/\varepsilon^{\rho_m+1}]^T$$
(1.23)

The observer gains, $h_{i_1}, \dots, h_{i_{\rho_i+1}}$ are chosen that the polynomials

$$\lambda^{\rho_i+1} + h_{i_1}\lambda^{\rho_i} + \dots + h_{i_{\rho_i}}\lambda + h_{i_{\rho_i+1}} \quad \text{for } i = 1, \dots, m$$
 (1.24)

are Hurwitz.

Extended high-gaion observers have been used for several applications. In [51], robust stabilization of non-minimum phase nonlinear system was considered using a continuous sliding-mode control and an extended high-gain observer. Using fast estimation speed of the extended high-gain observer, the derivative of system output was estimated and one of unknown functions in the last chain of integrator was also estimated by the extended high-gain observer. Then estimates were used for the sliding mode control. In [13], an extended high-gain observer as a fast time-scale was combined with an extended kalman filter as a slow time-scale to estimate states of internal dynamics. Estimates of the extended high-gain observer were used as a virtual measurement output for the extended kalman filter.

Chapter 2

Output Feedback Performance

Recovery in the Presence of

Uncertainties

2.1 Introduction

Control of dynamical systems is challenging in the presence of uncertainties. Uncertainties may arise from inaccurate description of the dynamics by the mathematical model used, or can be due to external disturbances that are not accounted for in the model. Additional challenges are posed when the states of the system are not available for measurement and the control variables do not appear linearly in the mathematical model. To achieve desired control objectives, many of these challenges have been addressed by several researchers.

To consider uncertain, nonaffine systems with external disturbances, Chakrabortty et al. [16,17] designed a time-scale separation method. Two filers were used in [17] to deal with system uncertainties and nonaffine input forms; one filter was designed to estimate the uncertainties and the other filter was used to deal with nonaffine input forms. The work in [16] is an extension of Chakrabortty et al. [17] where unmodeled dynamics in the control

inputs are additionally taken into account. Hovakimyan et al. [28] proposed a fast gradient algorithm for dynamic inversion to deal with Multi-Input-Multi-Output (MIMO) nonaffine systems. The control approaches developed by Chakrabortty et al. [16,17] and Hovakimyan et al. [28] are based on state feedback.

Tanelli et al. [64] designed a state feedback control scheme for uncertain, Single-Input-Single-Output (SISO) nonaffine systems. A second-order sliding mode controller with saturation was used to deal with uncertainties and nonaffine input forms. The system states were estimated using the first-order differentiator proposed by Lavant [40] but the stability analysis was based on state feedback control.

In [23], Extended High-Gain Observers (EHGOs) were designed to estimate unmeasured states and uncertainties by combining the High-Gain Observers (HGOs) proposed by Atassi and Khalil [7] with an additional integrator. Back and Shim [9] developed controllers for uncertain, SISO nonline systems using a time-scale separation approach and the circle criterion; the unmeasured states and external disturbances were estimated using an observer. These results were extended in [10] to deal with uncertain MIMO systems using the multi-variable circle criterion. The results in [23] and [9, 10] are applicable to systems with affine inputs.

Hovakimyan et al. [27] proposed an output feedback controller for uncertain, SISO nonaffine input systems using neural network observers together with dynamic inversion. Ge
and Zhang et al. [24] used neural networks to deal with SISO nonaffine systems and highgain observers were used to estimate the unmeasured states. Chen et al. [18] proposed state
feedback control for uncertain, MIMO nonaffine systems using neural networks. Neural
networks were used to model the system dynamics, uncertainties in the system, and input
nonlinearities and uncertainties. A robust backstepping controller, combining backstepping
with variable structure control, was used to deal with neural networks approximation errors.
All of these methods based on neural networks require heavy computations and good prior
knowledge of the system.

In this chapter, we propose an output feedback control scheme for uncertain nonlinear

systems with nonaffine inputs and external disturbances; it is an extension of our earlier work [41,42]. By operating an EHGO in the fastest time scale, unmeasured system states, model uncertainties, and external disturbance were estimated. For the fast recovery of target system inputs in the presence of uncertainties, dynamic inversion was used based on the estimates provided by the EHGO together with sector conditions for the inputs. Using a multi-time-scale controller, the performance of target system states and inputs is recovered in the presence of uncertainties. The singular perturbation method is used to analyze the closed-loop system behavior and establish stability and performance recovery.

This chapter is organized as follows. In the Section 2.2, the problem is formulated for uncertain, MIMO, systems. In Section 2.3 the output feedback controller is presented along with the EHGO and the dynamic inversion algorithm. Section 2.4 provides the stability analysis and establishes performance recovery. Simulation results are presented in Section 2.5 and compared with results of other algorithms in the literature. Performance recovery is also verified through the simulations. Concluding remarks are provided in Section 2.6.

2.2 Problem Statements

The goal of this chapter is to design an output feedback controller that can make an uncertain, MIMO, nonlinear system follow a target system. Consider a MIMO nonlinear system given by

$$\dot{x} = Ax + Bf(x, z, u), \quad x(0) = x_0$$

$$\dot{z} = f_0(x, z), \quad z(0) = z_0$$

$$y = Cx,$$
(2.1)

where A, B, and C represent n chains of integrators as

$$A = \operatorname{block} \operatorname{diag}[A_1, \dots, A_n], B = \operatorname{block} \operatorname{diag}[B_1, \dots, B_n]$$

$$A_{i} = \begin{bmatrix} 0 & 1 & 0 & \cdots & 0 \\ 0 & 0 & 1 & \cdots & 0 \\ \vdots & \vdots & \ddots & \ddots & \vdots \\ 0 & 0 & \cdots & 0 & 1 \\ 0 & 0 & \cdots & \cdots & 0 \end{bmatrix}_{\rho_{i} \times \rho_{i}}, \quad B_{i} = \begin{bmatrix} 0 \\ 0 \\ \vdots \\ 0 \\ 1 \end{bmatrix}_{\rho_{i} \times 1}$$

 $C = \text{block diag}[C_1, \dots, C_n], \ C_i = [1, 0, \dots, 0]_{1 \times \rho_i},$

and $f(x, z, u) = f_n(x, u) + \sigma(x, z, u)$ with

$$f_n(x, u) = \begin{bmatrix} f_{n,1} \\ \vdots \\ f_{n,n} \end{bmatrix}_{n \times 1}, \ \sigma(x, z, u) = \begin{bmatrix} \sigma_1(x, z, u) \\ \vdots \\ \sigma_n(x, z, u) \end{bmatrix}_{n \times 1}$$

 $1 \le i \le n$, $\rho = \rho_1 + \dots + \rho_n$, $x \in D_x \subset \mathbf{R}^{\rho}$, $z \in D_z \subset \mathbf{R}^m$, and $u \in D_u \subset \mathbf{R}^n$. The domains D_x , D_z , and D_u contains their respective origins. The output $y \in D_y \subset \mathbf{R}^n$ is measured, the nominal function $f_n(x, u)$ is known, and $\sigma(x, z, u)$ is unknown. Assumptions for the system are made as follows.

Assumption 1. The functions $f_n(x,u)$, $\sigma(x,z,u)$, and $f_0(x,z)$ are continuously differentiable.

In this chapter, we are designing controllers for minimum-phase systems. Assumption 2, below, implies that the z-subsystem in (2.1) is bounded-input-bounded-state stable.

Assumption 2. There exists a radially unbounded positive definite function V_z such that for all $x \in \mathbb{R}^{\rho}$ and $z \in \mathbb{R}^m$

$$\dot{V}_z \le 0 \quad for \ z \ge W_z(x) \tag{2.2}$$

where $W_z(x)$ is a nonnegative continuous function.

A target system is defined by

$$\dot{x}_r = (A - BL)x_r + Bu_c(t), \quad x_r(0) = x_{r0}, \tag{2.3}$$

where the matrix L is block diagonal such that the matrix (A - BL) is Hurwitz and $u_c(t)$ is a bounded command input belonging to the compact set $D_r \subset \mathbf{R}^n$ and its derivative \dot{u}_c is chosen to be bounded. With the variable $e = x - x_r$, the error dynamics are given by

$$\dot{e} = (A - BL)e + BF(x, z, u, u_c), \quad e_0 = e(0)$$
(2.4)

where $F(x, z, u, u_c) = f(x, z, u) + Lx - u_c(t)$. With the error dynamics of (2.4), we have the following assumption.

Assumption 3. • There is a unique continuously differentiable function $\phi(x, z, u_c)$ such that $u_r = \phi(x, z, u_r)$ solves the equation

$$F(x, z, u_r, u_c) = 0 (2.5)$$

The derivative $\dot{u}_r = \phi_d(x, z, u_c, \dot{u}_c)$ is bounded on compact sets of x and z.

• There is a known matrix $K(x, s + u_r, u_c)$ such that the function F satisfies the sector condition

$$s^{T}K(x, s + u_r, u_c)F(x, z, s + u_r, u_c) \ge \beta s^{T}s, \quad \beta > 0$$
 (2.6)

for all (x, z, u_d) , with $s = u - u_r$.

Remark 1. When the system is affine in u, i.e., f(x,z,u) = h(x,z) + G(x,z)u, condition

(2.6) is equivalent to the existence of a known matrix $K(x, s + u_r, u_c)$ such that

$$K(x, s + u_r, u_c)G(x, z) + G^T(x, z)K^T(x, s + u_r, u_c) \ge kI$$
 (2.7)

with k > 0. This condition holds with K = I when G(x, z) satisfies

$$G(x,z) + G^{T}(x,z) \ge kI, \quad k > 0$$
 (2.8)

This will be the case for single-input systems when G is positive and bounded away from zero. Condition (2.7) is less restrictive than (2.8) as it will be shown in Section 2.5 by an example.

Remark 2. Earlier work on systems that are nonaffine in the input, in particular, [17] requires the Jacobian matrix $(\partial f/\partial u)$ to satisfy the condition.

$$\left(\frac{\partial f}{\partial u}\right) + \left(\frac{\partial f}{\partial u}\right)^T \ge kI, \quad k > 0 \tag{2.9}$$

and [27–29] require the Jacobian matrix $(\partial f/\partial u)$ to satisfy either the condition (2.9) or the condition

$$\zeta^{T} \left(\frac{\partial f}{\partial u}^{T} (x, u_{1}, u_{c}) \right) \left(\frac{\partial f}{\partial u} (x, u_{2}, u_{c}) \right) \zeta \ge 2k_{c} \|\zeta\|^{2} \quad \forall \zeta \in \mathbf{R}^{n}$$
 (2.10)

where u_1 and u_2 are distinct variables and k_c is a positive constant. The sector condition (2.6) is less restrictive than (2.9) and (2.10). For single-input systems, (2.9) requires the Jacobian to be positive for all u. The sector condition (2.6), on the other hand, allows the Jacobian to be negative as long as f(x, z, u) belongs to the sector $[k, \infty)$, uniformly in x, z and u_c .

For multi-input systems, the sector condition does not require the Jacobian $(\partial f/\partial u)$ to be nonsingular. The relation between K in (2.7) and the Jacobian matrix $(\partial f/\partial u)$ will be

mentioned in Section 2.3. In Section 2.5, it is shown that the sector condition in (2.7) is less conservative than the conditions (2.9) and (2.10) through numerical simulations.

2.3 Control Design

We use dynamic inversion to deal with nonaffine and/ or uncertain functions. Had x and σ been available, the dynamic inversion would have been taken as

$$\mu \dot{u} = -K(x, u, u_c) F(x, z, u, u_c), \quad u(0) = u_0$$

$$= -K(x, u, u_c) [f_n(x, u) + \sigma(x, z, u) + Lx - u_c]$$
(2.11)

If the matrix K is chosen as the Jacobian matrix $(\partial f/\partial u)^T$, i.e., $K = (\partial f/\partial u)^T(x, u, u_c)$ and the function F in (2.11) is not a function of z, i.e., $F = F(x, u, u_c)$, the derivative of the Lyapunov function $V_s = s^T s/2$ along the trajectories (2.1) and (2.3), is

$$\dot{V}_{s} = (\dot{u} - \phi_{d})^{T} s + s^{T} (\dot{u} - \phi_{d})
= -\left(\frac{1}{2\mu}\right) s^{T} \left[KF(x, u, u_{c}) + F^{T}(x, u, u_{c}) K^{T} \right] s - \phi_{d}^{T} s$$
(2.12)

with $s = u - u_r$ and $\dot{u}_r = \phi_d(x, u_c, \dot{u}_c)$. By using the mean value theorem (Appendix B, [34]) with $F(x, u_r, u_c) = 0$ in (2.5),

$$F(x, u, u_c) - F(x, u_r, u_c)$$

$$= \int_0^1 \frac{\partial F}{\partial u} (x, (1 - \sigma)s + u_r, u_c) d\sigma s$$
(2.13)

for $0 \le \sigma \le 1$, and $\partial f/\partial u = \partial F/\partial u$, \dot{V}_s is rewritten as

$$\dot{V}_s = -\left(\frac{1}{2\mu}\right) s^T \left[P^T K^T + KP\right] s - \phi_d^T s \tag{2.14}$$

where

$$P = \int_0^1 \frac{\partial f}{\partial u}(x, (1 - \sigma)s + u_r, u_c) d\sigma$$
 (2.15)

With sufficiently small μ and the condition

$$s^{T}(P^{T}K^{T} + KP)s \ge k_{i}||s||^{2}$$
(2.16)

 $\dot{V}_s \leq -(k_s/\mu)V_s + \delta$ with k_j , $k_s > 0$, and $\delta > 0$ independent of μ . We note that the condition in (2.16) is similar to the condition in (2.10).

In output feedback control, x and σ are estimated using the EHGO:

$$\dot{\hat{x}} = A\hat{x} + B[f_n(\hat{x}, u) + \hat{\sigma}(t)] + H(\varepsilon)(y - C\hat{x})
\dot{\hat{\sigma}} = H_{n+1}(y - C\hat{x}), \quad \hat{x}(0) = \hat{x}_0, \quad \hat{\sigma}(0) = \hat{\sigma}_0$$
(2.17)

where $\hat{\sigma}(t) = [\hat{\sigma}_1, \dots, \hat{\sigma}_n]^T \in \mathbb{R}^n$ is the estimate of $\sigma(x, z, u)$, and

$$H = \text{block diag}[H_1, \dots, H_n],$$

$$H_i(\varepsilon) = [\alpha_{i,1}/\varepsilon, \dots, \alpha_{i,\rho_i}/\varepsilon^{\rho_i}]^T,$$

$$H_{n+1} = \text{block diag}[\alpha_{1,\rho_1}/\varepsilon^{\rho_1+1}, \dots, \alpha_{n,\rho_n}/\varepsilon^{\rho_n+1}]$$

$$(2.18)$$

The constants $\alpha_{i,1}, \dots, \alpha_{i,\rho_i+1}$ are chosen such that the polynomials

$$\lambda^{\rho_i+1} + \alpha_{i,1}\lambda^{\rho_i} + \dots + \alpha_{i,\rho_i}\lambda + \alpha_{i,\rho_i+1}$$
 for $i = 1,\dots, n$

are Hurwitz and the control parameter $\varepsilon > 0$ is small enough. We note that the small parameter ε is smaller than μ to make the dynamics of the EHGO faster than the dynamics of the dynamic inversion since the dynamic inversion uses estimates provided by the EHGO. Therefore, the control parameters ε and μ are chosen such that $0 < \varepsilon \ll \mu \ll 1$.

Using the EHGO in (2.17) together with the dynamic inversion in (2.11), the output feedback control is designed as

$$\mu \dot{u} = -K[f_n(\hat{x}_s, u) + \hat{\sigma}_s + L\hat{x}_s - u_c]$$

$$\hat{x}_s = [\hat{x}_{s1}^T, \dots, \hat{x}_{sn}^T]^T, \quad \hat{\sigma}_s = [\hat{\sigma}_{s1}, \dots, \hat{\sigma}_{sn}]^T$$

$$\hat{x}_{si} = \left[M_{x_{i,1}} \operatorname{sat} \left(\frac{\hat{x}_{i,1}}{M_{x_{i,1}}} \right), \dots, M_{x_{i,\rho_i}} \operatorname{sat} \left(\frac{\hat{x}_{i,\rho_i}}{M_{x_{i,\rho_i}}} \right) \right]^T$$

$$\hat{\sigma}_{si} = \left[M_{\sigma_1} \operatorname{sat} \left(\frac{\hat{\sigma}_1}{M_{\sigma_1}} \right), \dots, M_{\sigma_n} \operatorname{sat} \left(\frac{\hat{\sigma}_n}{M_{\sigma_n}} \right) \right]^T$$
(2.19)

for i = 1, ..., n, where sat(·) is the saturation function defined by

$$\operatorname{sat}(k) = \begin{cases} k & |k| \le 1\\ \operatorname{sign}(k) & |k| > 1 \end{cases}$$
 (2.20)

The saturation function is used to prevent peaking from degrading the system performance. The saturation levels $M_{x_{i,j}}$ and M_{σ_i} for $j=1,\ldots,\rho_i$ and $i=1,\ldots,n$ in (2.19), are determined outside of a compact set of interest, which is specified next. Under Assumption 3, the error dynamics of (2.4) with $u=u_r$ is exponentially stable at e=0. Let $P=P^T>0$ be the solution of the Lyapunov equation $P(A-BL)+(A-BL)^TP=-I$. With $u=u_r$ and Assumption 2, for any given positive constant c_x and for all $x(t) \in \{V_x(x) \leq c_x\}$ where $V_x(x) = x^T P x$, and $u_c(t) \in D_r$, the positively invariant set $\{V_z(z) \leq c_z + \alpha_z(c_x)\}$ can be chosen for the dynamics of z in (2.1), where $\alpha_z(c_e)$ is a class K_∞ function and $c_z > 0$. Now, we can define the compact set

$$\Omega_s = \{V_x(x) \le c_x\} \times \{V_z(z) \le c_z + \alpha_z(c_x)\}$$
(2.21)

By choosing c_x sufficiently large, any compact subset of $\mathbf{R}^{\rho} \times \mathbf{R}^m$ can be included in the interior of Ω_s . Based on the compact set Ω_s , the levels of saturation are determined as

follows.

$$M_{x_{i,j}} > \max_{x \in \{V_x(x) \le c_x\}} |x_{i,j}|,$$

$$M_{\sigma_i} > \max_{(x,z) \in \Omega_s, u_c \in D_r} |\sigma_i(x, z, u_r(x, z, u_c))|$$
(2.22)

for $j = 1, ..., \rho_i$ and i = 1, ..., n.

2.4 Main Result

In this section, we will show that in the presence of uncertainties, the output feedback control (2.17) and (2.19) can recover the performance of both states and inputs of the target system (2.3). Consider the fast variables $\eta = [\eta_1^T, \dots, \eta_{n+1}^T]^T$ with $\eta_i = [\eta_{i,1}, \dots, \eta_{i,\rho_i}]^T \in \mathbb{R}^{\rho_i}$ for error dynamics of the EHGO

$$\eta_{i,j} = \frac{x_{i,j} - \hat{x}_{i,j}}{\varepsilon^{\rho_i + 1 - j}}, \quad \eta_{i,\rho_i + 1} = \sigma_i(x, z, u) - \hat{\sigma}_i(t)$$
for $1 \le i \le n, \quad 1 \le j \le \rho_i$

$$(2.23)$$

Using (2.4), the dynamics of z in (2.1), (2.17), and (2.19), the closed-loop system equations can be written in the standard singularly perturbed form

$$\dot{e} = (A - BL)e + B[f(x, z, s + u_r) + Lx - u_c(t)], \tag{2.24}$$

$$\dot{z} = f_0(x, z) \tag{2.25}$$

$$\mu \dot{s} = -K[f_n(\hat{x}_s, s + u_r) + \hat{\sigma}_s + L\hat{x}_s - u_c] - \mu \phi_d$$
 (2.26)

$$\varepsilon \dot{\eta} = \Lambda \eta + \varepsilon [\bar{B}_1 \psi_1 + (\bar{B}_2 / \mu) \psi_2] \tag{2.27}$$

where

$$\Lambda = \operatorname{block} \operatorname{diag}[\Lambda_{1}, \dots, \Lambda_{n}],$$

$$\Lambda_{i} = \begin{bmatrix}
-\alpha_{i,1} & 1 & 0 & \cdots & 0 \\
-\alpha_{i,2} & 0 & 1 & \ddots & 0 \\
\vdots & \vdots & \ddots & \vdots & \vdots \\
-\alpha_{i,\rho_{i}} & 0 & \cdots & 0 & 1 \\
-\alpha_{i,\rho_{i}+1} & 0 & \cdots & \cdots & 0
\end{bmatrix}_{\rho_{i} \times \rho_{i}}$$

$$\bar{B}_{1} = \operatorname{block} \operatorname{diag}[B_{1,1}, \dots, B_{1,n}],$$

$$\bar{B}_{2} = \operatorname{block} \operatorname{diag}[B_{2,1}, \dots, B_{2,n}],$$

$$B_{1,i} = \begin{bmatrix}
0 \\
B_{i}
\end{bmatrix}, \quad B_{2,i} = \begin{bmatrix}
B_{i} \\
0
\end{bmatrix}$$

for $i=1,\ldots,n$ and the functions ψ_1 and ψ_2 are given by

$$\psi_{1} = (1/\varepsilon)[f_{n}(x, s + u_{r}) - f_{n}(\hat{x}_{s}, s + u_{r})]$$

$$\psi_{2} = \mu \left\{ \left(\frac{\partial \sigma}{\partial x} \right)^{T} [Ax + Bf(x, z, s + u_{r})] + \left(\frac{\partial \sigma}{\partial z} \right)^{T} f_{0}(x, z) \right\} - \left(\frac{\partial \sigma}{\partial u} \right)^{T} KF_{s}$$

$$F_{s} = f_{n}(\hat{x}_{s}, s + u_{r}) + \hat{\sigma}_{s} + L\hat{x}_{s} - u_{c}$$

$$(2.29)$$

We note that u_r and $\phi_d(x, z, s + u_r)$ in (2.24) and (2.25), respectively, are mentioned in the Assumption 3, the nominal function $f_n(x, s + u_r)$ is Lipschitz in its arguments so that the inequality $||f_n(x, s + u_r) - f_n(\hat{x}_s, s + u_r)|| \le \varepsilon k_{\psi_1} ||\eta||$ is satisfied with k_{ψ_1} independent of ε .

we are going to show the stability of the boundary layer and reduced systems in the closed-loop system (2.24)-(2.27). Since the z-subsystem of (2.25) with the input x is bounded-input-bounded-state stable, we are focusing on the subsystems (2.24), (2.26), and (2.27).

Now, using the time-scale structure of the closed-loop system (2.24), (2.26), and (2.27),

the stability analysis of each subsystem will be shown. By considering the subsystem (2.27) as the fast system and the other subsystems (2.24) and (2.26) as the slow system, the boundary layer system in (2.27) can be obtained by

$$\varepsilon \dot{\eta} = \Lambda \eta, \quad \eta(0) = \eta_0$$
 (2.30)

Since the matrix Λ is Hurwitz, the boundary layer system (2.30) is exponentially stable at the origin.

After the fast variable η reaches its quasi-steady state, $\eta = 0$, the reduced system for (2.24) and (2.26) is obtained by setting $\eta = 0$ and $\varepsilon = 0$. In the reduced system, the dynamic inversion (2.26) is viewed as fast and the subsystem (2.24) is slow. The boundary layer system for (2.26) is given by

$$\mu \dot{s} = -KF(x, z, s + u_r, u_c), \quad s(0) = s_0$$
 (2.31)

To investigate the stability of the boundary layer system (2.31), the Lyapunov function $V_s = (s^T s)/2$ is defined. With the sector condition (2.6), its derivative \dot{V}_s along the trajectory (2.31) is

$$\mu \dot{V}_s = -s^T K F \le -\beta \|s\|^2 \tag{2.32}$$

Therefore, the boundary layer system (2.31) is exponentially stable at s = 0.

The reduced system for (2.24) is obtained by setting $\varepsilon = 0$, $\eta = 0$, $\mu = 0$, and s = 0. With the input $u = u_r$ and $x = \hat{x}$, the reduced system for (2.24) is obtained as

$$\dot{e} = (A - BL)e, \quad e(0) = e_0$$
 (2.33)

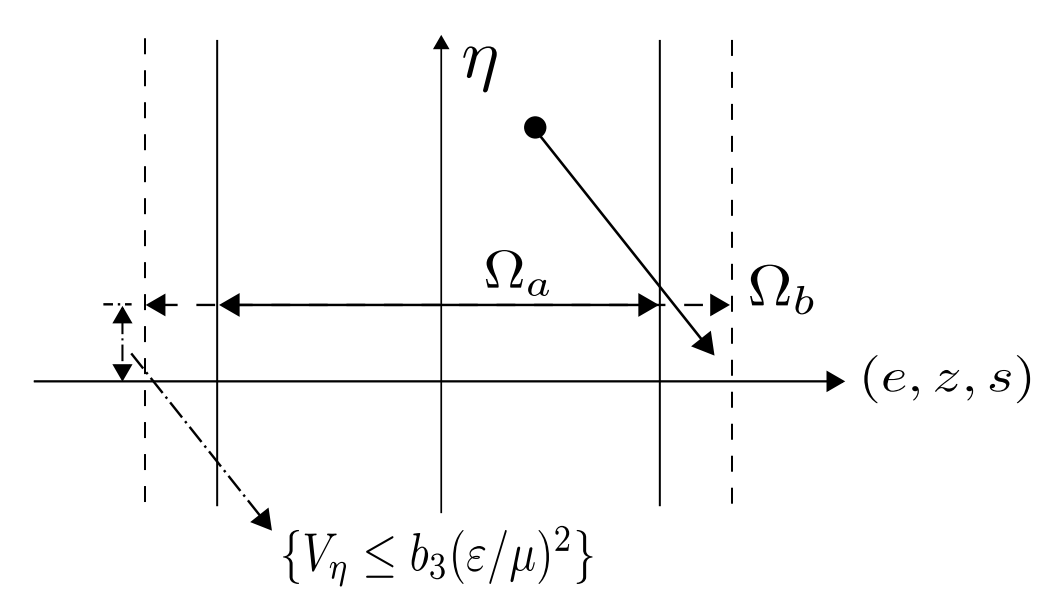


Figure 2.1: The trajectory starting from $(e_0, z_0, s_0) \in \Omega_a$ and $\eta_0 \notin \{V_\eta \leq b_3(\varepsilon/\mu)^2\}$ converges into $(e, z, s, \eta) \in \Omega_b \times \{V_\eta \leq b_3(\varepsilon/\mu)^2\}$.

which is exponentially stable at e = 0.

The following theorem shows that all trajectories will be bounded and (x, u) approach the trajectories of the target system (2.3) as μ , (ε/μ) , and ε tend to zero.

Theorem 1. Consider the closed-loop system (2.24) - (2.27) under Assumption 1, 2, and 3. Suppose the trajectories $(x, z, u, \hat{x}, \hat{\sigma})$ start from the compact sets $(x_0, z_0, u_0) \in S_x \times S_z \times S_u \subset D_x \times D_z \times D_u$ and $(\hat{x}_0, \hat{\sigma}_0) \in Q_x \times Q_s \subset \mathbf{R}^{\rho} \times \mathbf{R}^n$. Then, there exists a constant $\varsigma > 0$ such that for $\max\{\mu, (\varepsilon/\mu), \varepsilon\} < \varsigma$

- all trajectories are bounded;
- $||x x_r|| \to 0$ and $||u u_r|| \to 0$ as $\mu, (\varepsilon/\mu), \varepsilon \to 0$ for all $t \ge 0$.

Proof. As the first part of the proof, we are going to show that all trajectories enter a positively invariant set.

We define the Lyapunov functions $V_e = e^T P e$ and $V_{\eta} = \eta^T P_{\eta} \eta$ for the subsystems, (2.24) and (2.27), respectively, where P_{η} is the solutions for the Lyapunov equation $P_{\eta} \Lambda + \Lambda^T P_{\eta} = -I$. We define the sets

$$\Omega_a = \{V_e \le a_1\} \times \{V_z \le c_z + \alpha_z(c_x)\} \times \{V_s \le a_2\}$$

$$\Omega_b = \{V_e \le b_1\} \times \{V_z \le c_z + \alpha_z(c_x)\} \times \{V_s \le b_2\}$$

$$\Omega_c = \{V_e \le c_1\} \times \{V_z \le c_z + \alpha_z(c_x)\}$$
(2.34)

with the relations

$$0 < a_1 < b_1 < c_1, \quad 0 < a_2 < b_2 \tag{2.35}$$

The constant c_1 is chosen such as that

$$e \in \{V_e \le c_1\} \implies x \in \{V_x \le c_x\} \tag{2.36}$$

so that $\forall e \in \{V_e \leq c_1\}, z \in \{V_z \leq c_z + \alpha_z(c_x)\}$. The constant a_1 and a_2 are chosen such that $S_x \times S_z \times S_u \subset \Omega_a$.

Similar to earlier work on high-gain observers, e.g., [33], it can be shown that, for sufficiently small (ε/μ) , the set $\Omega_b \times \{V_\eta \leq b_3(\varepsilon/\mu)^2\}$, for some $b_3 > 0$, is positively invariant. This is done by showing that the derivatives of V_e , V_z , and V_s are negative on the boundaries $\{V_e = a_1\}$, $\{V_z = c_z + \alpha_z(c_x)\}$, and $\{V_s = a_2\}$, respectively. Similarly, it can be shown that for sufficiently small $\lambda = \max\{\mu, \varepsilon/\mu\}$, the set $\Omega_c \times \{V_s \leq c_2\lambda^2\} \times \{V_\eta \leq b_3(\varepsilon/\mu)^2\}$, for some $c_2 > 0$, is positively invariant.

We show boundedness of the trajectories in two steps:

- firstly, the trajectories (e, z, s) and η starting from $(e_0, z_0, s_0) \in \Omega_a$ and $\eta(0) \notin \{V_{\eta} \leq b_2(\varepsilon/\mu)^2\}$ enter the set $\Omega_b \times \{V_{\eta} \leq b_3(\varepsilon/\mu)^2\}$ in finite time as depicted in Fig. 2.1;
- secondly, the trajectories (e, z), s, and η starting from $\Omega_b \times \{V_{\eta} \leq b_3(\varepsilon/\mu)^2\}$ enters the set $\Omega_c \times \{V_s \leq c_2 \lambda^2\} \times \{V_{\eta} \leq b_3(\varepsilon/\mu)^2\}$ in finite time.

In the first step, consider that the initial conditions are in $(e_0, z_0, s_0) \in \Omega_a$ and $\eta(0)$ starting from outside the set $\{V_{\eta} \leq b_3(\varepsilon/\mu)^2\}$. Due to the scaling (2.23), $\eta(0)$ could be of the order of

 $1/\varepsilon^{\rho_m}$ where $\rho_m = \max_{i=1,...,n} \rho_i$. Because the term $[\bar{B}_1\psi_1 + (\bar{B}_2/\mu)\psi_2]$ in (2.27) is bounded by $k_1\|\eta\| + k_2$ for all $(x, z, s) \in \Omega_b$, for some positive constants k_1 and k_2 , it can be shown that

$$\varepsilon \dot{V}_{\eta} \le -\|\eta\|^2 + \varepsilon k_3 \|\eta\|^2 + \varepsilon k_4 \|\eta\| \tag{2.37}$$

for some positive constants k_3 and k_4 . Hence,

$$\varepsilon \dot{V}_{\eta} \le -\frac{1}{2} \|\eta\|^2 + \frac{\varepsilon}{\mu} \|\eta\| \tag{2.38}$$

for $\varepsilon < 1/(2k_3)$. It follows that there is $b_3 > 0$ such that

$$\varepsilon \dot{V}_{\eta} \le -\gamma_1 V_{\eta}, \quad \text{for } V_{\eta} \ge \left(\frac{\varepsilon}{\mu}\right)^2 b_3$$
 (2.39)

for some $\gamma_1 > 0$. Taking into consideration that $\|\eta(0)\| \le k_5/\varepsilon^{\rho_m}$ for some positive constant $k_5 > 0$, we obtain

$$V_{\eta} \le \frac{k_6}{\varepsilon^{2\rho_m}} e^{-\gamma_1 t/\varepsilon} \tag{2.40}$$

for some positive constant $k_6 > 0$. Since $\varepsilon \leq \varepsilon/\mu$, we can estimate the time the trajectory will enter $\{V_{\eta} \leq b_3(\varepsilon/\mu)^2\}$ by the more conservative time, $T_1(\varepsilon)$, when $V_{\eta} = b_3 \varepsilon^2$. The time $T_1(\varepsilon)$ is given by

$$\frac{k_6}{\varepsilon^{2\rho_m}} e^{-\gamma_1 T_1/\varepsilon} = b_3 \varepsilon^2 \Leftrightarrow T_1 = \frac{\varepsilon}{\gamma_1} \ln \left(\frac{k_6}{b_3 \varepsilon^{2(\rho_m + 1)}} \right)$$
 (2.41)

By L'Hopital's rule, it can be shown that $\lim_{\varepsilon\to 0} T_1(\varepsilon) = 0$. Because $a_1 < b_1$, $a_2 < b_2$, and the right-hand side functions of (2.24), (2.25), and (2.27) are bounded uniformly in ε , there is time T_0 such that $(x, z, s) \in \Omega_b$ for all $t \in [0, T_0]$. By choosing ε small enough we can have

$$T_1(\varepsilon) = (1/2)T_0.$$

In the second step, we repeat the same argument to show that s enters the set $\{V_s \leq c_2 \lambda^2\}$. The right-hand side of (2.26) is a perturbation of the right-hand side of (2.31) with the perturbation term bounded by $k_7 ||\eta|| + k_8 \mu$ for some positive constants k_7 and k_8 . Because η cannot leave the set $\{V_{\eta} \leq b(\varepsilon/\mu)^2\}$,

$$k_7 \|\eta\| + k_8 \mu \le k_9 \lambda$$
 for some $k_9 > 0$ (2.42)

where $\lambda = \max\{\mu, \varepsilon/\mu\}$. Hence

$$\mu \dot{V}_s \le -\beta \|s\|^2 + k_{10}\lambda \|s\| \tag{2.43}$$

Therefore, there is $c_2 > \text{such that}$

$$\mu \dot{V}_s < -\gamma_2 V_s, \quad \text{for } V_s > c_2 \lambda^2$$
 (2.44)

This show that there is time $T_2 = T_2(\mu)$ such that the trajectory enters $\{V_s \leq c_2\lambda^2\}$. Once again by choosing μ small enough, (e, z) stay in the set $\{V_e \leq c_1\} \times \{V_z \leq c_z + \alpha(c_x)\}$. Thus, with the time $T(\varepsilon, \mu) = T_1(\varepsilon) + T_2(\mu)$, the trajectory enters the positively invariant set $\Omega_c \times \{V_s \leq c_2\lambda^2\} \times \{V_\eta \leq b_3(\varepsilon/\mu)^2\}$.

Lastly, we are going to show the performance recovery for x and u. Since the proof is similar for both variables, we show it only for u. The nominal model of (2.26) is the system (2.31), which is exponential stable at s = 0. The difference between (2.26) and (2.31) is

$$G = -K[f_n(\hat{x}_s, s + u_r) - f_n(x, s + u_r) + \hat{\sigma}_s(t) - \sigma(x, z, s + u_r) + L(\hat{x}_s - x)] + \mu \dot{u}_r$$
(2.45)

where $\dot{u}_r = \phi_d(x, z, u_c, \dot{u}_c)$ is bounded on the compact set of x, z, u_c , and \dot{u}_c , i.e., $||\dot{u}_r|| \le u_{rm}$,

with $u_{rm} > 0$, uniformly in μ and ε . The function G is bounded

$$||G|| \le K_m[\varepsilon L_1 ||\eta|| + L_2 ||\eta||] + \mu u_{rm} \tag{2.46}$$

for some positive constants K_m , L_1 , L_2 , which can be made arbitrarily small by choosing sufficient small μ and ε/μ , for $t \geq T(\varepsilon, \mu)$. Using Theorem 9.1 in [33], we conclude that

$$||u(t) - u_r(t)|| \le \delta(\mu, \varepsilon/\mu), \quad \forall t \ge T(\mu, \varepsilon) > 0$$
 (2.47)

where $\delta(\mu, \varepsilon) \to 0$ as $\mu, (\varepsilon/\mu), \varepsilon \to 0$. For the time interval $t \in [0, T(\mu, \varepsilon)]$, since the trajectories u and u_r are in the compact set, we have two inequalities

$$||u(t) - u(0)|| \le k_t t, \quad ||u_r(t) - u(0)|| \le k_t t$$
 (2.48)

with $k_t > 0$, during the time interval. Using the triangle inequality, we obtain the inequality

$$||u - u_r|| \le 2k_t T(\mu, \varepsilon), \quad \forall t \in [0, T(\mu, \varepsilon)]$$
 (2.49)

Therefore, given any $\delta_1 > 0$, we can ensure that

$$||u(t) - u_r(t)|| \le \delta_1$$
, for all $t \ge 0$ (2.50)

by choosing ε , μ , and (ε/μ) sufficiently small.

2.5 Simulations

In this section, we choose examples for the comparison with other papers, [28], and [17]. The first example, which has nonaffine input, considers the case that the Jacobian matrix is singular at some values. As a second example, which has affine input forms and system

uncertainties, the camera image coordinate system in [17] is modified to show that our proposed control methods provide less conservative conditions than ones in [17].

2.5.1 Example 1

First, we are considering the case where the Jacobian matrix, $(\partial f/\partial u)$ in (2.10), is singular at some values. In this example, we assume that the state $x = [x_1, x_2]^T$ is available and there is no system uncertainty. The MIMO nonlinear nonaffine system is given by

$$\begin{bmatrix} \dot{x}_1 \\ \dot{x}_2 \end{bmatrix} = \begin{bmatrix} x_1 + 2u_1^3 - 15u_1^2 + 36u_1 \\ 2u_2^3 - 15u_2^2 + 36u_2 \end{bmatrix}$$
 (2.51)

The target system is

$$\dot{x}_r = (A - BL)x_r + u_c, \quad x_r = [x_{r1}, x_{r2}]^T$$

$$u_c = \begin{bmatrix} 100 \\ 100 \end{bmatrix}, \quad A - LB = \begin{bmatrix} -x_1 & 0 \\ 0 & -x_2 \end{bmatrix}$$
(2.52)

Our proposed controller for the dynamic inversion is

$$\mu \dot{u} = - \begin{bmatrix} x_1 + 2u_1^3 - 15u_1^2 + 36u_1 + x_1 - 100 \\ 2u_2^3 - 15u_2^2 + 36u_2 + x_2 - 100 \end{bmatrix},$$
 (2.53)

where $u = [u_1, u_2]^T$, the small constant $\mu = 0.1$, and K in (2.6) is chosen as an identity matrix, i.e., $K = I_{2\times 2}$ (a 2×2 -identity matrix). In Fig. 2.2, the solid lines x_1 and x_2 generated by the proposed controller in (2.52), converge into the reference trajectories (dashed lines) in (2.52). Since the proposed controller in (2.53) is designed based on the sector condition, the controller is not affected by the singularity of the Jacobian matrix in Fig. 2.3.

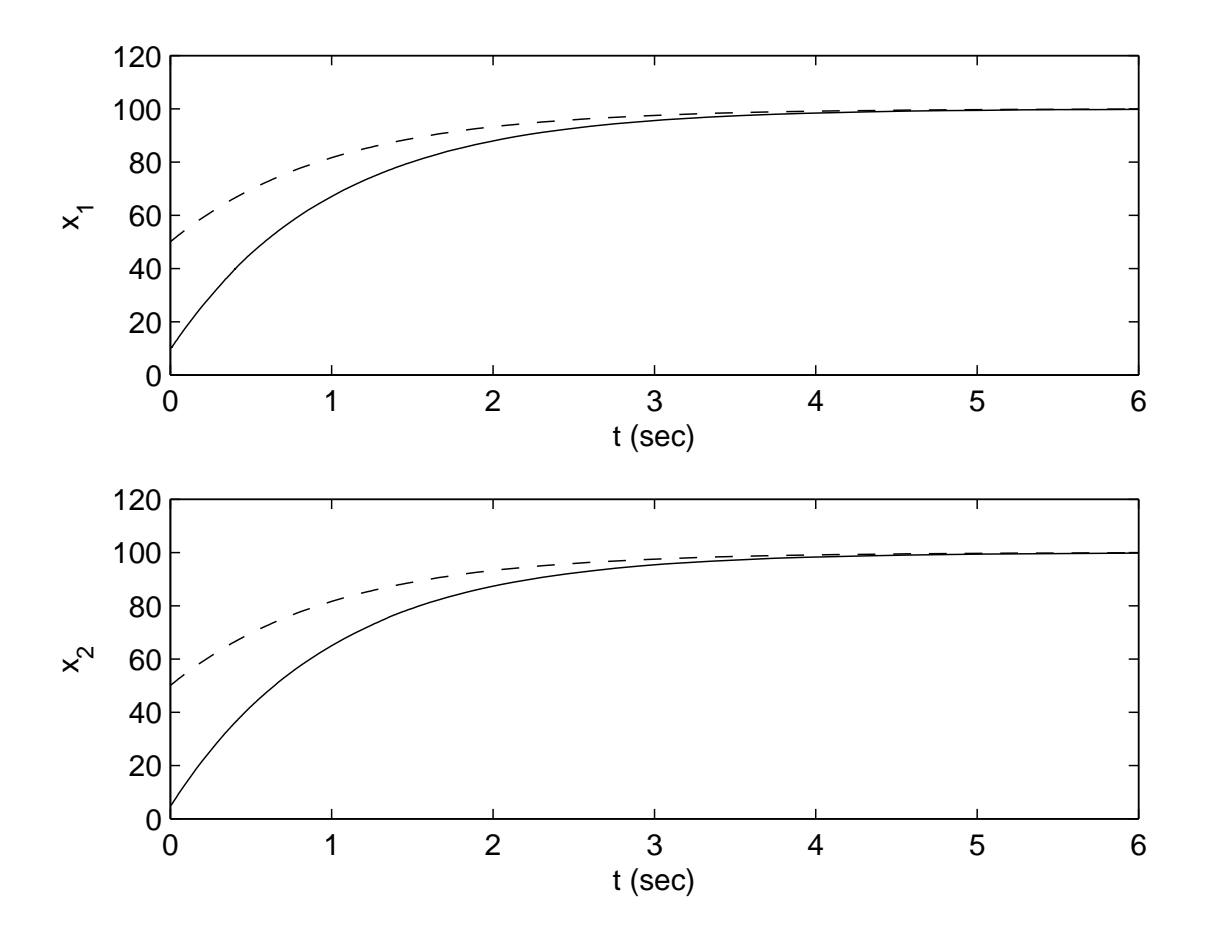


Figure 2.2: The solid and dashed lines represent trajectories x_i for i = 1, 2 driven by the proposed controller in (2.53) and reference trajectories x_{ri} for i = 1, 2 in (2.52), respectively.

2.5.2 Example 2

A modified model from [17] is given by

$$\dot{x} = R_m u, \quad y = [x_1, x_2]^T,$$

$$R_m = \begin{bmatrix} \cos \phi & \sin \phi \\ \sin \phi & -\cos \phi \end{bmatrix}$$
(2.54)

with $x = [x_1, x_2]^T$, $u = [u_1, u_2]^T$, and $\phi = 45^\circ$. The target system with $u_c = [0, 0]^T$ is the same as in (2.52). With the condition $\phi = 45^\circ$, the Jacobian condition $(\partial R_m/\partial u)^T + (\partial R_m/\partial u) \ge k_p I_{2\times 2}$ in [17] is not satisfied. Using the dynamic inversion, the control inputs are designed

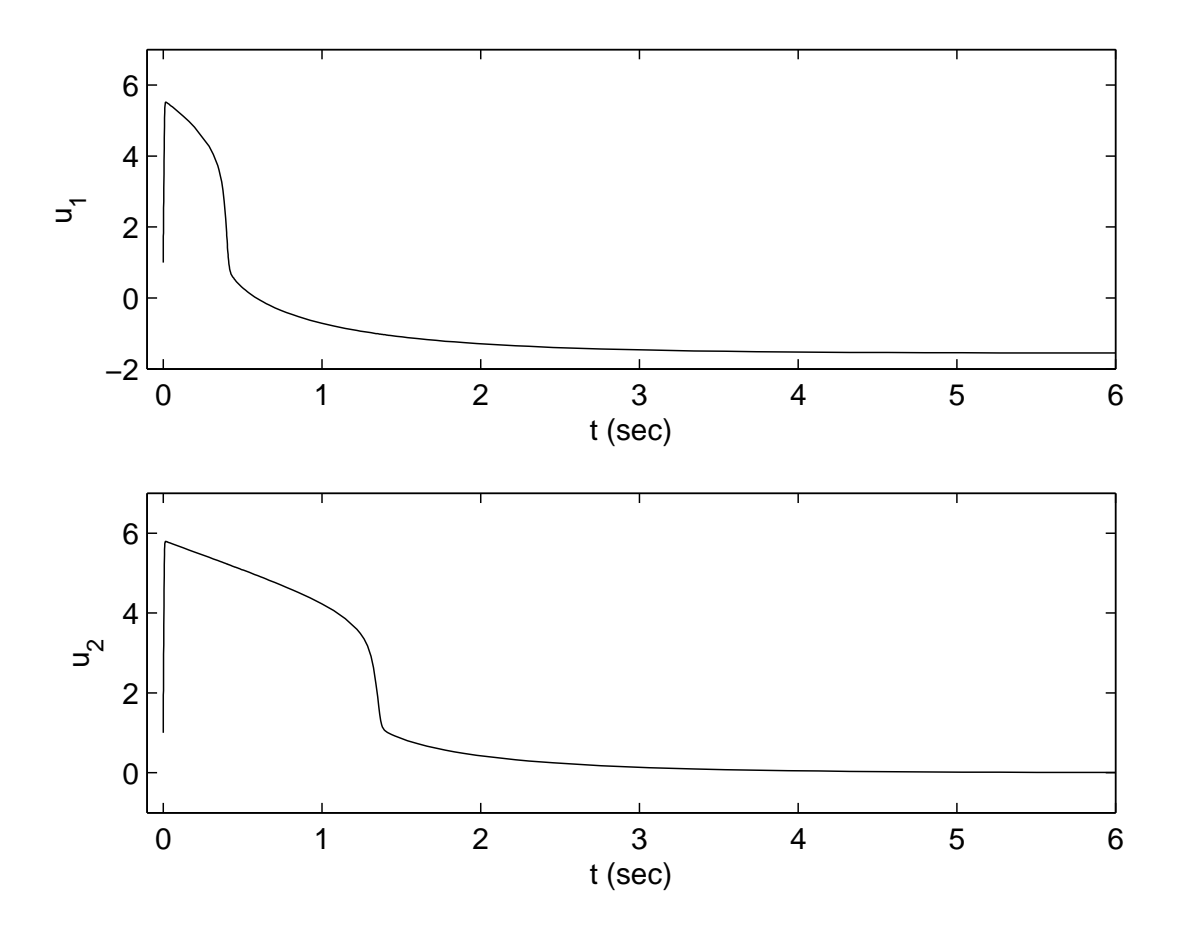


Figure 2.3: Input trajectories u_1 and u_2 in (2.53) are shown and both u_1 and u_2 cross the values $u_1=2,3$ and $u_2=2,3$ which make the Jacobian matrix $(\partial f/\partial u)$ singular.

by

$$\mu \dot{u} = -KF \tag{2.55}$$

where

$$KF = \begin{bmatrix} u_1 \cos \phi + u_2 \sin \phi + x_1 \\ -u_1 \sin \phi + u_2 \cos \phi - x_2 \end{bmatrix}$$
 (2.56)

The sector condition in Assumption 3 is satisfied as follows.

$$s^T K F \ge \beta \|s\|^2 \tag{2.57}$$

with the constant $\beta > 0$. Now, the EHGO is designed to estimate uncertainties i.e., the right-hand side of (2.54), $R_m u$,

$$\dot{\hat{x}}_1 = \hat{\sigma}_1 + \frac{h_{11}}{\varepsilon} (x_1 - \hat{x}_1), \quad \dot{\hat{\sigma}}_1 = \frac{h_{12}}{\varepsilon^2} (x_1 - \hat{x}_1)
\dot{\hat{x}}_2 = \hat{\sigma}_2 + \frac{h_{21}}{\varepsilon} (x_2 - \hat{x}_2), \quad \dot{\hat{\sigma}}_2 = \frac{h_{22}}{\varepsilon^2} (x_2 - \hat{x}_2)$$
(2.58)

where $\hat{\sigma}_1$ and $\hat{\sigma}_2$ are the estimates of \dot{x}_1 and \dot{x}_2 , respectively. The constants $h_{i,1}$ and $h_{i,2}$, i = 1, 2 are chosen such that the polynomials

$$\lambda^2 + h_{i,1}\lambda + h_{i,2} = 0$$
, for $i = 1, 2$ (2.59)

are Hurwitz. The output feedback control is

$$\mu \dot{u} = -KF_s, \quad KF_s = \begin{bmatrix} M_{\sigma_1} \operatorname{sat}(\hat{\sigma}_1/M_{\sigma_1}) + x_1 \\ -M_{\sigma_2} \operatorname{sat}(\hat{\sigma}_2/M_{\sigma_2}) - x_2 \end{bmatrix}$$

where the levels of saturation, M_{σ_1} and M_{σ_2} are chosen such that the saturations will not be activated in the range of state feedback control.

For the simulation, the parameters are given by

$$\mu = 0.02, \ \varepsilon = 0.0002, \ h_{i,1} = 3, \ h_{i,2} = 1$$
 (2.60)

for i = 1, 2. In Fig. 2.4, the states x_1 and x_2 (solid lines) and their estimates \hat{x}_1 and \hat{x}_2 (dotted lines), respectively are plotted. The initial conditions of trajectories are given by $x(0) = [2, 4]^T$, $u(0) = [0, 0]^T$, the estimates $\hat{x}_1(0) = 0$ and $\hat{x}_2(0) = 0$, and $\hat{\sigma}_1(0) = 0$ and

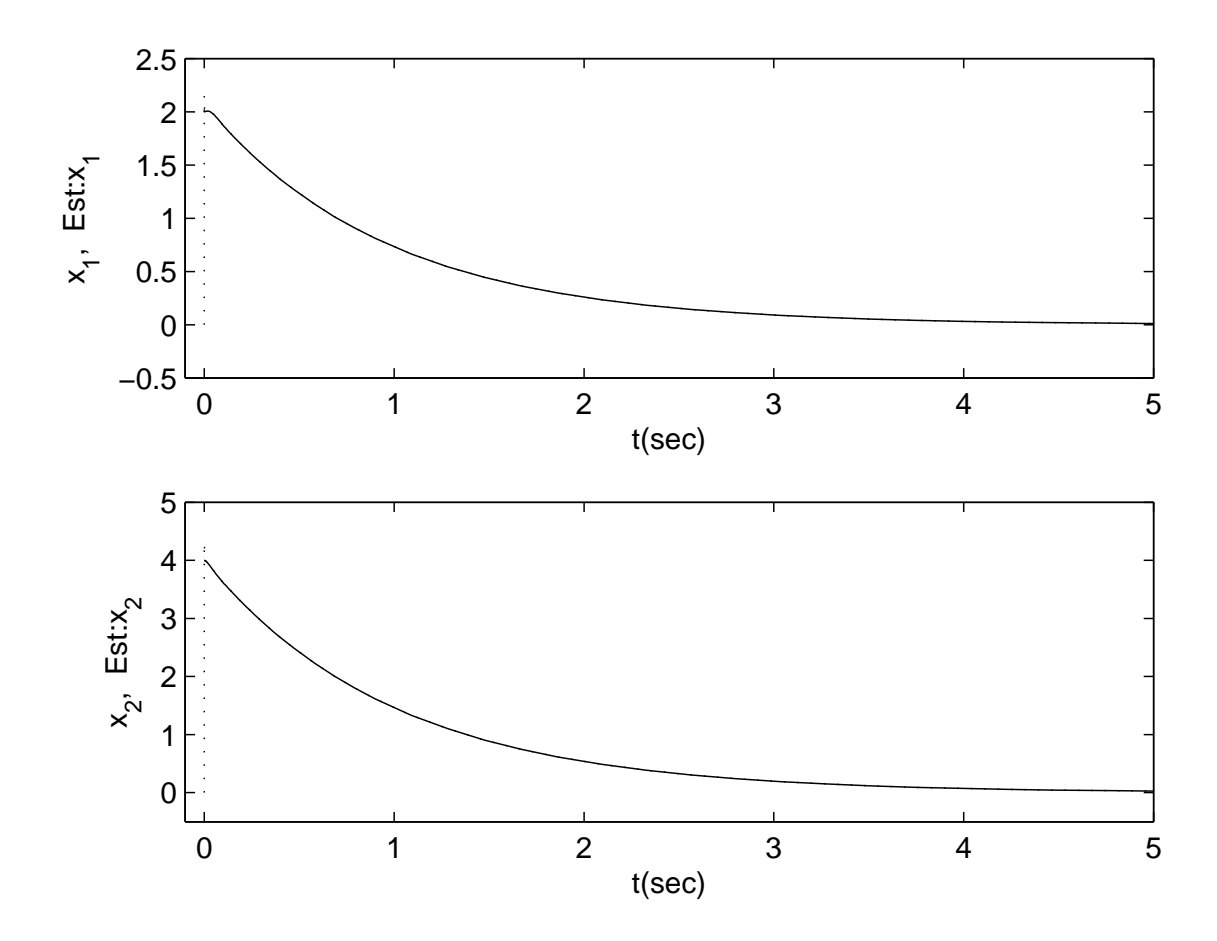


Figure 2.4: The solid and dotted lines represent the system states x_1 and x_2 , and estimates \hat{x}_1 and \hat{x}_2 , respectively.

 $\hat{\sigma}_2(0) = 0$. In Fig. 2.4, the estimate trajectories quickly converge into the system states and both the states and estimates are indistinguishable. The results shown in Fig. 2.5, indicate the EHGO successfully estimates the uncertainties (i.e., the entire terms in the right-hand side of (2.54)) in a short period of time. At beginning of the simulations in Fig. 2.5, the peaking phenomena are shown and quickly disappear, which are overcome by the use of saturation functions. To illustrate the performances recovery for inputs, we choose the same rate of $(\varepsilon/\mu) = 0.01$ with different values $\mu = 0.2$ and $\mu = 0.02$. The other parameters in the EHGO are the same as in (2.60). In Fig. 2.6, the input $u_r = R_m^{-1} x$ is solid lines, the dashed lines represents the inputs under the output feedback with parameters $\mu = 0.02$ and $\varepsilon/\mu = 0.01$, and the dotted lines are trajectories for the input under the output feedback

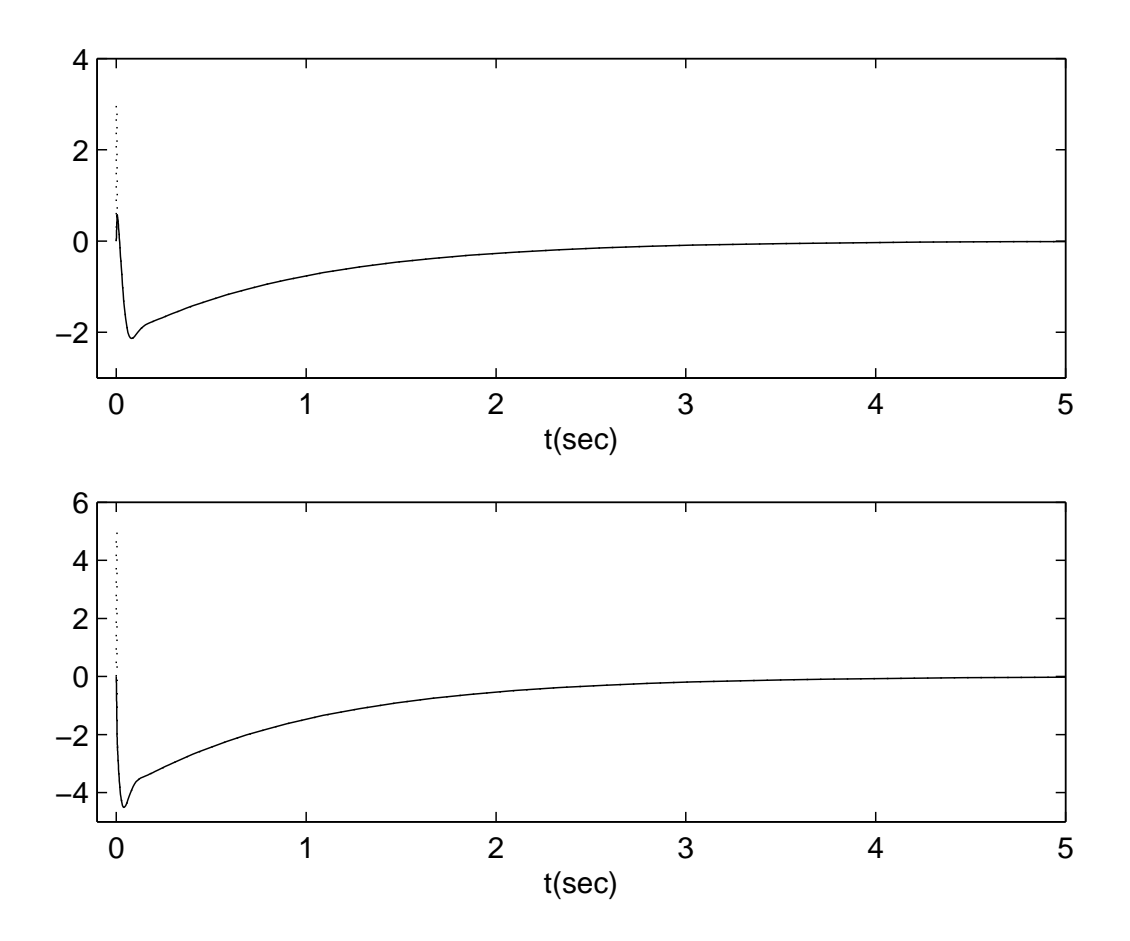


Figure 2.5: The solid and dotted lines represent the system states \dot{x}_1 and \dot{x}_2 , and estimates $\hat{\sigma}_1$ and $\hat{\sigma}_2$, respectively.

with parameters $\mu = 0.2$ and $\varepsilon/\mu = 0.01$. The input u with the control parameters $\mu = 0.02$ and $\varepsilon/\mu = 0.01$, has an faster convergence into u_r than the input with control parameters $\mu = 0.2$ and $\varepsilon/\mu = 0.01$.

2.6 Conclusions

Unmeasured states, uncertainties, and nonaffine inputs pose challenges in control design for nonlinear systems. An output feedback control design was proposed to address these challenges. The unmeasured states and uncertainties were estimated using an EHGO and sector conditions were utilized for dynamic inversion to deal with nonaffine and uncertain

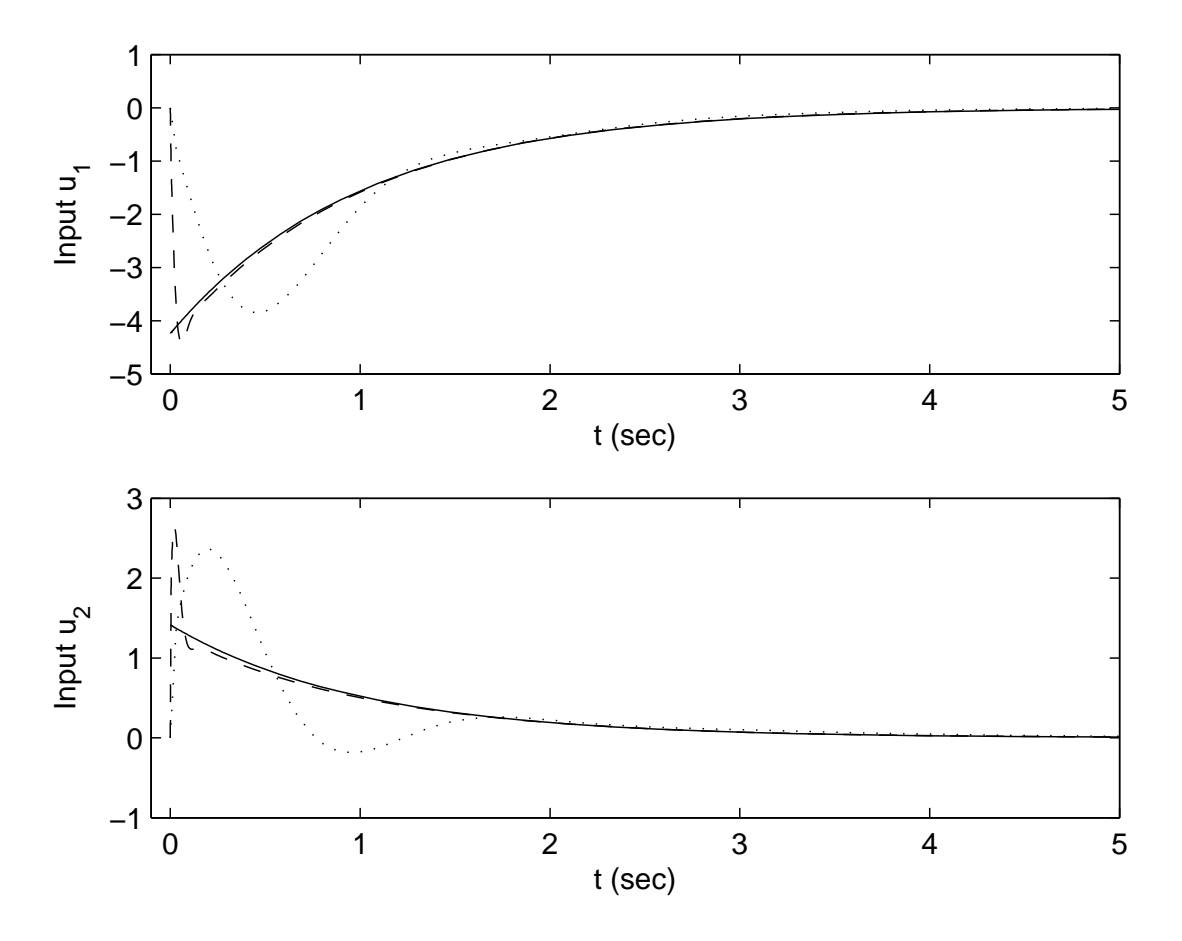


Figure 2.6: The solid, dashed, and dotted lines represent the inputs $u_r = R_m^{-1} x$, u with $\mu = 0.02$ and $\varepsilon/\mu = 0.01$, and u with $\mu = 0.2$ and $\varepsilon/\mu = 0.01$, respectively.

inputs. The EHGO and the dynamic inversion together result in exponential convergence of the states to those of a target system. The stability and performance of the system were analyzed using singular perturbation methods and the effectiveness of the proposed controller was verified through numerical simulations. Our future work will consider extension of our approach to non-minimum phase systems.

Chapter 3

Output Feedback Stabilization of Inverted Pendulum on a Cart in the Presence of Uncertainties

3.1 Introduction

An inverted pendulum on a cart is a classical example of an underactuated mechanical system and its stabilization problem has been investigated by many researchers. Based on linearized system dynamics, controllers can be designed to stabilize the equilibrium but the size of the region of attraction is typically small. Furthermore, these controllers are not very effective in the presence of significant uncertainties in the system model. In this chapter we present an output feedback control design that can stabilize the equilibrium in the presence of significant uncertainties and provide a large region of attraction.

One representative approach for stabilization of the inverted pendulum on a cart is based on the energy of the system. Spong and Praly [62] used partial feedback linearization to linearize the cart dynamics followed by transfer of energy from the cart to the pendulum. A stabilizing controller is invoked when the configuration of the system reaches a neighbour-

hood of the equilibrium. Astrom and Furuta [6] used a Lyapunov function based on the potential energy of the pendulum, and Lozano et al. [46] stabilized the pendulum around its homoclinic orbit prior to stabilization. Fradkov [22] developed a control method using an energy-based objective function and the speed-gradient, and Shiriaev et al. [61] proposed a modified controller using the idea of variable structure systems. Muralidharan et al. [50] designed a controller for the two-wheeled inverted pendulum using the interconnection and damping-passivity-based control (IDA-PBC) method proposed by Ortega et al. [55] for underactuated systems. Sarras et al. [59] combined the approach of the Immersion & Invariance proposed by Astolfi et al [5] with the Hamiltonian formulation to accommodate underactuation degree greater than one. Bloch et al. [12], [11] used the controlled Lagrangian approach to derive a desired closed-loop system dynamics for stabilization. The controller is designed by matching the dynamic equations for the uncontrolled and controlled Lagrangians. In [12], only the kinetic energy was shaped to obtain the desired dynamics whereas both kinetic and potential energies were shaped in [11]. Angeli [4] developed a smooth feedback law for almost-global stabilization based on the energy-shaping control strategy in [12]. Auckly [8] derived a stabilizing controller by solving a set of linear partial differential equations; these equations were obtained by matching the desired closed-loop system dynamics based on the potential energy with the original dynamics.

Among other approaches, Mazenc et al. [49] and Teel [66] developed control methods based on the concept of interconnected systems. In [49], the stability analysis was carried out using a Lyapunov function whereas in [66] a nonlinear small gain theorem was used. Olfati-Saber [54] proposed a transformation to convert the system into cascade normal form, for which existing control methods can be used for stabilization. A two-time-scale approach was proposed by Getz et al. [26] and Srinivasan et al. [63]. In [26], the trajectories of the pendulum were rapidly converged to a reference trajectory and the reference trajectory was slowly varied to converge the cart to its desired position. In [63], low gains were used near the equilibrium for separation of time scales. All of the methods discussed above require

exact knowledge of the system dynamics and are unlikely to guarantee stabilization in the presence of significant uncertainties.

To deal with uncertainties of the system model, Ravichandran et al. [57] used a two-time-scale approach together with Lyapunov redesign. However, the transient behavior of the fast system was not analyzed. Park et al. [56] utilized two sliding surfaces for the pendulum and cart subsystems to stabilize the system in the presence of disturbances but uncertainties in system parameters were not considered. Adhikary et al. [2] used backstepping and sliding mode control to the normal form of the system. Both uncertainties and disturbances were considered but they were introduced after the system was converted into normal form. Xu et al. [68] used integral sliding-mode control [15] to deal with uncertainties in the two-wheeled mobile inverted pendulum but the size of the region of attraction of the equilibrium is small since the controller is designed based on the linearized system dynamics.

In this chapter we present an output feedback controller to stabilize the inverted pendulum on a cart in the presence of significant uncertainties. Extended High-Gain Observers and dynamic inversion are combined together with a multi-time-scale structure to deal with model uncertainties. The stability analysis for the multi-time-scale structure is carried out using singular perturbation methods; the advantage of this approach is that the behavior of the system can be analyzed independently for each time scale. The multi-time-scale structure of the controller effectively provides a large region of attraction and this is illustrated through simulations. Output feedback control of the inverted pendulum on a cart has not been proposed earlier and it is shown here that it can recover the performance of the system under state feedback.

The chapter is organized as follows. In section 3.2, a state feedback controller is designed using a two-time-scale structure; uncertainties are not considered. In section 3.3, the output feedback controller is designed in the presence of uncertainties. Simulation and experimental results are presented in section 3.4 and conclusions are provided in section 3.5.

3.2 Stabilization in the Absence of Uncertainties

We present a control strategy to stabilize the desired equilibrium of the inverted pendulum on a cart system, in the absence of uncertainties. The controller is based on the designs proposed by [25] and [63]; here we cast the closed-loop system dynamics in two-time scale format for the purpose of stability analysis. The stability analysis is done by transforming the system into a standard singularly perturbed one.

Remark 3. As an intermediate step for the output feedback controller in Section 3.3, we design a controller in this section in the absence of uncertainties.

3.2.1 Dynamics of an inverted pendulum on a cart

The dynamics of an inverted pendulum on a cart are given by

$$\begin{bmatrix} m_p + m_c & \ell m_p \cos \alpha \\ \ell m_p \cos \alpha & \ell^2 m_p \end{bmatrix} \begin{bmatrix} \ddot{x} \\ \ddot{\alpha} \end{bmatrix} = \begin{bmatrix} \ell m_p \dot{\alpha}^2 \sin \alpha \\ g \ell m_p \sin \alpha \end{bmatrix} + \begin{bmatrix} F \\ 0 \end{bmatrix}$$
(3.1)

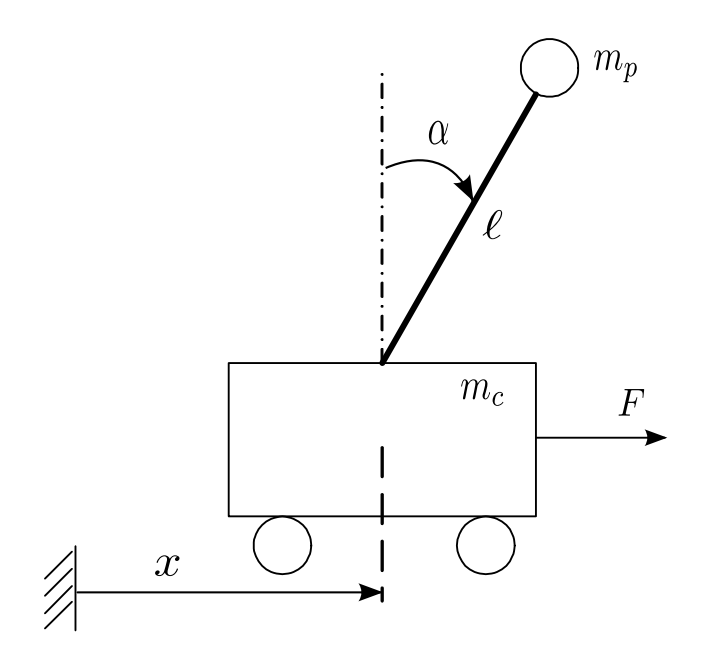


Figure 3.1: Inverted pendulum on a cart

where m_p , m_c are masses of the pendulum and the cart, respectively; g is the acceleration due to gravity; and ℓ is the length of the pendulum - see Fig. 3.1. The variables x and α denote the position of the cart and the angular displacement of the pendulum, respectively; α is measured clockwise from the vertical following the notation in [25]. The variable F denotes the force applied on the cart and is the control input. With the choice of state variables

$$x_1 = x$$
, $x_2 = \dot{x}$, $\alpha_1 = \alpha$, $\alpha_2 = \dot{\alpha}$

the system equations of (3.1) take the form

$$\dot{x}_1 = x_2, \ \dot{x}_2 = f_x(\alpha_1, \alpha_2, F), \ \dot{\alpha}_1 = \alpha_2, \ \dot{\alpha}_2 = f_\alpha(\alpha_1, \alpha_2, F)$$
 (3.2)

where

$$f_{x} = \frac{1}{(m_{p} + m_{c} - m_{p} \cos^{2} \alpha_{1})} F + G_{x}$$

$$f_{\alpha} = \frac{-\cos \alpha_{1}}{\ell(m_{p} + m_{c} - m_{p} \cos^{2} \alpha_{1})} F + G_{\alpha}$$

$$G_{x} = \frac{(\ell m_{p} \alpha_{2}^{2} \sin \alpha_{1} - m_{p} g \cos \alpha_{1} \sin \alpha_{1})}{(m_{p} + m_{c} - m_{p} \cos^{2} \alpha_{1})}$$

$$G_{\alpha} = \left(\frac{g}{\ell}\right) \sin \alpha_{1} - \frac{\cos \alpha_{1}}{\ell} G_{x}$$

$$(3.3)$$

We consider equations in (3.2) over the domain $x = [x_1, x_2]^T \in D_x$ and $\alpha = [\alpha_1, \alpha_2]^T \in D_\alpha$ where $D_x = \{-a_{x_1} < x_1 < a_{x_1}\} \times \{-a_{x_2} < x_2 < a_{x_2}\} \subset \mathbf{R}^2$ and $D_\alpha = \{-a_{\alpha_1} < \alpha_1 < a_{\alpha_1}\} \times \{-a_{\alpha_2} < \alpha_2 < a_{\alpha_2}\} \subset \mathbf{R}^2$ are bounded. The constants, a_{x_1} , a_{x_2} , a_{α_1} , and a_{α_2} are positive numbers and $a_{\alpha_1} < \pi/2$.

3.2.2 Control Design

The choice of the control input

$$F = (m_c + m_p - m_p \cos^2 \alpha_1)(u - G_x)$$
(3.4)

with

$$u = g \tan \alpha_1 - \left(\frac{\ell}{\cos \alpha_1}\right) \nu_d \tag{3.5}$$

results in

$$\dot{x}_1 = x_2$$

$$\dot{x}_2 = g \tan \alpha_1 - \left(\frac{\ell}{\cos \alpha_1}\right) \nu_d$$
(3.6)

$$\dot{\alpha}_1 = \alpha_2$$

$$\dot{\alpha}_2 = \nu_d$$
(3.7)

We choose

$$\nu_d = -\beta_1(\alpha_1 - \alpha_r) - \beta_2 \alpha_2 \tag{3.8}$$

where α_r is a reference trajectory for α_1 , which will be chosen using the concept of equilibrium manifold [25].

The desired dynamics of the x-subsystem is

$$\dot{x}_1 = x_2$$

$$\dot{x}_2 = v_{ext} - \left(\frac{\ell}{\cos \alpha_1}\right) \nu_d \tag{3.9}$$

where v_{ext} is chosen as

$$v_{ext} = -\gamma_1 x_1 - \gamma_2 x_2 (3.10)$$

and $(\ell/\cos\alpha_1)\nu_d$ is considered to be a vanishing perturbation. By comparing the actual x-subsystem in (3.6) with the desired x-subsystem in (3.9), the desired reference trajectory for α_r can be determined as follows

$$g \tan \alpha_r = v_{ext} \iff \alpha_r = \tan^{-1} \left(\frac{v_{ext}}{g} \right)$$
 (3.11)

The control input ν_d in (3.8) can now be designed as follows:

$$\nu_d = -\beta_1 \left[\alpha_1 - \tan^{-1} \left(\frac{v_{ext}}{g} \right) \right] - \beta_2 \alpha_2 \tag{3.12}$$

3.2.3 Closed-loop system

Using (3.4), (3.5), and (3.8), the closed-loop system dynamics can be represented as

$$\dot{x}_1 = x_2
\dot{x}_2 = g \tan \alpha_1 + \left(\frac{\ell}{\cos \alpha_1}\right) \left[\beta_2 \alpha_2 + \beta_1 (\alpha_1 - \alpha_r)\right]
\dot{\alpha}_1 = \alpha_2
\dot{\alpha}_2 = -\beta_2 \alpha_2 - \beta_1 (\alpha_1 - \alpha_r)$$
(3.13)

The above system is comprised of two subsystems: the cart dynamics described by states x_1 and x_2 , and the pendulum dynamics described by states α_1 and α_2 . Through proper choice of β_1 and β_2 , we can ensure that α_1 converges to α_r quickly and α_2 converges to 0. Then,

the cart dynamics is described by

$$\dot{x}_1 = x_2$$

$$\dot{x}_2 = g \tan \alpha_r = v_{ext} = -\gamma_1 x_1 - \gamma_2 x_2$$
(3.14)

which guarantees asymptotic stability of the origin $(x, \dot{x}) = (0, 0)$.

3.2.4 Analysis using singular perturbations

To make the cart dynamics slower than the pendulum dynamics, we choose low gains for the cart controller: $\gamma_1 = \varepsilon_1^2 k_1$ and $\gamma_2 = \varepsilon_1 k_2$, where ε_1 is a small positive parameter and positive constants k_1 and k_2 are independent of ε_1 . We note that instead of using the low gains in the cart controller, high gains can be used in the pendulum controller. However, the use of high gains results in peaking in the slow dynamics. The change of variables

$$y = [y_1, y_2]^T, \quad y_1 = \varepsilon_1^2 x_1, \quad y_2 = \varepsilon_1 x_2$$
 (3.15)

$$\theta = [\theta_1, \theta_2]^T, \quad \theta_1 = \alpha_1 - \alpha_r, \quad \theta_2 = \alpha_2 \tag{3.16}$$

transforms the system (3.13) into the singularly perturbed form

$$\dot{y}_{1} = \varepsilon_{1} y_{2}$$

$$\dot{y}_{2} = \varepsilon_{1} [-k_{1} y_{1} - k_{2} y_{2} + h_{x}(\theta, \alpha_{r})]$$

$$\dot{\theta}_{1} = \theta_{2} + \varepsilon_{1} h_{\alpha}(y, \theta, \alpha_{r}, F)$$

$$\dot{\theta}_{2} = -\beta_{1} \theta_{1} - \beta_{2} \theta_{2}$$

$$(3.17)$$

where h_x and h_α are given by the expressions

$$h_{x} = g \left[\tan(\theta_{1} + \alpha_{r}) - \tan \alpha_{r} \right]$$

$$+ \left[\frac{\ell}{\cos(\theta_{1} + \alpha_{r})} \right] (\beta_{1}\theta_{1} + \beta_{2}\theta_{2}),$$

$$h_{\alpha} = \left[\frac{g}{g^{2} + (-k_{1}y_{1} - k_{2}y_{2})^{2}} \right] (k_{1}y_{2} + k_{2}f_{x})$$
(3.18)

and f_x is defined in (3.3), except that α_1 should now be replaced by $(\theta_1 + \alpha_r)$ in accordance with (3.15). We note that h_x and h_α are bounded by constants independent of ε_1 for all $\varepsilon_1 \ll 1$ over the domains D_x and D_α . The boundary layer system is obtained by setting $\varepsilon_1 = 0$ in (3.17):

$$\dot{\theta} = A_{\theta}\theta, \quad A_{\theta} = \begin{bmatrix} 0 & 1 \\ -\beta_1 & -\beta_2 \end{bmatrix}$$
(3.19)

where β_1 and β_2 are chosen such that A_{θ} is Hurwitz. The reduced system is obtained by setting $\varepsilon_1 = 0$:

$$\dot{y} = \varepsilon_1 A_y y, \quad A_y = \begin{bmatrix} 0 & 1 \\ -k_1 & -k_2 \end{bmatrix}$$
(3.20)

where k_1 and k_2 are chosen such that A_y is Hurwitz. The two time-scale structure of the system is depicted in Fig. 3.2.

It follows from Theorem 11.4 of [33] that there exists a positive constant ε_1^* such that for $\varepsilon_1 \in (0, \varepsilon_1^*)$ the origin of the closed-loop system (3.17) is exponentially stable.

The design of β_1 and β_2 should ensure that α_1 stays in the set $|\alpha_1| < a_{\alpha_1}$ where $a_{\alpha_1} < \pi/2$. Since $\theta_1 = \alpha_1 - \alpha_r = \alpha_1 - \tan^{-1}(v_{ext}/g)$, by choosing ε_1 small enough we can constrain θ_1 to the set $|\theta_1| \le b_{\theta_1}$ with $b_{\theta_1} < \pi/2$. The initial state $\theta(0)$ belongs to a compact set $\{|\theta_1| \le a_{\theta_1}, |\theta_2| \le a_{\theta_2}\}$ where $a_{\theta_1} < \pi/2$ and a_{θ_2} is some positive constant. We are going to design β_1 and β_2 to obtain a Lyapunov function V_{θ} for the system:

$$\dot{\theta}_1 = \theta_2, \quad \dot{\theta}_2 = -\beta_1 \theta_1 - \beta_2 \theta_2$$

such that the compact set $\{V_{\theta} \leq c_{\theta}\}$ contains the set $\{|\theta_{1}| \leq a_{\theta_{1}}, |\theta_{2}| \leq a_{\theta_{2}}\}$ and is contained in the strip $|\theta_{1}| \leq b_{\theta_{1}}$ with $a_{\theta_{1}} < b_{\theta_{1}} < \pi/2$. By showing that \dot{V}_{θ} is negative definite we ensure that the set $\{V_{\theta} \leq c_{\theta}\}$ is positively invariant and all trajectories starting in $\{|\theta_{1}| \leq a_{\theta_{1}}, |\theta_{2}| \leq a_{\theta_{2}}\}$ stay in the strip $|\theta_{1}| \leq b_{\theta_{1}}$ for all $t \geq 0$. The gains β_{1} and β_{2} are taken as $\beta_{1} = (\beta_{c1}/\mu)$ and $\beta_{2} = (\beta_{c2}/\mu)$ with positive constants β_{c1} and β_{c2} , and a small positive constant μ . The Lyapunov function is taken as

$$V_{\theta} = \tilde{\theta}^T P_{\alpha} \tilde{\theta}, \quad \tilde{\theta} = \begin{bmatrix} \theta_1 \\ \left(\frac{\beta_1}{\beta_2}\right) \theta_1 + \theta_2 \end{bmatrix}, \quad P_{\alpha} = \begin{bmatrix} \frac{1}{2} & 0 \\ 0 & \frac{d}{2} \end{bmatrix}$$
(3.21)

By choosing $c_{\theta} < \frac{1}{2}b_{\theta_1}^2$ we have

$$V_{\theta} \le c_{\theta} \Rightarrow \frac{1}{2}\theta_1^2 \le c_{\theta} < \frac{1}{2}b_{\theta_1}^2 \Rightarrow |\theta_1| < b_{\theta_1}$$

Over the set $\{|\theta_1| \le a_{\theta_1}, |\theta_2| \le a_{\theta_2}\},\$

$$V_{\theta} \le \frac{1}{2}a_{\theta_1}^2 + \frac{d}{2}\left[\left(\frac{\beta_1}{\beta_2}\right)a_{\theta_1} + a_{\theta_2}\right]^2$$

Therefore by choosing

$$d < \frac{(2c_{\theta} - a_{\theta_1}^2)}{[(\beta_1/\beta_2)a_{\theta_1} + a_{\theta_2}]^2}$$

we ensure that $\{|\theta_1| \leq a_{\theta_1}, |\theta_2| \leq a_{\theta_2}\} \subset \{V_{\theta} \leq c_{\theta}\}$. As in standard analysis of singularly perturbed systems (Theorem 2.1 of Chapter 7.2 of [36]), the derivative \dot{V}_{θ} will be negative

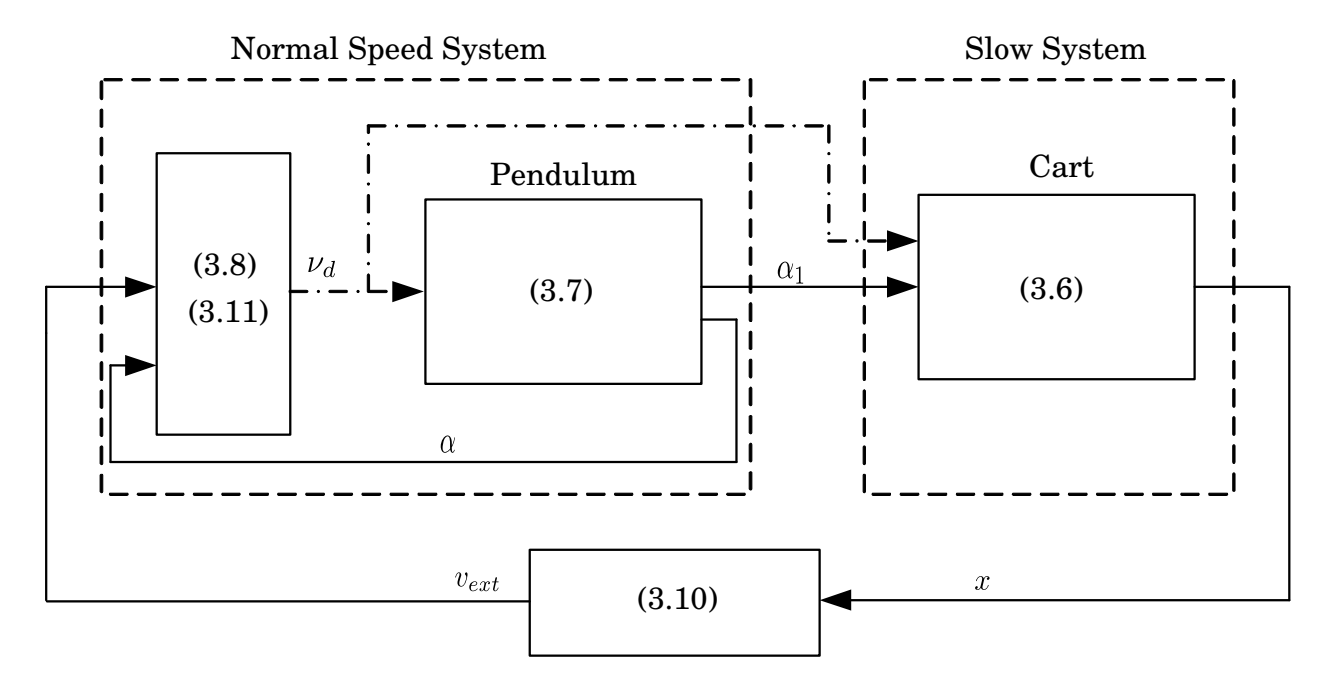


Figure 3.2: The two-time-scale structure of the inverted pendulum on a cart system

definite by choosing μ sufficiently small.

3.3 Stabilization in the Presence of Uncertainties

In the presence of parameter uncertainties, f_x and f_α of (3.2) are unknown. We however note that the following conditions (the sign of the input coefficients in (3.3)) hold in D_x and D_α :

$$sign(c_x) > 0, \ c_x = \frac{1}{m_p + m_c - m_p \cos^2 \alpha_1}$$

$$sign(c_\alpha) > 0, \ c_\alpha = \frac{c_x \cos \alpha_1}{\ell}$$
(3.22)

Extended High-Gain Observers will be used to estimate the uncertain terms in f_x and f_α in addition to the states; and dynamic inversion will be used to compute the inputs F and u, described by (3.4) and (3.5), using the estimates of f_x and f_α .

3.3.1 Dynamic inversion

With the knowledge of the sign of the input coefficients, as shown in (3.22), we use a dynamic inversion scheme which is different from ones in [25], [29], and [28], in order to compute the control inputs F and u. The proposed dynamic inversion scheme in the chapter is an extension in our earlier work [42] since our earlier work dealt with SISO systems. In particular, had f_x and f_α been known, we could have used

$$\varepsilon_2 \begin{bmatrix} \dot{F} \\ \dot{u} \end{bmatrix} = \begin{bmatrix} -f_x + u \\ f_\alpha - \nu_d \end{bmatrix}$$
 (3.23)

to solve for F and u, starting from arbitrary initial conditions. In the above equation, ε_2 is a small positive number; its relationship with ε_1 will be discussed later. As $\varepsilon_2 \to 0$ and the stability of (3.23) is guaranteed, $f_x \approx u$ and $f_\alpha \approx \nu_d$. The equation (3.23) is a singularly perturbed system of the form

$$\varepsilon_{2} \begin{bmatrix} \dot{F} \\ \dot{u} \end{bmatrix} = A_{z} \begin{bmatrix} F \\ u \end{bmatrix} + \begin{bmatrix} G_{x} \\ G_{\alpha} - \nu_{d} \end{bmatrix}, \ A_{z} = \begin{bmatrix} -c_{x} & 1 \\ -c_{\alpha} & 0 \end{bmatrix}$$
(3.24)

whose quasi-steady-state solution is given by (3.4) and (3.5). Since the foregoing equation is linear in F and u and the matrix A_z with frozen x and α is Hurwitz, it can be seen that for sufficiently small ε_2 , F and u converge fast to their values that satisfy (3.4) and (3.5). The stability analysis for the system in (3.24) will be discussed in Section 3.3.

Remark 4. The dynamic inversion scheme used in this section is different from ones in [25], [29], and [28].

• In [25] and [28], the dynamic inversion schemes were developed by the Jacobian with respect to inputs whereas the proposed one in the chapter is based on the stability of the fast dynamics in (3.24), which only requires the knowledge on the signs of inputs.

- In [25], the stability analysis for the dynamic inversion is limited to a local neighborhood of the equilibrium, whereas our stability analysis is based on Lyapunov functions, which covers a larger domain than one in [25].
- In [29], the dynamic inversion is only for SISO systems whereas our dynamic inversion scheme is able to deal with MIMO systems since the dynamic inversion has the inputs F and u in (3.24).

3.3.2 Extended High-Gain Observers (EHGOs)

Now, we assume that velocity and acceleration terms, x_2 , α_2 , $\sigma_x(x,\alpha,u)$, and $\sigma_\alpha(x,\alpha,u)$, which are used in the dynamic inversion, are unknown. EHGOs are designed to estimate the acceleration and velocity terms. The EHGOs for the cart and pendulum systems are designed as

$$\dot{\hat{x}}_{1} = \hat{x}_{2} + \left(\frac{h_{11}}{\varepsilon_{3}}\right) (x_{1} - \hat{x}_{1})$$

$$\dot{\hat{x}}_{2} = \bar{f}_{x}(\hat{\alpha}_{1}, \hat{\alpha}_{2}, F) + \hat{\sigma}_{x} + \left(\frac{h_{12}}{\varepsilon_{3}^{2}}\right) (x_{1} - \hat{x}_{1})$$

$$\dot{\hat{\sigma}}_{x} = \left(\frac{h_{13}}{\varepsilon_{3}^{3}}\right) (x_{1} - \hat{x}_{1})$$

$$\dot{\hat{\alpha}}_{1} = \hat{\alpha}_{2} + \left(\frac{h_{21}}{\varepsilon_{3}}\right) (\alpha_{1} - \hat{\alpha}_{1})$$

$$\dot{\hat{\alpha}}_{2} = \bar{f}_{\alpha}(\hat{\alpha}_{1}, \hat{\alpha}_{2}, F) + \hat{\sigma}_{\alpha} + \left(\frac{h_{22}}{\varepsilon_{3}^{2}}\right) (\alpha_{1} - \hat{\alpha}_{1})$$

$$\dot{\hat{\sigma}}_{\alpha} = \left(\frac{h_{23}}{\varepsilon_{3}^{3}}\right) (\alpha_{1} - \hat{\alpha}_{1})$$
(3.25)

where \bar{f}_x and \bar{f}_α are the nominal values of f_x and f_α in (3.3); $\hat{\sigma}_x$ and $\hat{\sigma}_\alpha$ denote the estimates of σ_x and σ_α , which are the uncertainties in the values of f_x and f_α , respectively, i.e. $f_x = \bar{f}_x + \sigma_x$ and $f_\alpha = \bar{f}_\alpha + \sigma_\alpha$. The constants h_{ij} for i = 1, 2 and j = 1, 2, 3 are chosen such that the

following polynomials

$$s^3 + h_{i1}s^2 + h_{i2}s + h_{i3}$$
, for $i = 1, 2$

are Hurwitz and ε_3 is a small positive number.

Remark 5. The parameters ε_1 , ε_2 and ε_3 should satisfy $\varepsilon_1 \ll 1$, $\varepsilon_2 \ll 1$, and $(\varepsilon_3/\varepsilon_2) \ll 1$. This requirement can be intuitively explained as follows. Since the EHGOs' estimates $\hat{\sigma}_x$ and $\hat{\sigma}_{\alpha}$ are used in dynamic inversion, the observer dynamics should be faster than the dynamic inversion algorithm; hence, $(\varepsilon_3/\varepsilon_2) \ll 1$. Since the dynamic inversion computes u and F, which are used to implement the controller, it's dynamics should be faster than the dynamics of the closed-loop system with no uncertainty (3.13); hence $\varepsilon_2 \ll 1$. Since the x-dynamics is much slower than the α -dynamics, $\varepsilon_1 \ll 1$.

3.3.3 Output feedback control

Using the dynamic inversions together with the EHGOs, the output feedback control is

$$\varepsilon_{2} \begin{bmatrix} \dot{F} \\ \dot{u} \end{bmatrix} = \begin{bmatrix} -\bar{f}_{x} \left(\alpha_{1}, M_{\theta} \operatorname{sat} \left(\frac{\hat{\alpha}_{2}}{M_{\theta}} \right), F \right) - M_{x} \operatorname{sat} \left(\frac{\hat{\sigma}_{x}}{M_{x}} \right) + u \\ \bar{f}_{\alpha} \left(\alpha_{1}, M_{\theta} \operatorname{sat} \left(\frac{\hat{\alpha}_{2}}{M_{\theta}} \right), F \right) + M_{\alpha} \operatorname{sat} \left(\frac{\hat{\sigma}_{\alpha}}{M_{\alpha}} \right) - \hat{\nu}_{d} \end{bmatrix}$$

$$(3.26)$$

where

$$\hat{\nu}_{d} = -\beta_{1}(\alpha_{1} - \hat{\alpha}_{r}) - \beta_{2}M_{\theta}\operatorname{sat}\left(\frac{\hat{\alpha}_{2}}{M_{\theta}}\right),$$

$$\hat{\alpha}_{r} = \tan^{-1}\left(\frac{\hat{v}_{ext}}{g}\right),$$

$$\hat{v}_{ext} = -\gamma_{1}x_{1} - \gamma_{2}\hat{x}_{2}$$

$$(3.27)$$

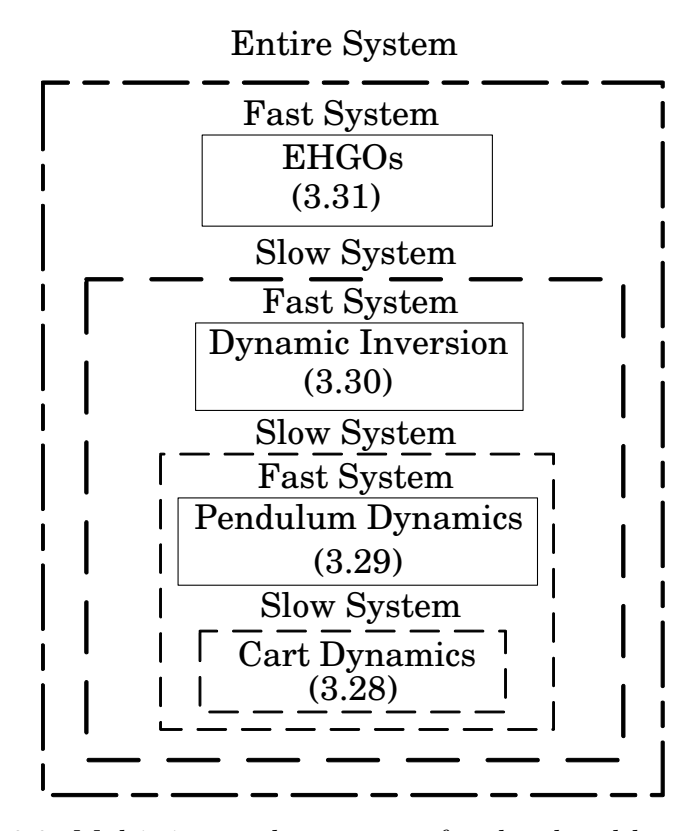


Figure 3.3: Multi-time-scale structure for the closed-loop system

To protect the system from peaking, the saturation function $sat(\cdot)$

$$\operatorname{sat}(e) = \begin{cases} e, & \text{if } |e| \le 1\\ \operatorname{sign}(e), & \text{if } |e| > 1 \end{cases}$$

is used. The saturation limits M_x , M_{α} , and M_{θ} are determined such that the saturation functions will not be invoked under state feedback.

3.3.4 Stability analysis in the presence of uncertainties

The closed-loop system is represented in the singularly perturbed form

$$\dot{y}_1 = \varepsilon_1 y_2
\dot{y}_2 = \varepsilon_1 f_x \left(\theta_1 + \alpha_r, \theta_2, F \right)$$
(3.28)

$$\dot{\theta}_1 = \theta_2 + \varepsilon_1 h_\alpha(y, \theta, \alpha_r, F)
\dot{\theta}_2 = f_\alpha (\theta_1 + \alpha_r, \theta_2, F)$$
(3.29)

$$\varepsilon_2 \dot{z} = A_z z + \psi(\cdot) - \varepsilon_2 \phi(\cdot) \tag{3.30}$$

$$\varepsilon_3 \dot{\eta} = A_\eta \eta + \varepsilon_3 \left[\bar{B}_1 \Delta_1 + \bar{B}_2 \Delta_2 + \left(\frac{1}{\varepsilon_2} \right) \bar{B}_2 \Delta_3 \right]$$
 (3.31)

where A_{η} , \bar{B}_1 and \bar{B}_2 are given in Appendix and $z=[z_F,z_u]^T$ with

$$z_F = F - F^*, \quad z_u = u - u^*$$

With the variables F^* and u^* , the conditions $f_x(\theta_1 + \alpha_r, \theta_2, F^*) - u^* = 0$ and $f_\alpha(\theta_1 + \alpha_r, \theta_2, F^*) - \nu_d = 0$ in (3.23) hold, and $\psi(\cdot) = 0$ when $\eta = 0$, and $\phi(\cdot)$ is bounded uniformly in ε_2 . The fast variables $\eta = [\eta_x, \eta_\alpha]^T$, $\eta_x = [\eta_{x_1}, \eta_{x_2}, \eta_{x_3}]^T$ and $\eta_\alpha = [\eta_{\alpha_1}, \eta_{\alpha_2}, \eta_{\alpha_3}]^T$ are defined by

$$\eta_{x_1} = \frac{x_1 - \hat{x}_1}{\varepsilon_3^2}, \ \eta_{x_2} = \frac{x_2 - \hat{x}_2}{\varepsilon_3},$$

$$\eta_{x_3} = \sigma_x(\theta_1 + \alpha_r, \theta_2, F) - \hat{\sigma}_x$$

$$\eta_{\alpha_1} = \frac{\alpha_1 - \hat{\alpha}_1}{\varepsilon_3^2}, \ \eta_{\alpha_2} = \frac{\alpha_2 - \hat{\alpha}_2}{\varepsilon_3},$$

$$\eta_{\alpha_3} = \sigma_\alpha(\theta_1 + \alpha_r, \theta_2, F) - \hat{\sigma}_\alpha,$$

We note that f_x and f_α of (3.28) and (3.29) are bounded uniformly in ε_2 and ε_3 .

The stability analysis for the each subsystem will be done by starting from the fastest one, i.e. the error dynamics of the two EHGOs (3.31) to the slowest one, i.e. the cart dynamics (3.28). The singularly perturbed system can be viewed as a two-time-scale structure if the error dynamics of the two EHGOs (3.31) are the fast subsystem, while other subsystems (3.28), (3.29), (3.30) are the slow one as depicted in Fig.3.3. The boundary layer system,

which is obtained by setting $\varepsilon_3 = 0$ in (3.31),

$$\varepsilon_3 \left(\frac{d\eta}{dt} \right) = A_\eta \eta$$

is exponentially stable. We note that in the error dynamics of the EHGOs, the matrix A_{η} is Hurwitz, and Δ_1 , Δ_2 , and Δ_3 and the constant matrix \bar{B}_1 , \bar{B}_2 , and \bar{B}_3 are uniformly bounded in ε_3 whose definitions are given in the Appendix.

Next, the dynamic inversion (3.30) is slow relative to the EHGOs and fast relative to the systems (3.28) and (3.29) as depicted in Fig.3.3. Setting $\varepsilon_3 = 0$ and $\eta = 0$, which yields

$$x = \hat{x}, \ \alpha = \hat{\alpha}, \ f_x = \bar{f}_x + \hat{\sigma}_x, \ f_\alpha = \bar{f}_\alpha + \hat{\sigma}_\alpha,$$

results in the boundary layer system

$$\varepsilon_2 \dot{z} = A_z z + \begin{bmatrix} -f_x(\theta_1 + \alpha_r, \theta_2, F^*) + u^* \\ f_\alpha(\theta_1 + \alpha_r, \theta_2, F^*) - \nu_d \end{bmatrix} - \varepsilon_2 \begin{bmatrix} \dot{F}^* \\ \dot{u}^* \end{bmatrix}$$

with

$$f_x(\theta_1 + \alpha_r, \theta_2, F^*) = c_x F^* + G_x,$$

$$f_\alpha(\theta_1 + \alpha_r, \theta_2, F^*) = -c_\alpha F^* + G_\alpha$$

Since $f_x(\theta_1 + \alpha_r, \theta_2, F^*) - u^* = 0$ and $f_\alpha(\theta_1 + \alpha_r, \theta_2, F^*) - \nu_d = 0$ with the inputs F^* and u^* , we have

$$\varepsilon_2 \dot{z} = A_z z - \varepsilon_2 \begin{bmatrix} \dot{F}^* \\ \dot{u}^* \end{bmatrix}$$

Setting $\varepsilon_2 = 0$ yields exponential stability of z = 0.

After the EHGOs and dynamic inversion reach quasi-steady state, hierarchically, i.e.,

$$\varepsilon_3 = 0, \ \eta = 0, \ \varepsilon_2 = 0, \ z = 0$$

we have the reduced system for the inverted pendulum on a cart which is the same as the system in (3.17). The reduced system also has a time-scale structure and its stability analysis is given in Section 3.2.4.

Typically, a slow variable in a multi-time-scale structure is assumed to be constant although it is evolving slowly. We consider the behavior of the slow variable and define sets for stability analysis of our multi-time-scale structure using Lyapunov functions. Lyapunov functions for three of the four subsystems are defined by; $V_y = y^T P_y y$, $V_z = z^T P_z z$, and $V_{\eta} = \eta^T P_{\eta} \eta$, where P_y , P_z , and P_{η} are solutions of Lyapunov equations with right-hand sides equal to the negative identity matrix. The Lyapunov function V_{θ} is defined in (3.21). The fastest variable η converges quickly into the set $\{V_{\eta} \leq \rho(\varepsilon_3/\varepsilon_2)^2\}$ with a positive constant ρ , while the variables y, θ , and z move relatively slowly. We define a set $(y, \theta, z) \in \{V_y \le a_1\} \times \{V_\theta \le a_1\}$ a_2 \times $\{V_z \leq a_3\}$ with positive constants a_1 , a_2 , and a_3 . Although a short convergence time period $T_1(\varepsilon_3)$ exists for the fastest variable η , the trajectories of variables y, θ , and zcan leave the set $\{V_y \leq a_1\} \times \{V_\theta \leq a_2\} \times \{V_z \leq a_3\}$. Therefore, we define the superset $\{V_y \le b_1\} \times \{V_\theta \le b_2\} \times \{V_z \le b_3\}$, where b_i , $(b_i > a_i)$ can be arbitrarily close to a_i , i = 1, 2, 3, (for a sufficiently small ε_3) that satisfies the condition for the constrained domain for θ . After the variable η converges into the set $\{V_{\eta} \leq \rho(\varepsilon_3/\varepsilon_2)^2\}$, we consider the time period $T_2(\varepsilon_2)$ for convergence of the second fastest variable z. During the time period $T_2(\varepsilon_2)$, the trajectories of y and θ can leave the set $\{V_y \leq b_1\} \times \{V_\theta \leq b_2\}$. To guarantee that the condition for the constrained domain for θ is satisfied during both time periods $T_1(\varepsilon_3)$ and $T_2(\varepsilon_2)$, we define the superset $(y, \theta) \in \{V_y \leq A_1\} \times \{V_\theta \leq A_2\}$ where $A_i \ (A_i > b_i)$ can be arbitrarily close to b_i , i = 1, 2, (for a sufficiently small ε_2).

The main result of this chapter is presented next with the help of the following theorem.

Theorem 2. Let X_1 be any compact set of (x, α) in the domain $D_x \times D_\alpha$, X_2 any compact subset of \mathbb{R}^2 , and X_3 any compact subset of \mathbb{R}^6 . There exists ε^* such that for all

$$\varepsilon_1 < \varepsilon^*, \ \varepsilon_2 < \varepsilon^*, \ \frac{\varepsilon_3}{\varepsilon_2} < \varepsilon^*, \ \varepsilon_3 < \varepsilon^*$$

and for all initial states $(x(0), \alpha(0)) \in X_1$, $(F(0), u(0)) \in X_2$, and $(\hat{x}(0), \hat{\alpha}(0)) \in X_3$, the closed-loop system (3.28) - (3.31) has an exponentially stable equilibrium point, at which x = 0 and $\alpha = 0$, and the set $X_1 \times X_2 \times X_3$ is a subset of the region of attraction.

Proof. It is shown in the Appendix that the closed-loop system (3.28) - (3.31) can be written as

$$\dot{y} = \varepsilon_1 \left[A_y y + B \left(h_x(\theta, \alpha_r) + c_x z_F \right) \right] \tag{3.32}$$

$$\dot{\theta} = A_{\theta}\theta + \varepsilon_1 E h_{\alpha}(y, \theta, \alpha_r, F) - B c_{\alpha} z_F \tag{3.33}$$

$$\varepsilon_2 \dot{z} = A_z z + \psi(\cdot) - \varepsilon_2 \phi(\cdot) \tag{3.34}$$

$$\varepsilon_3 \dot{\eta} = A_\eta \eta + \varepsilon_3 \left[\bar{B}_1 \Delta_1 + \bar{B}_2 \Delta_2 + \left(\frac{1}{\varepsilon_2} \right) \bar{B}_2 \Delta_3 \right]$$
 (3.35)

For the first part of the proof, all trajectories starting from $(x(0), \alpha(0), F(0), u(0)) \in X_1 \times X_2$, will converge into the desired equilibrium while α_1 satisfies the condition for the constrained domain. We are going to show that all trajectories converge to a positive invariant set $\{V_y \leq d_1\} \times \{V_\theta \leq (\varepsilon_\theta^*)^2 d_2\} \times \{V_z \leq (\varepsilon_z^*)^2 c_3\} \times \{V_\eta \leq (\varepsilon_3/\varepsilon_2)^2 \rho\}$ with the positive constants $d_1, d_2, c_3, \rho, \varepsilon_\theta^* = \max\{\varepsilon_1, \varepsilon_z^*\}$, and $\varepsilon_z^* = \max\{\varepsilon_2, (\varepsilon_3/\varepsilon_2)\}$. Note that it is shown that in section 3.2.4, the condition for the constrained domain for α_1 with sufficiently small $\varepsilon_1 > 0$, is satisfied even though change of variables is used. We are going to use the following hierarchical, repeated process

• First, we are going to prove that a subset $\{V_z \leq b_3\} \times \{V_\eta \leq (\varepsilon_3/\varepsilon_2)^2 \rho\}$ of $\{V_y \leq b_1\} \times \{V_\theta \leq b_2\} \times \{V_z \leq b_3\} \times \{V_\eta \leq (\varepsilon_3/\varepsilon_2)^2 \rho\}$ is positively invariant by properly choosing ρ .

while the variable η is viewed as fast and the other variables y, θ , and z are considered as slow. The time period $T_1(\varepsilon_3)$ for η to converge into the set $\{V_{\eta} \leq (\varepsilon_3/\varepsilon_2)^2 \rho\}$, can be arbitrarily small as $\varepsilon_3 \to 0$.

- Second, it will be shown that the subset $\{V_{\theta} \leq c_2\} \times \{V_z \leq (\varepsilon_z^*)^2 c_3\} \times \{V_{\eta} \leq (\varepsilon_3/\varepsilon_2)^2 \rho\}$ of $\{V_y \leq c_1\} \times \{V_{\theta} \leq c_2\} \times \{V_z \leq (\varepsilon_z^*)^2 c_3\} \times \{V_{\eta} \leq (\varepsilon_3/\varepsilon_2)^2 \rho\}$ with $b_1 < c_1 < A_1$ and $b_2 < c_2 < A_2$ is positively invariant by properly choosing c_3 . In this stage, the variable η is already in the set $\{V_{\eta} \leq (\varepsilon_3/\varepsilon_2)^2 \rho\}$ and the variable z converges rapidly into the set $\{V_z \leq (\varepsilon_z^*)^2 c_3\}$ with the convergence time period $T_2(\varepsilon_2)$. The time $T_2(\varepsilon_2)$ can be arbitrarily small as $\varepsilon_2 \to 0$.
- Lastly, it will be claimed that the set of $\{V_y \leq d_1\} \times \{V_\theta \leq (\varepsilon_\theta^*)^2 d_2\} \times \{V_z \leq (\varepsilon_z^*)^2 c_3\} \times \{V_\eta \leq (\varepsilon_3/\varepsilon_2)^2 \rho\}$ with $c_1 < d_1 < A_1$ is positively invariant by properly choosing d_2 . In this stage, the variables z and η are in the set $\{V_z \leq (\varepsilon_z^*)^2 c_3\} \times \{V_\eta \leq (\varepsilon_3/\varepsilon_2)^2 \rho\}$ and the fast variable θ converges into $\{V_\theta \leq (\varepsilon_\theta^*)^2 d_2\}$.

In this proof, we are going to show only the first bullet out of three since proofs for the others are the same as the first bullet. There is an upper bound $\|\eta\| \leq (\varepsilon_3/\varepsilon_2)\sqrt{\rho/\lambda_{\min}(P_{\eta})}$, where symbols $\lambda_{\max}(N)$ and $\lambda_{\min}(N)$ are used to denote maximum and minimum eigenvalues of a matrix N, respectively, and the variables y and θ are in a compact set. The derivative of V_z along the trajectory (3.34) is

$$\dot{V}_{z} \leq -\left(\frac{1}{\varepsilon_{2}}\right) \|z\|^{2} + \left(\frac{2}{\varepsilon_{2}}\right) P_{z_{m}} k_{\psi} \|\eta\| \|z\|
+2P_{z_{m}} \left[k_{\phi_{1}} \|y\| + k_{\phi_{2}} \|\theta\| + k_{\phi_{3}} \|z\|\right] \|z\| \leq -\frac{a_{z}}{2\varepsilon_{2}} \|z\|^{2}
\text{for } \|z\| \geq \varepsilon_{z}^{*} \left(\frac{4P_{z_{m}}}{a_{z}}\right) k_{z_{b}}$$
(3.36)

for all $(y, \theta, z, \eta) \in \{V_y \leq b_1\} \times \{V_\theta \leq b_2\} \times \{V_z = b_3\} \times \{V_\eta \leq (\varepsilon_3/\varepsilon_2)^2 \rho\}$, where $a_z = 1 - 2\varepsilon_2 k_{\phi_1} P_{z_m}$, $P_{z_m} = \lambda_{\max}(P_z)$, and the positive constants k_{z_b} , k_{ψ} , k_{ϕ_1} , k_{ϕ_2} , and k_{ϕ_3} are

independent of ε_z^* . The derivative of V_{η} along the trajectory (3.35) is

$$\dot{V}_{\eta} \leq -\frac{1}{\varepsilon_{3}} \|\eta\|^{2} + 2P_{\eta_{m}} \Big[(k_{\eta_{1}} \|y\| + k_{\eta_{2}} \|\theta\| + k_{\eta_{3}} \|z\|) + \left(\frac{1}{\varepsilon_{2}}\right) (k_{\eta_{4}} \|z\| + k_{\eta_{5}} \|\eta\|) + k_{\eta_{6}} \|\eta\| \Big] \|\eta\|$$

$$\dot{V}_{\eta} \le -\frac{a_{\eta}}{2\varepsilon_3} \|\eta\|^2, \quad \text{for } |\eta| \ge \left(\frac{\varepsilon_3}{\varepsilon_2}\right) \left(\frac{4P_{\eta_m}}{a_{\eta}}\right) b_{\eta}$$
 (3.37)

for all $(y, \theta, z, \eta) \in \{V_y \leq b_1\} \times \{V_\theta \leq b_2\} \times \{V_z \leq (\varepsilon_z^*)^2 b_3\} \times \{V_\eta = \rho(\varepsilon_3/\varepsilon_2)^2\}$, where $a_\eta = 1 - 2P_{\eta_m} \left[(\varepsilon_3/\varepsilon_2) k_{\eta_5} + \varepsilon_3 k_{\eta_6} \right]$, $P_{\eta_m} = \lambda_{\max}(P_\eta)$, and the positive constants b_η and k_{η_1} to k_{η_6} are independent of $(\varepsilon_3/\varepsilon_2)$. By choosing $\rho = 16P_{\eta_m}^3 (b_\eta/a_\eta)^2$ and using (3.36) and (3.37), we conclude that the set $\{V_z \leq b_3\} \times \{V_\eta \leq (\varepsilon_3/\varepsilon_2)^2 \rho\}$ is positively invariant.

Now, it will be shown that for sufficiently small ε_3 , trajectories starting from $(F, u) \in X_2$ and $(\hat{x}, \hat{\alpha}) \in X_3$ enter the corresponding the invariant set of $\{V_z \leq b_3\} \times \{V_\eta \rho(\varepsilon_3/\varepsilon_2)^2\}$ in the finite time $T_1(\varepsilon_3)$, where $\lim_{\varepsilon_3 \to 0} T_1(\varepsilon_3) = 0$. There exists the error bound $\|\eta(0)\| \leq k_t/\varepsilon_3^2$ with a non-negative constant k_t . Due to the continuity and boundedness of \dot{y} , $\dot{\theta}$, and \dot{z} , we have

$$||y(t)-y(0)|| \le k_f t$$
, $||\theta(t)-\theta(0)|| \le k_f t$, $||z(t)-z(0)|| \le k_f t$

with the constant $k_f > 0$. Instead of computing the time T_n when the trajectory η enters into the set $\{V_{\eta} \leq \rho(\varepsilon_3/\varepsilon_2)^2\}$, we will find the longer time T_1 than T_n to ensure that the trajectory enters the set in a finite time. Using the bound for the initial condition of η and the property of exponential stable Lyapunov function V_{η} in (3.37), we have

$$V_{\eta} \le \left(\frac{\sigma_2}{\varepsilon_3^4}\right) \exp(-\sigma_1 t/\varepsilon_3)$$

where $\sigma_1 = a_{\eta}/(2P_{\eta_m})$ and $\sigma_2 = P_{\eta_m}k_t^2$. Due to $\varepsilon_3 < (\varepsilon_3/\varepsilon_2)$, we obtain

$$\varepsilon_3^2 \rho = \left(\frac{\sigma_2}{\varepsilon_3^4}\right) \exp(-\sigma_1 T_1/\varepsilon_3)$$

The bound for the time $T_1(\varepsilon_3) \in (0, T_0]$ is obtained

$$T_1(\varepsilon_3) = \left(\frac{\varepsilon_3}{\sigma_1}\right) \ln\left(\frac{\sigma_2}{\rho_4 \varepsilon_3^6}\right) \le \frac{1}{2} T_0$$

As $\varepsilon_3 \to 0$, $T_1(\varepsilon_3) \to 0$.

As the second part of the proof, we are going to show that the closed-loop system (3.28) - (3.31) has an exponentially stable equilibrium point, at which x = 0, $\alpha = 0$. Consider the derivative of the Lyapunov functions V_{θ} and V_z along the trajectories (3.33) and (3.34), respectively, are

$$\dot{V}_{\theta} \leq -k_{m} \|\theta\|^{2} + \left[\varepsilon_{1} k_{h_{1}} \|y\| + \varepsilon_{1} k_{h_{2}} \|\theta\| + (\varepsilon_{1} k_{h_{3}} + c_{\alpha_{m}}) \|z\| \right] \|\theta\|$$
(3.38)

$$\dot{V}_{y} \le \varepsilon_{1}[-\|y\|^{2} + 2k_{\theta}P_{y_{m}}\|\theta\|\|y\| + 2c_{x_{m}}P_{y_{m}}\|z\|\|y\|]$$
(3.39)

where $P_{y_m} = \lambda_{\max}(P_y)$, $||c_x|| \le c_{x_m}$, $||c_\alpha|| \le c_{\alpha_m}$ and the positive constants k_m , k_{h_1} , k_{h_2} , k_{h_3} , and k_{θ} are independent of ε_1 , ε_2 , ε_3 , and $(\varepsilon_3/\varepsilon_2)$.

By defining $W_y = \sqrt{V_y}$, $W_\theta = \sqrt{V_\theta}$, $W_z = \sqrt{V_z}$, and $W_\eta = \sqrt{V_\eta}$ and using (3.36), (3.37),

(3.38), and (3.39), we have

$$D^{+}W \leq -MW, \ W = [W_{y}, W_{\theta}, W_{z}, W_{\eta}]^{T}$$

$$M = \begin{bmatrix} \varepsilon_{1}k_{11} & -\varepsilon_{1}k_{12} & -\varepsilon_{1}k_{13} & 0\\ -\varepsilon_{1}k_{21} & (1 - \varepsilon_{1}k_{22})k_{22}^{*} & -(\varepsilon_{1}k_{23} + k_{23}^{*}) & 0\\ -k_{31} & -k_{32} & (\frac{k_{33}}{\varepsilon_{2}})(1 - \varepsilon_{2}k_{33}^{*}) - \frac{k_{34}}{\varepsilon_{2}}\\ -k_{41} & -k_{42} & -(k_{43} + \frac{k_{43}^{*}}{\varepsilon_{2}}) & k_{M} \end{bmatrix}$$

where $k_M = \frac{1}{\varepsilon_3} \left(1 - \varepsilon_3 k_{44} - \frac{\varepsilon_3}{\varepsilon_2} k_{44}^* \right)$ and $D^+W(\cdot)$ denotes the upper right-hand derivative, and k_{ij} and k_{ij}^* for $i,j=1,\ldots,4$ are positive constants independent of ε_1 , ε_2 , ε_3 , and $(\varepsilon_3/\varepsilon_2)$. Consider the differential equation $\dot{U} = -MU$ with $U = [U_y, U_\theta, U_z, U_\eta]^T$ and the same initial condition U(0) = W(0), whose origin is exponentially stable since the leading principal minors of the matrix M can be all positive (i.e., the matrix M can be Hurwitz) by choosing $\varepsilon_1 \ll 1$, $\varepsilon_2 \ll 1$, $\varepsilon_3 \ll 1$, and $\varepsilon_3/\varepsilon_2 \ll 1$ small enough. Using a vectorial comparison method in Chapter IX of [58], we conclude that $W \leq U$ for all $t \geq 0$. Therefore, the closed-loop system (3.28) - (3.31) has an exponentially stable equilibrium point, at which x = 0, $\alpha = 0$.

3.4 Simulation and Experiment

3.4.1 Simulation results

For simulations, the system parameters were assumed to be

$$m_c = 0.94 \text{ kg}, \quad m_p = 0.23 \text{ kg}$$

 $g = 9.8 \text{ m/s}^2, \quad \ell = 0.3206 \text{ m}$ (3.40)

The state feedback controller described by (3.4), (3.5), (3.10), and (3.12) was implemented using the following parameter values; The control parameters for the state feedback are

$$\gamma_1 = \varepsilon_1^2 k_1, \ \gamma_2 = \varepsilon_1 k_2, \ \beta_1 = 5, \ \beta_2 = 3$$
 (3.41)

where ε_1 , k_1 , and k_2 were chosen as

$$\varepsilon_1 = 0.2, \ k_1 = 2, \ k_2 = 1$$
 (3.42)

For the output feedback controller, we assume that the system dynamics is completely unknown except for the sign conditions in (3.22). The output feedback controller with dynamic inversion described by (3.25), (3.26), and (3.27) was implemented by setting $\bar{f}_x(\cdot) = 0$ and $\bar{f}_\alpha(\cdot) = 0$ in (3.25) and (3.26). The following parameter values were used

$$h_{i1} = 5, h_{i2} = 5, h_{i3} = 4, i = 1, 2$$

The parameters ε_1 and β_i , γ_i , i = 1, 2, are the same as those used in state feedback control - see (3.41) and (3.42). The saturation limits M_x , M_α , and M_θ are chosen to be slightly greater than the maximum absolute values of f_x , f_α , and α_2 , respectively, observed in state feedback control simulations.

For both state feedback and output feedback, the initial states $x_1(0)$, $x_2(0)$, $\alpha_1(0)$, and $\alpha_2(0)$ were chosen as

$$x_1(0) = 0 \text{ m}, \quad x_2(0) = 0 \text{ m/s},$$

 $\alpha_1(0) = 0.8727 \text{ rad } (50^\circ), \quad \alpha_2(0) = 0 \text{ rad/s}$

The initial conditions used for the dynamic inversion and the EHGOs were

$$F(0) = 0, \ u(0) = 0,$$

$$\hat{x}_1(0) = 0.1, \ \hat{x}_2(0) = 0.1, \ \hat{f}_x(0) = 0,$$

$$\hat{\alpha}_1(0) = 0.1, \ \hat{\alpha}_2(0) = 0.1, \ \hat{f}_{\alpha}(0) = 0$$

To investigate the performance of output feedback vis-a-vis state feedback, we simulate two cases with: $(\varepsilon_2, \varepsilon_3) = (0.02, 0.002)$ and $(\varepsilon_2, \varepsilon_3) = (0.01, 0.0001)$. The results are shown in Figs.3.4 and 3.5.

The plots of x_1 and x_2 are shown in Fig.3.4 and the plots of α_1 and α_2 are shown in Fig.3.5; these plots have different time horizons since the dynamics of x_1 and x_2 are slower than the dynamics of α_1 and α_2 . Both Figs.3.4 and 3.5 indicate that the states converge to the desired values and the output feedback controller is able to recover the performance of the state feedback controller when ε_2 and ε_3 are chosen small enough.

We present results from a second simulation where the initial configuration of the pendulum is almost horizontal with different initial conditions. The initial conditions were assumed to be

$$x_1(0) = 0$$
 m, $x_2(0) = -3$ m/s,
 $\alpha_1(0) = 1.3963$ rad (80°) , $\alpha_2(0) = \frac{\pi}{2}$ rad/s

The time-scale control parameters ε_1 , ε_2 , and ε_3 were chosen as $\varepsilon_1 = 0.05$, $\varepsilon_2 = 0.002$ and $\varepsilon_3 = 0.0001$, and the control parameters β_1 and β_2 were chosen as $\beta_1 = 15$, $\beta_2 = 10$. The remaining control parameters and initial conditions were chosen to be identical to the first simulation. The results, shown in Fig.3.6, indicate that the pendulum and the cart are both successfully stabilized to their desired configuration.

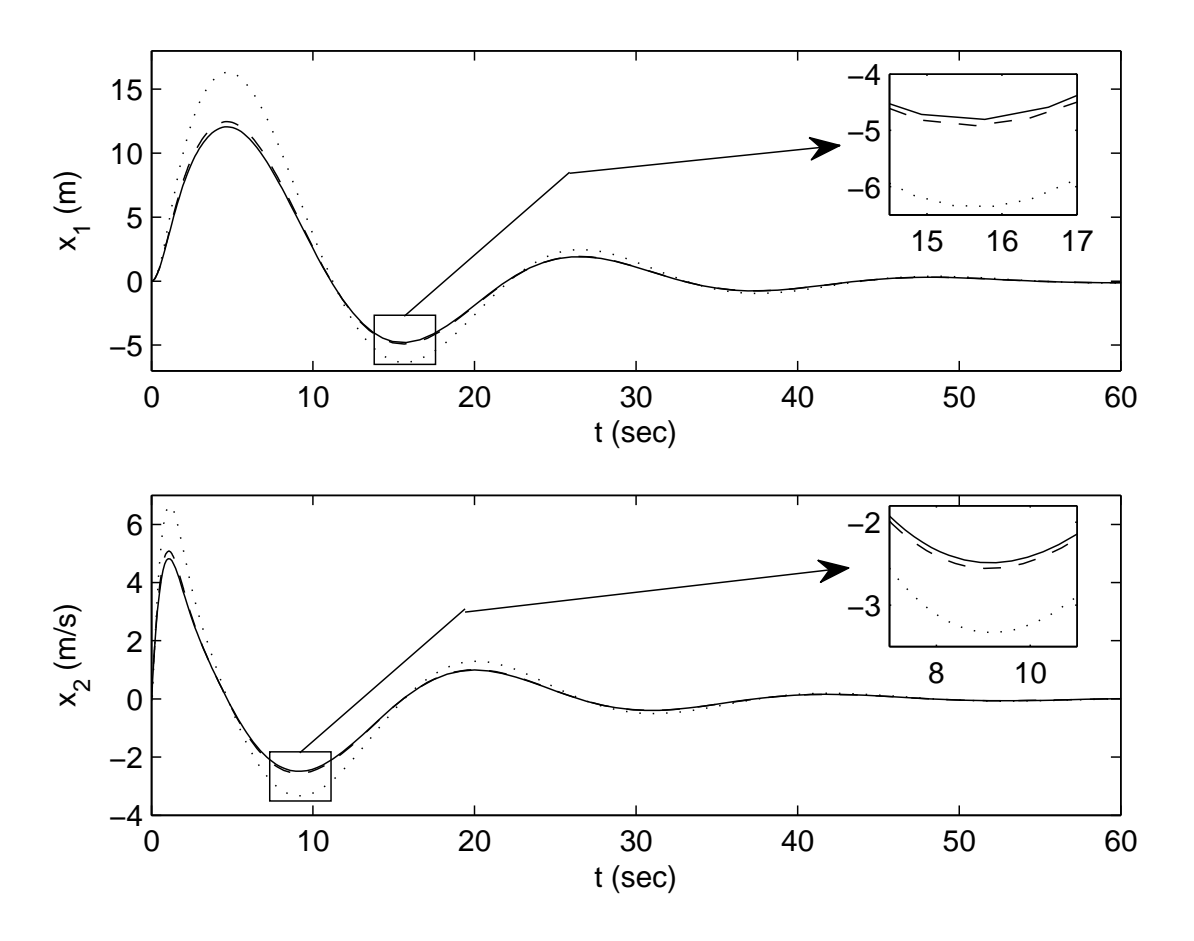


Figure 3.4: Trajectories of x_1 and x_2 for state feedback (solid line), output feedback with $(\varepsilon_2, \varepsilon_3) = (0.02, 0.002)$ (dotted line), and output feedback with $(\varepsilon_2, \varepsilon_3) = (0.01, 0.0001)$ (dashed line)

3.4.2 Experimental results

The experimental testbed for the inverted pendulum on a cart is shown in Fig.3.7. A 6V-DC motor with a planetary gearhead (reduction ratio 3.71:1) drives the cart on the racks. The angle of the pendulum and the position of the cart are measured by optical encoders that have a resolution of 1024 lines per revolution. The experimental hardware was interfaced with a dSPACE board and the output feedback controller was implemented in the Matlab/Simulink environment with a sampling interval of 0.0006 sec.

The dynamics of the inverted pendulum on a cart is described by (3.2) and (3.3) and the nominal parameter values are given by (3.40). The dynamic inversion based output feed-

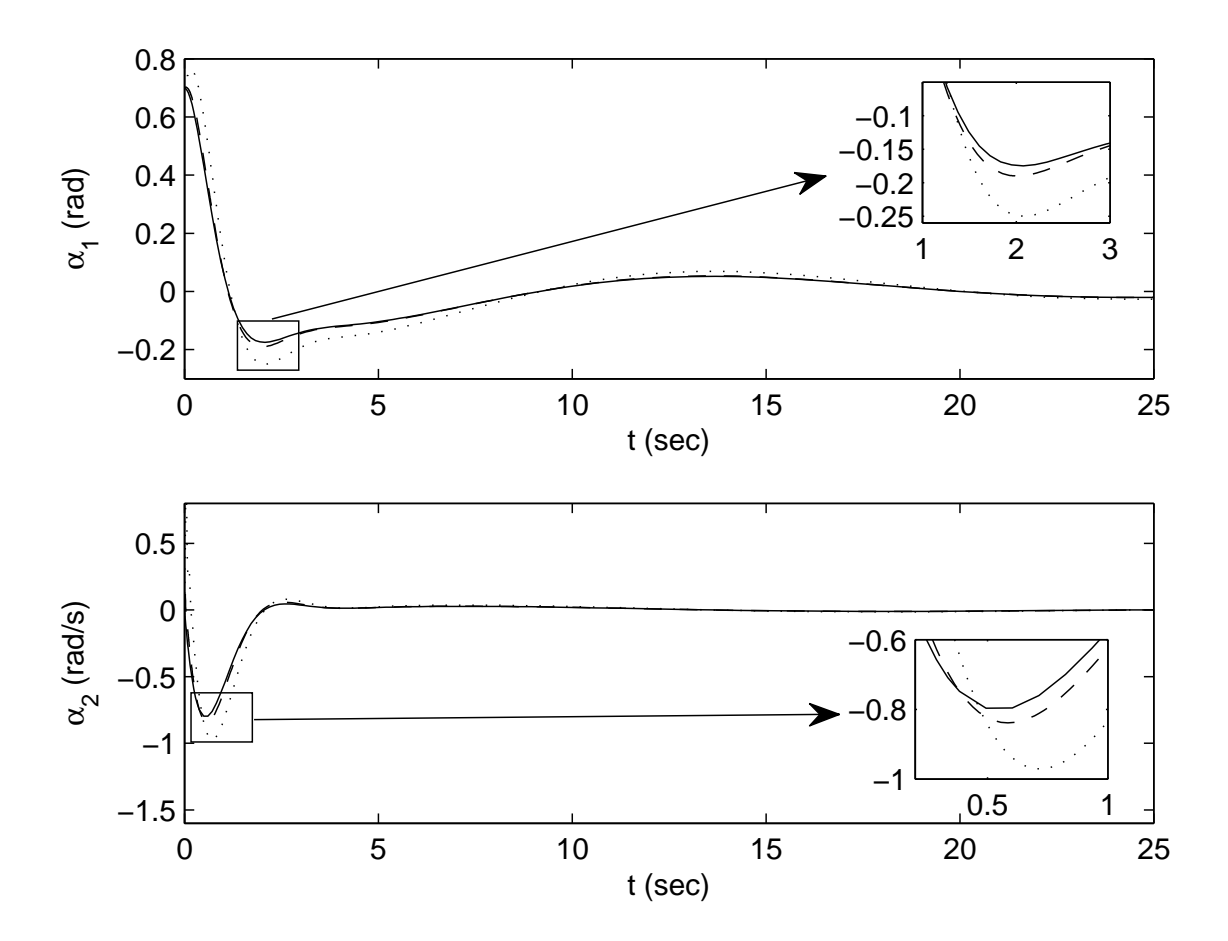


Figure 3.5: Trajectories of α_1 and α_2 for state feedback (solid line), output feedback with $(\varepsilon_2, \varepsilon_3) = (0.02, 0.002)$ (dotted line), and output feedback with $(\varepsilon_2, \varepsilon_3) = (0.01, 0.0001)$ (dashed line).

back controller described by (3.25), (3.26), and (3.27) was implemented using the following parameter values

$$k_1 = 9, \ k_2 = 5, \ \gamma_1 = \varepsilon_1^2 k_1, \ \gamma_2 = \varepsilon_1 k_2,$$

 $\beta_1 = 50, \ \beta_2 = 30,$
 $h_{i1} = 3, \ h_{i2} = 3, \ h_{i3} = 1, \ \text{for} \quad i = 1, 2$
 $\varepsilon_1 = 0.2, \ \varepsilon_2 = 0.01, \ \varepsilon_3 = 0.005$

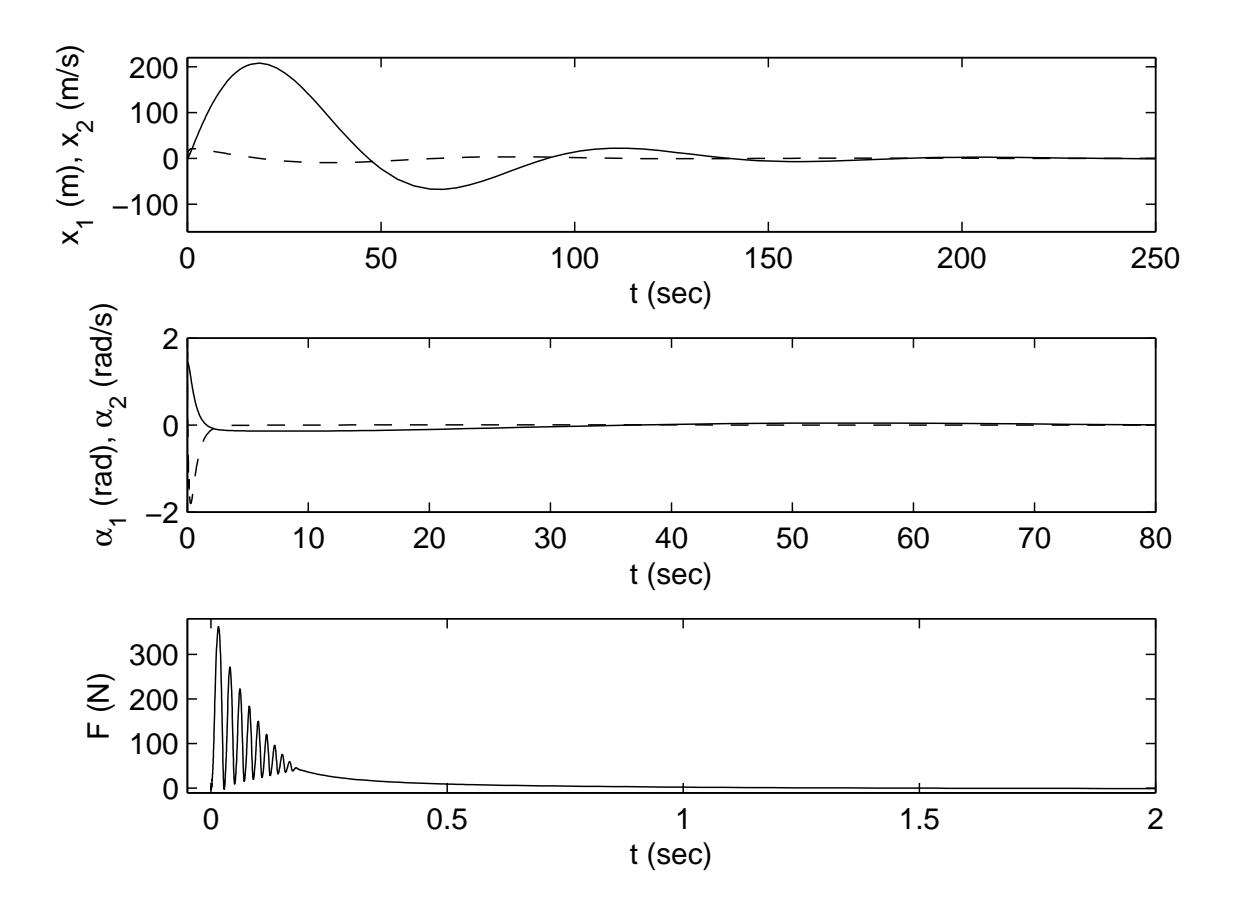


Figure 3.6: Trajectories of x_1 and α_1 (solid lines), and x_2 and α_2 (dashed lines) are shown in the top and middle subfigures. In the bottom subfigure, a trajectory of the input F in (3.26) is shown.

The initial conditions were chosen as follows

$$x_1(0) = -0.38 \text{ m}, \ x_2(0) = 0 \text{ m/sec},$$

 $\alpha_1(0) = 0.19 \text{ rad } (10.9^\circ), \ \alpha_2(0) = 0 \text{ rad/sec}$

The initial angle of the pendulum was chosen close to the upright configuration such that the cart position did not exceed the physical limit of the racks and the motor did not exceed its torque limit. To reduce the effect of measurement noise, the encoder signals were passed through low-pass filters of bandwidth 1000 Hz.

The experimental results are shown in Fig.3.8. Until around 0.5 sec, the pendulum on the

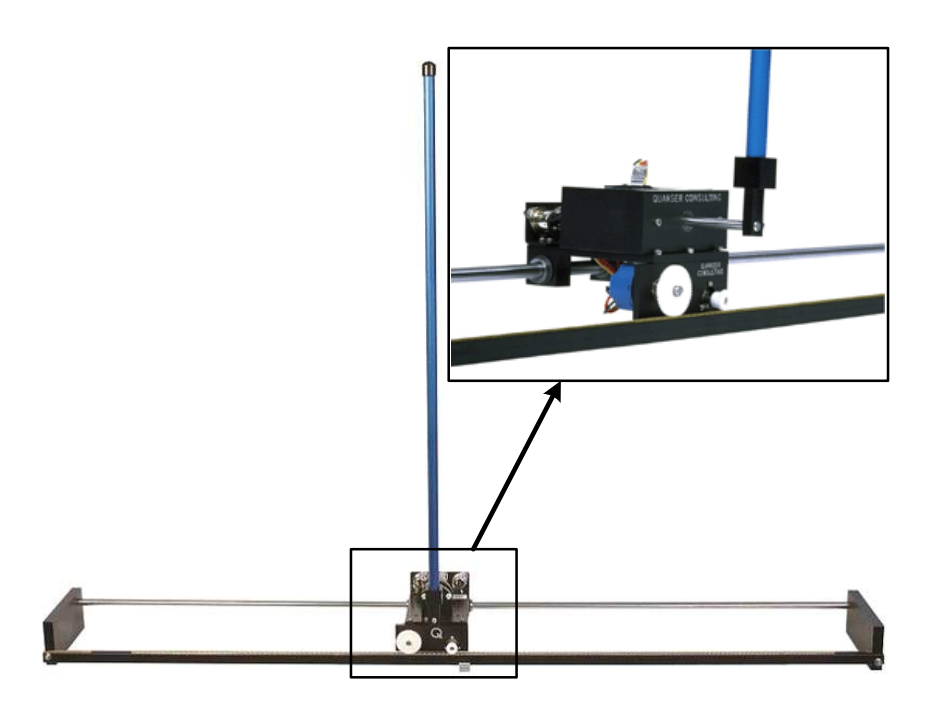


Figure 3.7: Experimental testbed for the inverted pendulum on a cart - a product of Quanser [1]

cart is held manually while the power switch is off. At around 0.5 sec, the power switch is turned on. The trajectories of x_1 and its estimate \hat{x}_1 , and α_1 and its estimate $\hat{\alpha}_1$, all converge to the origin.

Within an allowable operation range of the system, we compared experimentally results generated by our control algorithm with ones provided by an LQR controller and the control algorithm in [63]. The LQR controller is designed by following instructions in manufacturer manuals. The stabilization control scheme proposed by [63] was also implemented to check the effectiveness of estimates of uncertainties by the EHGOs. In Fig. 3.9, we show the ultimate boundedness results from system uncertainties, which could be due to friction between cart's pion and racks, mass of the cart and pendulum, etc. In Fig. 10, the effectiveness of fast estimates by the EHGOs with the dynamic inversion results in the appropriate control input F whereas the other two controllers use high gains to stabilize the system at the equilibrium in the presence of uncertainties.

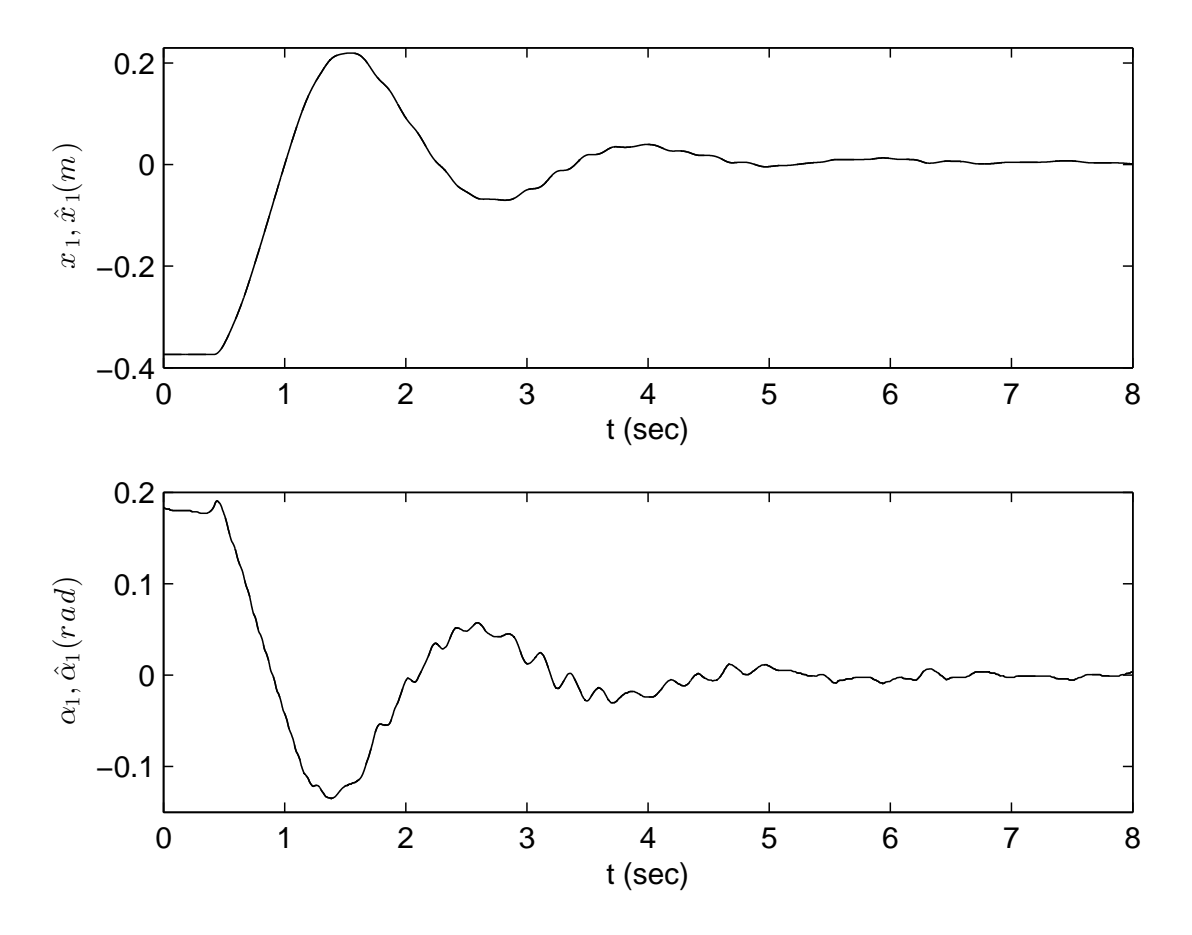


Figure 3.8: Trajectories of x_1 and its estimate \hat{x}_1 , and α_1 and its estimate $\hat{\alpha}_1$ are shown. The estimated values are indistinguishable from their true (measured) values.

3.5 Conclusion

An output feedback controller for stabilization of an inverted pendulum on a cart was presented. From a practical point of view, this is an important contribution since all states of the system are typically not accessible and uncertainties reside in the system. To estimate the unmeasured states and to compensate for the uncertain dynamics, Extended High-Gain Observers were used. To deal with uncertainties in the input coefficients, dynamic inversion was used. Both Extended High-Gain Observers and dynamic inversion introduce fast time scales and this required the controller to be designed using a multi-time-scale structure. The multi-time-scale structure is well-suited for control of underactuated systems, and for the

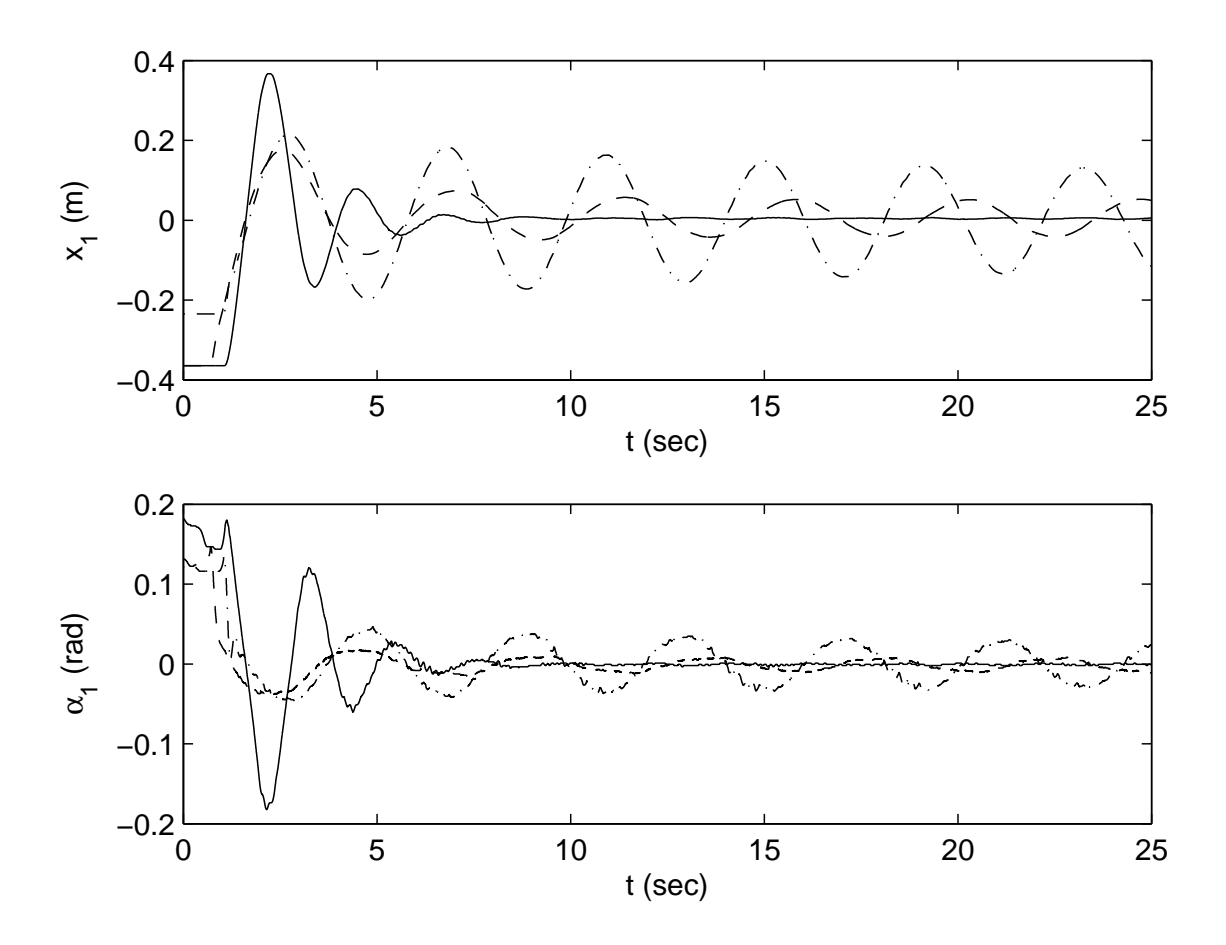


Figure 3.9: Trajectories of x_1 and α_1 are shown with different control schemes. Solid lines driven by our control scheme, converge into the origin. Dotted lines generated by a LQR controller, have ultimate boundedness. Dash-dot lines provided by the control algorithm in [63] have the biggest ultimate boundedness.

inverted pendulum on a cart, additional time scale separation was used to first converge the pendulum to a reference trajectory and then converge the cart to its desired configuration. Using singular perturbation methods, the stability of the closed-loop system was analyzed and exponential stability of the equilibrium was established. Numerical simulations were used to show that the output feedback controller recovers the performance of state feedback and to demonstrate a large region of attraction of the equilibrium. Experimental results were used to demonstrate the feasibility of practical implementation with uncertainties in system parameters. Our future work will focus on extending our approach to output feedback stabilization of other underactuated mechanical systems.

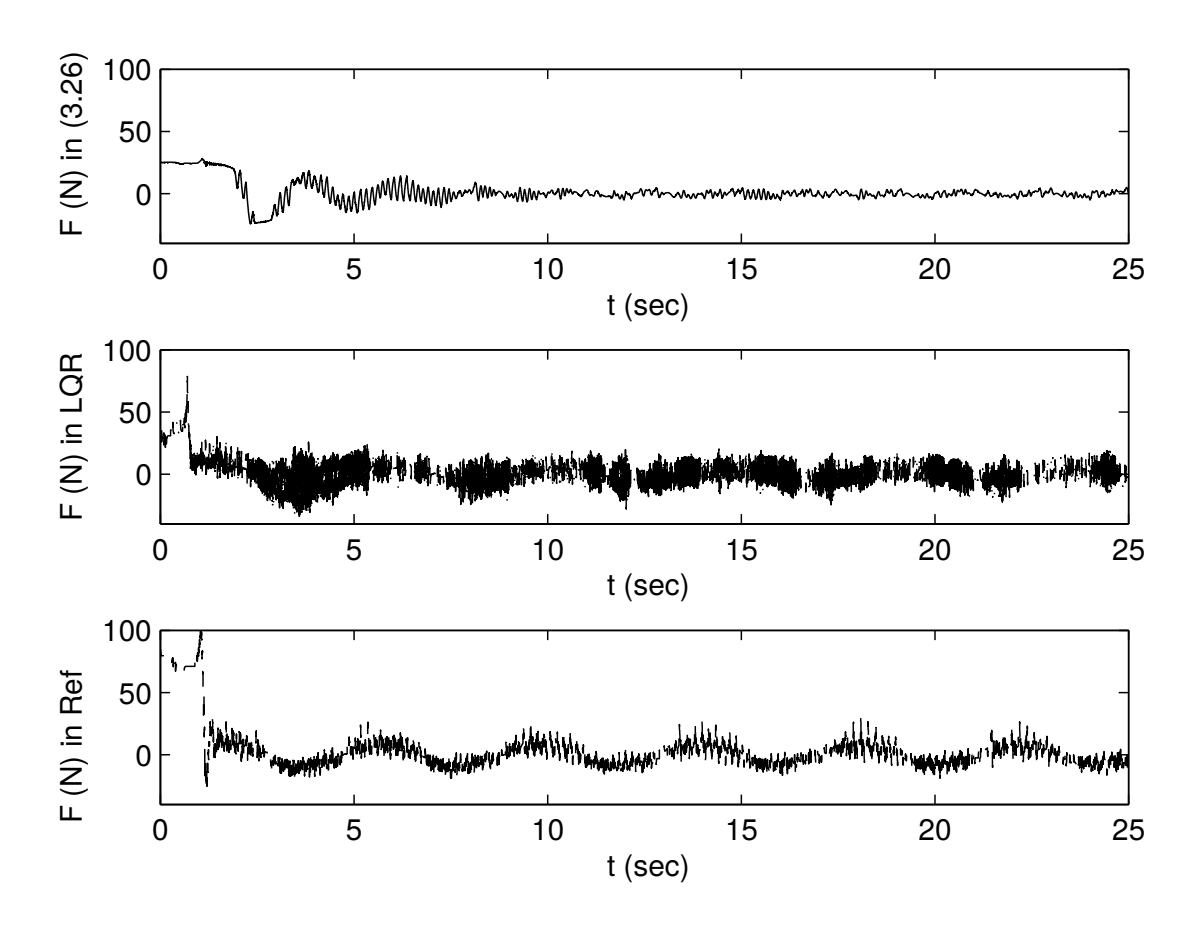


Figure 3.10: Trajectories of inputs F in (3.26) (the top subfigure), LQR (the middle subfigure), and [63] (the bottom subfigure) are shown.

Chapter 4

Output Feedback Control for an Autonomous Helicopter in the

Presence of Disturbances

4.1 Introduction

In recent years, autonomous helicopter operation has been used in various areas such as above-ground transportation, forest fire monitoring, monitoring criminal activity, and multiagent, multi-objective UAV mission in [60,67]. However designing a control system for an autonomous helicopter is a challenging task. Since helicopter dynamics have nonaffine control inputs and are underactuated mechanical systems, it is difficult to control and it can easily become unstable compared to other mechanical systems like ground vehicles.

In [3, 20, 38, 39], controllers were proposed for helicopters without considering unmeasured states and uncertainties. In [38], a dynamic extension concept from [30] was used to eliminate internal dynamics in an approximate model of a helicopter. In [39], a differential flatness method was proposed through an approximation model. In [39], using the concept of a natural two-time-scale separation, it was possible to design outer-loop (position dynam-

ics) and inner-loop (the rest of the system) controls separately and overcome the feature of underactuated mechanical systems. In [3], while considering dynamics of actuators, the approximated (input-affine) model was combined with backstepping to control a helicopter. Since an approximate model was used in both [38,39] and [3], and neither disturbance nor model uncertainties were considered, the proposed methods are not valid in the presence of disturbance.

In [31, 47, 48], using high gains a two-time-scale approach for helicopter dynamics was proposed considering the helicopter system parameter uncertainties. In [31], based on a two time-scale separation approach between rotational and translational dynamics, a controller with an affine control input model was designed to track the vertical reference trajectory which has unknown phase, amplitude, and frequency, while stabilizing the lateral, longitudinal, and attitude dynamics. In [31], the robustness of the controller to uncertainties was considered through numerical simulations. In [47,48], a state feedback controller robust to uncertain aerodynamical parameters of the helicopter was proposed, which is based on the linear approximation of control inputs. In [48], high gains were used to dominate uncertain parameters and to render the helicopter rotational dynamics quickly converge into desired trajectories which are control inputs for the translational dynamics. Moreover, nested saturation control was used to prevent the controller having singularities. In [47], the systematic control design process was presented, based on the earlier work of [48]. For the three papers, it was assumed that states of the system were measurable and external disturbances were not considered. Nonaffine control inputs were approximated to affine control inputs.

In [14,19,65], neural networks were proposed to deal with nonaffine control inputs and uncertainties. In [14], neural networks were used to deal with uncertain, input-nonaffine, nonlinear systems (for example, attitude dynamics of a helicopter). In [19], using neural networks and backstepping scheme, uncertain system parameters and external disturbances were dealt with under state feedback control. In [65], robust adaptive neural networks control was designed in the absence of uncertainties for vertical flight of helicopters, i.e., a

single-input-single-output nonaffine system. The system states were estimated by high-gain observers [33] and adaptive nenural networks were used to deal with a nonaffine control input. However, neural networks require training, and selection of the basis and weights often requires significant computation.

Disturbance estimators were used to consider uncertainties in helicopter dynamics in [41, 45]. In [45], nonlinear model predictive control with disturbance observers was used to deal with parameter uncertainties and external disturbances under the assumption that states of the system were measurable and control inputs were affine. In [41], output feedback control design for an unmanned helicopter in the presence of uncertainties was developed for the rotational dynamics; the dynamic inversion scheme was used to deal with nonaffine control inputs and an extended high-gain observer estimated unmeasured states, system parameter uncertainties, and external disturbances.

In this chapter, the output feedback control of a helicopter is proposed as an extension of [41] from a Single-Input-Single-Output (SISO) systems to MIMO systems. We propose to use an Extended High-Gain Observer (EHGO) to estimate the system states and disturbances of a helicopter instead of a neural network. In order to deal with nonaffine control inputs in a helicopter, the EHGO is used together with the method of dynamic inversion. The combined system has five time scales: two-time scales are required by plant dynamics between translational and rotational dynamics; the third time-scale is required by dynamic inversion for the translational dynamics; the fourth time-scale is required by the dynamic inversion for the rotational dynamics; and the fifth, fastest, time scale is required by the EHGO for estimation of the states, uncertain system parameter, and external disturbances.

This chapter is organized as follow. In Section 4.2, a helicopter model is given. In Section 4.3, we define the problem and design state feedback control in the absence of uncertainties. The stability analysis for the closed-loop system is conducted under state feedback. In Section 4.4, output feedback control for full helicopter dynamics is designed in the presence of uncertainties using the EHGO and dynamic inversion. Based on the singular perturbation

method, the stability for the multi-time-scale closed-loop system is analyzed. The effectiveness of the proposed control scheme is verified through numerical simulations in Section 4.5. Section 4.6 presents concluding remarks.

4.2 Dynamics of a Helicopter

In this section, the rigid body dynamics of a helicopter are presented. It is assumed that the actuator dynamics are sufficiently fast compared to the rigid body dynamics and can be ignored in the mathematical model. The rigid body dynamics are based on [38] and written as

$$\begin{bmatrix} M & 0 \\ 0 & I \end{bmatrix} \begin{bmatrix} \dot{v}^b \\ \dot{\omega}^b \end{bmatrix} + \begin{bmatrix} \omega^b \times m v^b \\ \omega^b \times I \omega^b \end{bmatrix} = \begin{bmatrix} f^b \\ \tau^b \end{bmatrix},$$

where M = diag[m, m, m] and $I = \text{diag}[I_{xx}, I_{yy}, I_{zz}]$ are mass matrix and the inertia matrix of the helicopter, respectively; m is the mass of a helicopter; I_{xx} , I_{yy} , and I_{zz} are the principle moments of inertia; $v^b = \begin{bmatrix} v_x^b, v_y^b, v_z^b \end{bmatrix}^T$ is the body velocity vector; v_i^b for i = x, y, z are the linear velocities in the x, y, and z directions; $\tau^b = [\tau_1^b, \tau_2^b, \tau_3^b]^T$ is the torque, specified later in next Subsection 4.2.1; and $\omega^b = [\omega_1, \omega_2, \omega_3]^T$ is the angular velocity vector where ω_j for j = 1, 2, 3 are the angular velocities about x, y, and z axes. The input force matrix is expressed as

$$f^{b} = \begin{bmatrix} X_{M} \\ Y_{M} + Y_{T} \\ Z_{M} \end{bmatrix} + R^{T}(\Theta_{b}) \begin{bmatrix} 0 \\ 0 \\ mg \end{bmatrix},$$

where the set of forces $(X_M, Y_M, Y_T, \text{ and } Z_M)$ or moments $(R_M, M_M, N_M, \text{ and } M_T)$ acting on a helicopter is given by

$$\begin{split} X_M &= -T_M \sin a_{1s}, \quad Y_M = T_M \sin b_{1s}, \\ Z_M &= -T_M \cos a_{1s} \cos b_{1s}, \quad Y_T = -T_T, \\ R_M & \simeq \frac{\partial R_M}{\partial b_{1s}} b_{1s} - Q_M \sin a_{1s}, \quad M_M \simeq \frac{\partial M_M}{\partial a_{1s}} a_{1s} + Q_M \sin b_{1s}, \\ N_M & \simeq -Q_M \cos a_{1s} \cos b_{1s}, \quad M_T = -Q_T. \end{split}$$

 $Q_M = C_M^Q T_M^{1.5} + D_M^Q$ and $Q_T = C_T^Q T_T^{1.5} + D_T^Q$ are the approximate rotor torque equations for main and tail rotors, respectively (we follow the model in [38]). C_M^Q and C_T^Q are the thrust coefficients of T_M and T_T , respectively, and D_M^Q and D_T^Q are the lift drag coefficients of T_M and T_T , respectively. The system parameters are given in Section 4.5. a_{1s} and b_{1s} are longitudinal and lateral tilts of the tip path plane of the main rotor with respect to the shaft, respectively; and T_M and T_T are main rotor thrust and tail rotor thrust, respectively. The gravitational acceleration is $g = 9.8 \ m/s^2$ and the rotation matrix $R(\Theta_b)$ is defined by

$$R(\Theta_b) = \begin{bmatrix} c\theta c\psi & s\phi s\theta c\psi - c\theta s\psi & c\phi s\theta c\psi + s\phi s\psi \\ c\theta s\psi & s\phi s\theta s\psi + c\phi c\psi & c\phi s\theta s\psi - s\phi c\psi \\ -s\theta & s\phi c\theta & c\phi c\theta \end{bmatrix},$$

where $\Theta_b = [\phi, \theta, \psi]^T$, ϕ (roll), θ (pitch), ψ (yaw) are the Euler angels and $s(\cdot) = \sin(\cdot)$, $c(\cdot) = \cos(\cdot)$. Control inputs, T_M , T_T , a_{1s} , and b_{1s} are used for a helicopter control under the assumption that the dynamics of a_{1s} and b_{1s} are sufficiently fast. In Table. 4.1,

Table 4.1: Parameters in a helicopter

h_M	Distance from COM(Center of Mass) to the main rotor along the z axis
h_T	Distance from COM to the tail rotor along the z axis
l_M	Distance from COM to the main rotor along the x axis
l_T	Distance from COM to the tail rotor along the x axis
y_M	Distance from COM to the main rotor along the y axis

parameters are given for the helicopter. The side and top view of the helicopter is shown with the parameters in Fig. 4.1.

4.2.1 Rotational Dynamics of a Helicopter

The helicopter dynamics can be divided into two parts, an inner-loop and an outer-loop due to a natural time-scale separation [38] as shown in Fig. 4.2. In Fig. 4.2, ϕ , θ , ψ are actual Euler angle values of a helicopter, and $\Theta_r = [\phi_r, \theta_r, \psi_r]^T$ is the reference trajectory which is generated from the controller of translational dynamics, C_T . The inner-loop is rotational dynamics of a helicopter whereas the outer-loop is translational dynamics.

The inner-loop dynamics of a helicopter (attitude dynamics) are given by

$$\dot{\Theta}_b = \Psi(\Theta_b)\omega^b$$

$$\dot{\omega}^b = -I^{-1}\omega^b \times I\omega^b + B\tau^b,$$
(4.1)

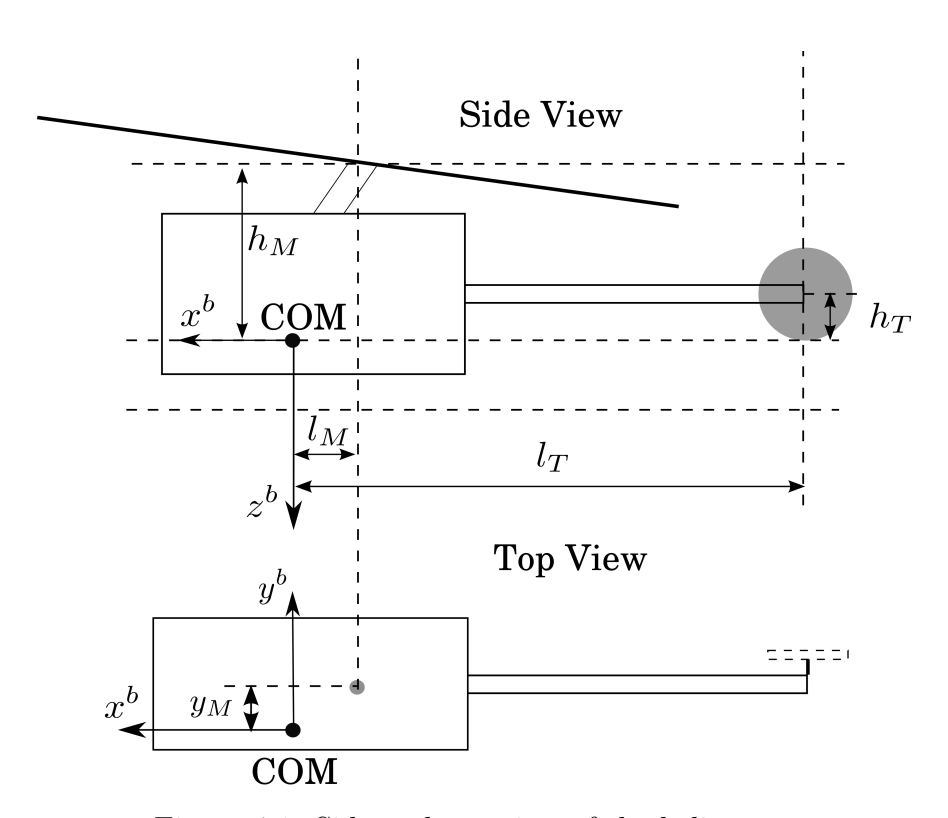


Figure 4.1: Side and top view of the helicopter

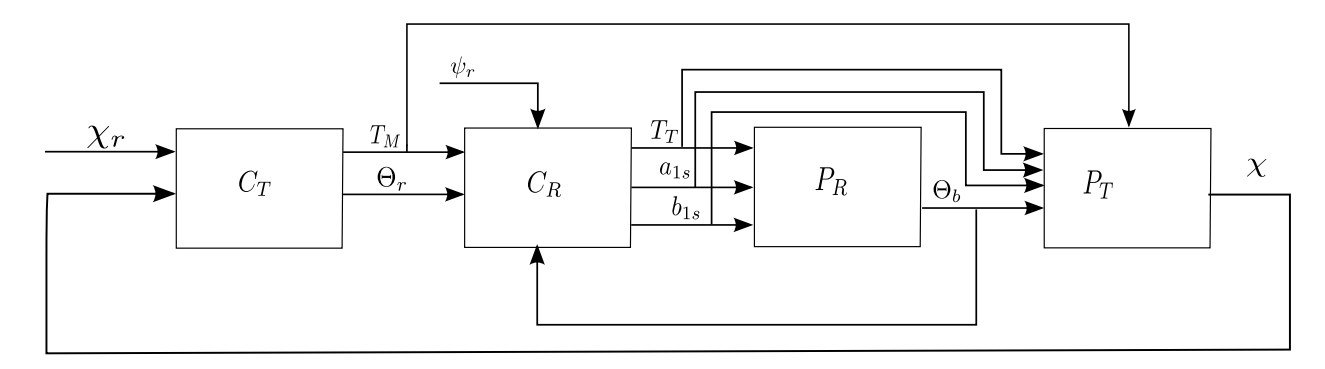


Figure 4.2: The block diagram is shown for rotational dynamics (inner-loop) and translational dynamics (outer-loop) control structure via two time-scale separation. The blocks P_R , P_T are rotational dynamics and translational dynamics, respectively. The blocks C_R , C_T are controllers for rotational and translational dynamics, respectively. χ is the position of the helicopter and χ_r and Θ_r are reference trajectories for the translational and rotational dynamics, respectively.

where $B = \text{diag}[1/I_{xx}, 1/I_{yy}, 1/I_{zz}];$ and

$$\Psi(\Theta_b) = \begin{bmatrix}
1 & \sin\phi \tan\theta & \cos\phi \tan\theta \\
0 & \cos\phi & -\sin\phi \\
0 & \sin\phi \sec\theta & \cos\phi \sec\theta
\end{bmatrix}, \quad \Psi^{-1}(\Theta_b) = \begin{bmatrix}
1 & 0 & -\sin\theta \\
0 & \cos\phi & \sin\phi \cos\theta \\
0 & -\sin\phi & \cos\phi \cos\theta
\end{bmatrix} \quad (4.2)$$

In order to make (4.1) compatible to extended high-gain observer method, the following coordinates are used as

$$\dot{\Theta}_b = \Omega$$

$$\dot{\Omega} = F_I(\Theta_b, \Omega, \tau^b),$$
(4.3)

where $\Omega = \Psi(\Theta_b)\omega^b = \left[\dot{\phi}, \dot{\theta}, \dot{\psi}\right]^T$ is a vector of the Euler angle rates. In (4.3), $\dot{\Omega} = F_I(\Theta_b, \Omega, \tau^b) = [\ddot{\phi}, \ddot{\theta}, \ddot{\psi}]^T$ is obtained from (4.1) as

$$\ddot{\phi} = (\omega_2 \cos \phi \tan \theta - \omega_3 \sin \phi \tan \theta) \dot{\phi} + (\omega_2 \sec^2 \theta \sin \phi + \omega_3 \cos \phi \sec^2 \theta) \dot{\theta}$$

$$- \frac{(I_{zz} - I_{yy})}{I_{xx}} \omega_2 \omega_3 + \frac{(I_{zz} - I_{xx})}{I_{yy}} \omega_1 \omega_3 \sin \phi \tan \theta - \frac{(I_{yy} - I_{xx})}{I_{zz}} \omega_1 \omega_2 \cos \phi \tan \theta$$

$$+ \frac{1}{I_{xx}} \tau_1^b + \frac{\sin \phi \tan \theta}{I_{yy}} \tau_2^b + \frac{\cos \phi \tan \theta}{I_{zz}} \tau_3^b,$$

$$(4.4)$$

$$\ddot{\theta} = -(\omega_2 \sin \phi + \omega_3 \cos \phi)\dot{\phi} + \frac{(I_{zz} - I_{xx})}{I_{yy}}\omega_1\omega_3 \cos \phi + \frac{(I_{yy} - I_{xx})}{I_{zz}}\omega_1\omega_2 \sin \phi + \frac{\cos \phi}{I_{yy}}\tau_2^b - \frac{\sin \phi}{I_{zz}}\tau_3^b$$

$$(4.5)$$

$$\ddot{\psi} = (\omega_2 \cos \phi \sec \theta - \omega_3 \sec \theta \sin \phi)\dot{\phi} + (\omega_2 \sec \theta \sin \phi \tan \theta + \omega_3 \cos \phi \sec \theta \tan \theta)\dot{\theta}$$

$$+ \frac{(I_{zz} - I_{xx})}{I_{yy}}\omega_1\omega_3 \sec \theta \sin \phi - \frac{(I_{yy} - I_{xx})}{I_{zz}}\omega_1\omega_2 \cos \phi \sec \theta$$

$$+ \frac{\sec \theta \sin \phi}{I_{yy}}\tau_2^b + \frac{\cos \phi \sec \theta}{I_{zz}}\tau_3^b,$$
(4.6)

and $\tau = [\tau_1^b, \tau_2^b, \tau_3^b]^T$ is given by

$$\tau_1^b = \frac{\partial R_M}{\partial b_{1s}} b_{1s} - Q_M \sin(a_{1s}) + T_M \sin(b_{1s}) h_M - T_M \cos(a_{1s}) \cos(b_{1s}) y_M - T_T h_T,$$

$$\tau_2^b = \frac{\partial M_M}{\partial a_{1s}} a_{1s} + Q_M \sin(b_{1s}) - Q_T + T_M \sin(a_{1s}) h_M - T_M \cos(a_{1s}) \cos(b_{1s}) l_M,$$

$$\tau_3^b = -Q_M \cos(a_{1s}) \cos(b_{1s}) - T_M \sin(b_{1s}) l_M + T_T l_T,$$

4.2.2 Translational Dynamics of a Helicopter

The translational dynamics of a helicopter (i.e., position dynamics) are given by

$$\dot{P} = v^b$$

$$\dot{v}^b = \frac{1}{m} R(\Theta) f^b = F_P,$$
(4.7)

where $P = [x, y, z]^T$, $v^b = [\dot{x}, \dot{y}, \dot{z}]^T$ are a position vector and a velocity vector in North-East-Down orientation, respectively, and $F_P = [f_x, f_y, f_z]^T$ is

$$f_x = \left(\frac{1}{m}\right) \left\{ -T_M \cos \theta \cos \psi \sin a_{1s} + (\sin \phi \sin \theta \cos \psi - \cos \phi \sin \psi) [T_M \sin b_{1s} - T_T] \right.$$

$$\left. - T_M (\cos \phi \sin \theta \cos \psi + \sin \phi \sin \psi) \cos a_{1s} \cos b_{1s} \right\}$$

$$f_y = \left(\frac{1}{m}\right) \left\{ -T_M \cos \theta \sin \psi \sin a_{1s} + (\sin \phi \sin \theta \sin \psi + \cos \phi \cos \psi) [T_M \sin b_{1s} - T_T] \right.$$

$$\left. - T_M (\cos \phi \sin \theta \sin \psi - \sin \phi \cos \psi) \cos a_{1s} \cos b_{1s} \right\}$$

$$f_z = \left(\frac{1}{m}\right) \left\{ T_M \sin \theta \sin a_{1s} + (\sin \phi \cos \theta) [T_M \sin b_{1s} - T_T] \right.$$

$$\left. - T_M \cos \phi \cos \theta \cos a_{1s} \cos b_{1s} \right\} + g$$

$$(4.8)$$

4.3 Stability Analysis in the Absence of Disturbances

In this section, we describe a control strategy for a helicopter in the absence of uncertainties, based on a time-scale separation strategy between the translational and rotational dynamics. The control objective is to follow given reference trajectories x_r , y_r , z_r , and ψ_r with inputs T_M , T_T , a_{1s} and b_{1s} .

In this section we assume that all system states and dynamic models are known. For the translational dynamics, we neglect flapping dynamics a_{1s} and b_{1s} and the tail rotor thrust T_T in y-direction in [38], [31], [48], [47] and the translational dynamics are given by

$$\ddot{P} = \frac{1}{m}R(\Theta) \begin{bmatrix} 0 \\ 0 \\ -T_M \end{bmatrix} + \begin{bmatrix} 0 \\ 0 \\ g \end{bmatrix}$$

$$(4.9)$$

We are going to design a controller which renders the rotational dynamics faster than the translational dynamics while dealing with nonaffine control inputs. Based on the time-scale separation between the rotational and translation dynamics, new control inputs $u_r = [T_T, a_{1s}, b_{1s}]^T$ for the rotational dynamics and $u_t = [T_M, \phi_d, \theta_d]^T$ for the translational dynamics are designed, where ϕ_d and θ_d in dynamic inversion control will be specified later. As depicted in Fig. 4.2, an inner-loop controller for the rotational dynamics is designed to force the rotational dynamics to follow the desired reference trajectories ϕ_r , θ_r , and ψ_r with a fast convergence rate. An outer-loop controller for the translational dynamics is designed to provides desired reference trajectories ϕ_r , θ_r , and ψ_r for the rotational dynamics and to obtain slower translation dynamics than rotational dynamics. A dynamic inversion controller will be designed to deal with nonaffine input forms.

4.3.1 State feedback control

With state variables

$$\chi_{x} = [x_{1}, x_{2}]^{T} = [x, \dot{x}]^{T}, \quad \chi_{y} = [y_{1}, y_{2}]^{T} = [y, \dot{y}]^{T}, \quad \chi_{z} = [z_{1}, z_{2}]^{T} = [z, \dot{z}]^{T}
\Theta_{\phi} = [\phi_{1}, \phi_{2}]^{T} = [\phi, \dot{\phi}]^{T}, \quad \Theta_{\theta} = [\theta_{1}, \theta_{2}]^{T} = [\theta, \dot{\theta}]^{T}, \quad \Theta_{\psi} = [\psi_{1}, \psi_{2}]^{T} = [\psi, \dot{\psi}]^{T}$$
(4.10)

the translational dynamics of (4.9) are rewritten as

$$\dot{\chi} = A\chi + BF_O \tag{4.11}$$

where $\chi = [\chi_x^T, \chi_y^T, \chi_z^T]^T \in D_{\chi}$, $D_{\chi} \subset \mathbf{R}^6$ is bounded, $A = \text{block diag}[A_1, A_1, A_1]$, $B = \text{block diag}[B_1, B_1, B_1]$ with

$$A_1 = \begin{bmatrix} 0 & 1 \\ 0 & 0 \end{bmatrix}, \quad B_1 = \begin{bmatrix} 0 \\ 1 \end{bmatrix} \tag{4.12}$$

and

$$F_O = \begin{bmatrix} f_x \\ f_y \\ f_z \end{bmatrix} = \begin{bmatrix} -\frac{1}{m} (\cos \phi_1 \sin \theta_1 \cos \psi_1 + \sin \phi_1 \sin \psi_1) T_M \\ -\frac{1}{m} (\cos \phi_1 \sin \theta_1 \sin \psi_1 - \sin \phi_1 \cos \psi_1) T_M \\ -\frac{1}{m} (\cos \phi_1 \cos \phi_1 \cos \theta_1) T_M + g \end{bmatrix}$$
(4.13)

We note that in the translational dynamics in (4.11), control inputs are ϕ_1 , θ_1 , and T_M where ϕ_1 and θ_1 are viewed as the virtual control provided by the rotational dynamics as the fast time scale. A target system for the translational dynamics is given by

$$\dot{\chi}_r = (A - BL)\chi_r + Bu_c \tag{4.14}$$

where $\chi_r = [x_r, \dot{x}_r, y_r, \dot{y}_r, z_r, \dot{z}_r]^T \in D_{\chi_r}$, $D_{\chi_r} \subset \mathbf{R}^6$ is bounded, the matrix $L = \mathrm{block} \ \mathrm{diag}[L_\chi, L_\chi, L_\chi]$ with $L_\chi = [k_p, k_v]$ is block diagonal such that the matrix (A - BL) is Hurwitz, and $u_c = [r_x, r_y, r_z]^T$ is a bounded commend input and continuously differentiable. To track the reference trajectories for the translational dynamics, it is required to find ϕ_r , θ_r and T_m^* given ψ_r such that

$$F_{\chi} = \begin{bmatrix} f_x(\phi_r, \theta_r, \psi_r, T_M^*) \\ f_y(\phi_r, \theta_r, \psi_r, T_M^*) \\ f_z(\phi_r, \theta_r, T_M^*) \end{bmatrix} + L\chi - u_c(t) = 0$$

$$(4.15)$$

The dynamic inversion in the translational dynamics is used to obtain approximated solutions ϕ_d , θ_d , and T_M for (4.15).

With the state variables in (4.10), the rotational dynamics of a helicopter in (4.3) can be represented as

$$\dot{\Theta} = A\Theta + BF_I, \tag{4.16}$$

where $\Theta = [\Theta_{\phi}^T, \Theta_{\theta}^T, \Theta_{\psi}^T]^T \in D_{\Theta} \subset \mathbf{R}^6$ and $F_I = [f_{\phi}, f_{\theta}, f_{\psi}]^T = F_I(\Theta_b, \Omega, \tau^b) \in \mathbf{R}^3$ in (4.3). The domain D_{Θ} is given by $D_{\Theta} = D_{\Theta_{\phi}} \times D_{\Theta_{\theta}} \times D_{\Theta_{\psi}}, D_{\Theta_p} = \{-a_p \leq p \leq a_p\} \times \{b_p \leq \dot{p} \leq b_p\},$ for $p = \phi, \theta, \psi$ with bounded $0 < a_p < \pi/2$ and b > 0.

There are two tasks of a controller for the rotational dynamics: one is to deal with nonaffine input forms which is required to find solutions a_{1s}^* , b_{1s} , and T_T^* such that

$$F_{\Theta} = \begin{bmatrix} f_{\phi}(\Theta, T_{M}, a_{1s}^{*}, b_{1s}^{*}, T_{T}^{*}) + k_{\phi_{1}}(\phi_{1} - \phi_{d}) + k_{\phi_{2}}\phi_{2}) \\ f_{\theta}(\Theta, T_{M}, a_{1s}^{*}, b_{1s}^{*}, T_{T}^{*}) + k_{\theta_{1}}(\theta_{1} - \theta_{d}) + k_{\theta_{2}}\theta_{2}) \\ f_{\psi}(\Theta, T_{M}, a_{1s}^{*}, b_{1s}^{*}, T_{T}^{*}) + k_{\psi_{1}}(\psi_{1} - \psi_{r}) + k_{\psi_{2}}\psi_{2}) \end{bmatrix} = 0,$$

$$(4.17)$$

where f_{ϕ} , f_{θ} , and f_{ψ} given in in (4.13), and k_{ϕ_i} , k_{θ_i} , k_{ψ_i} for i = 1, 2 are high gains specified later; and the other is to make the rotational dynamics converge quickly into the desired reference trajectories ϕ_d , θ_d , and ψ_r provided by a dynamic inversion controller. For the rotational dynamics, the dynamic inversion is used to find approximated solutions a_{1s} , b_{1s} , and T_T for (4.17).

Two dynamic inversion controllers in [43,44] are designed to deal with nonaffine inputs $u_t = [T_M, \phi_d, \theta_d]^T$ and $u_r = [T_T, a_{1s}, b_{1s}]^T$. The dynamic inversion for the translational dynamics is

$$\varepsilon_2 \dot{u}_t = -\left(\frac{\partial F_{\chi_d}}{\partial u_t}\right)^T F_{\chi_d}(\Theta, \chi, u_t, u_c) \tag{4.18}$$

where $u_t \in D_t \subset \mathbf{R}^3$; $(\partial F_{\chi_d}/\partial u_t)$ is given in Appendix Appendix B;

$$F_{\chi_d}(\Theta, \chi, u_t, u_c) = \begin{bmatrix} f_x(\phi_d, \theta_d, \psi_r, T_M) \\ f_y(\phi_d, \theta_d, \psi_r, T_M) \\ f_z(\phi_d, \theta_d, T_M) \end{bmatrix} + L\chi - u_c(t), \quad u_c(t) = \begin{bmatrix} r_x(t) \\ r_y(t) \\ r_z(t) \end{bmatrix}$$
(4.19)

 f_x , f_y and f_z are given in (4.13); and $r_x(t)$, $r_y(t)$, and $r_z(t)$ are bounded reference commends. The dynamic inversion for the rotational dynamics

$$\varepsilon_3 \dot{u}_r = -\left(\frac{\partial F_{\Theta}}{\partial u_r}\right)^T F_{\Theta}(\Theta, u_t, u_r, \psi_r) \tag{4.20}$$

where $u_r \in D_r \subset \mathbf{R}^3$, $(\partial F_{\Theta}/\partial u_r)$ is given in Appendix Appendix B, and

$$F_{\Theta}(\Theta, u_t, u_r, \psi_r) = \begin{bmatrix} f_{\phi}(\Theta, u_t, u_r) + k_{\phi_1}(\phi_1 - \phi_d) + k_{\phi_2}\phi_2) \\ f_{\theta}(\Theta, u_t, u_r) + k_{\theta_1}(\theta_1 - \theta_d) + k_{\theta_2}\theta_2) \\ f_{\psi}(\Theta, u_t, u_r) + k_{\psi_1}(\psi_1 - \psi_r) + k_{\psi_2}\psi_2) \end{bmatrix}$$
(4.21)

To obtain the fast rotational dynamics, k_{ϕ_i} , k_{θ_i} , k_{ψ_i} for i=1,2 are chosen as

$$k_{\phi_1} = k_{\theta_1} = k_{\psi_1} = \frac{k_1}{\varepsilon_1^2}, \quad k_{\phi_2} = k_{\theta_2} = k_{\psi_2} = \frac{k_2}{\varepsilon_1}$$
 (4.22)

where $k_{r,1}$ and $k_{r,2}$ are positive constants independent of ε_1 and ε_2 . The assumption for the Jacobian matrices $(\partial F_{\chi_d}/\partial u_t)$ and $(\partial F_{\Theta}/\partial u_r)$ are as follows.

Assumption 4. In the domains D_{χ} , D_{χ_r} , D_{Θ} , D_t and D_r ,

- the Jacobian matrices $(\partial F_{\chi_d}/\partial u_t)$ and $(\partial F_{\Theta}/\partial u_r)$ are nonsingular;
- $\lambda_{\min} \left((\partial F_{\chi_d} / \partial u_t) (\partial F_{\chi_d} / \partial u_t)^T \right) > a \text{ with } a > 0 \text{ and } \lambda_{\min} \left((\partial F_{\Theta} / \partial u_r) (\partial F_{\Theta} / \partial u_r)^T \right) > b$ with b > 0;
- F_{χ} and F_{Θ} are continuously differentiable,

where $\lambda_{\min}(P)$ denotes the minimum eigenvalue of the matrix P.

4.3.2 Stability analysis

Using the systems (4.11), (4.14), and (4.16) with the control (4.18) and (4.20), the standard singularly perturbed form for the closed-loop system is derived. Error variables for the

translational dynamics are

$$e_{x_1} = x_1 - x_r, \quad e_{x_2} = x_2 - \dot{x}_r$$

$$e_{y_1} = y_1 - y_r, \quad e_{y_2} = y_2 - \dot{y}_r$$

$$e_{z_1} = z_1 - z_r, \quad e_{z_2} = z_2 - \dot{z}_r$$

$$(4.23)$$

Time-scaled variables for the rotational dynamics are

$$e_{\phi_1} = \phi_1 - \phi_r, \quad e_{\phi_2} = \varepsilon_1(\phi_2 - \dot{\phi}_r)$$

$$e_{\theta_1} = \theta_1 - \theta_r, \quad e_{\theta_2} = \varepsilon_1(\theta_2 - \dot{\theta}_r)$$

$$e_{\psi_1} = \psi_1 - \psi_r, \quad e_{\psi_2} = \varepsilon_1(\psi_2 - \dot{\psi}_r)$$

$$(4.24)$$

Error variables of the dynamic inversion for the translational and rotational dynamics are $s_t = u_t - u_t^*$ and $s_r = u_r - u_r^*$ with

$$u_{t} = \begin{bmatrix} T_{M} \\ \phi_{d} \\ \theta_{d} \end{bmatrix}, \quad u_{t}^{*} = \begin{bmatrix} T_{M}^{*} \\ \phi_{r} \\ \theta_{r} \end{bmatrix}, \quad u_{r} = \begin{bmatrix} T_{T} \\ a_{1s} \\ b_{1s} \end{bmatrix}, \quad u_{r}^{*} = \begin{bmatrix} T_{T}^{*} \\ a_{1s}^{*} \\ b_{1s}^{*} \end{bmatrix}$$

$$(4.25)$$

 u_t^* and u_r^* are satisfied with

$$F_{\Theta}(\Theta, u_{t}, u_{r}^{*}, \psi_{r}) = 0, \quad F_{\chi}(\Theta, \chi, u_{t}^{*}, u_{c}) = 0$$

$$F_{\chi}(\Theta, \chi, u_{t}^{*}, u_{c}) = \begin{bmatrix} f_{x}(\phi_{r}, \theta_{r}, \psi_{r}, T_{M}^{*}) \\ f_{y}(\phi_{r}, \theta_{r}, \psi_{r}, T_{M}^{*}) \\ f_{z}(\phi_{r}, \theta_{r}, T_{M}^{*}) \end{bmatrix} + L\chi - u_{c}(t),$$

$$(4.26)$$

In view of Assumption 4 and the Lipschitz property of F_{χ_d} in its arguments, it is reasonable to have the following assumption on the relation between $||F_{\chi_d}||$ and ||s||:

Assumption 5. $k_l ||s_t|| \le ||F_{\chi_d}(\Theta, \chi, u_t, u_c) - F_{\chi_d}(\Theta, \chi, u_t^*, u_c)|| \le k_l ||s||$ with some constants

 $k_l, k_p > 0$ on the domains $D_{\chi}, D_{\chi_r}, D_{\Theta}, D_t$, and D_r

So, u_r^* is a function, $u_r^* = u_r^*(\Theta, u_t, \psi_r)$ and u_t^* a function, $u_t^* = u_t^*(\Theta, \chi, u_c)$. Error dynamics of translational dynamics are represented as

$$\dot{e}_{\chi} = A_{\chi} e_{\chi} + BF_{\chi}(\Theta, \chi, u_t, u_c) \tag{4.27}$$

with $e_{\chi} = [e_x^T, e_y^T, e_z^T]^T$ and $A_{\chi} = A - BL$. With the time-scaled variables in (4.24), the closed-loop standard singular perturbed form for error dynamics of the rotational dynamics is

$$\varepsilon_1 \dot{e}_{\Theta} = A_{\theta} e_{\Theta} + B[k_1(\Theta_d - \Theta_r) + \varepsilon_1^2 F_{\Theta}(\Theta, u_t, u_r, \psi_r) - \varepsilon_1^2 \ddot{\Theta}_r - \varepsilon_1 k_2 \dot{\Theta}_r]$$
(4.28)

with $A_{\theta} = A - BL_{\theta}$, $e_{\Theta} = [e_{\phi}^T, e_{\theta}^T, e_{\psi}^T]^T$, $e_{\phi} = [e_{\phi_1}, e_{\phi_2}]^T$, $e_{\theta} = [e_{\theta_1}, e_{\theta_2}]^T$, $e_{\psi} = [e_{\psi_1}, e_{\psi_2}]^T$, $L_{\theta} = \text{block diag}[L_1, L_1, L_1]$, $L_1 = [k_1, k_2]$, $\Theta_d = [\phi_d, \theta_d, \psi_r]^T$, and $\Theta_r = [\phi_r, \theta_r, \psi_r]^T$. The error dynamics for the variable s_t are

$$\varepsilon_2 \dot{s}_t = -\left(\frac{\partial F_{\chi_d}}{\partial u_t}\right)^T F_{\chi_d}(\Theta, \chi, u_t, u_c) - \varepsilon_2 \dot{u}_t^* \tag{4.29}$$

where \dot{u}_t^* is

$$\dot{u}_t^* = \left(\frac{\partial u_t}{\partial \Theta}\right) \dot{\Theta} + \left(\frac{\partial u_t}{\partial \chi}\right) \dot{\chi} + \left(\frac{\partial u_t}{\partial u_c}\right) \dot{u}_c \tag{4.30}$$

The error dynamics for s_r is

$$\varepsilon_3 \dot{s}_r = -\left(\frac{\partial F_{\Theta}}{\partial u_r}\right)^T F_{\Theta}(\Theta, u_t, u_r, \psi_r) - \varepsilon_3 \dot{u}_r^* \tag{4.31}$$

where \dot{u}_r^* is

$$\dot{u}_r^* = \left(\frac{\partial u_r}{\partial \Theta}\right) \dot{\Theta} - \left(\frac{1}{\varepsilon_2}\right) \left(\frac{\partial u_r}{\partial u_t}\right) \left(\frac{\partial F_{\chi_d}}{\partial u_t}\right)^T F_{\chi_d} + \left(\frac{\partial u_t}{\partial \psi_r}\right) \dot{\psi}_r \tag{4.32}$$

Using (4.27), (4.28), (4.29), and (4.31), the singularly perturbed form is

$$\dot{e}_{\chi} = A_{\chi} e_{\chi} + BF_{\chi}(e_{\Theta} + \Theta_{er}, e_{\chi} + \chi_r, s + u^*, u_c)$$

$$\tag{4.33}$$

$$\varepsilon_1 \dot{e}_{\Theta} = A_{\theta} e_{\Theta} + B[k_1(\Theta_d - \Theta_r) + \varepsilon_1^2 F_{\Theta}(\Theta, s + u^*, \psi_r) - \varepsilon_1^2 \ddot{\Theta}_r - \varepsilon_1 k_2 \dot{\Theta}_r]$$
(4.34)

$$\varepsilon_2 \dot{s}_t = -\left(\frac{\partial F_{\chi_d}}{\partial u_t}\right)^T F_{\chi_d}(\Theta, e_\chi + \chi_r, s_t + u_t^*, u_c) - \varepsilon_2 \dot{u}_t^* \tag{4.35}$$

$$\varepsilon_3 \dot{s}_r = -\left(\frac{\partial F_{\Theta}}{\partial u_r}\right)^T F_{\Theta}(\Theta, e_{\chi} + \chi_r, s_t + u_t^*, s_r + u_r^*, \psi_r) - \varepsilon_3 \dot{u}_r^*$$
(4.36)

We have a three-time-scale structure in (4.33), (4.34), (4.35), and (4.36). We note that the small parameters ε_1 , ε_2 , and ε_3 have the relation, $0 < \varepsilon_3 \ll \varepsilon_2 \ll \varepsilon_1 \ll 1$. Since \dot{u}_t^* in (4.35) has the term $(1/\varepsilon_1)$, it is required to have $0 < \varepsilon_2 \ll \varepsilon_1 \ll 1$. ε_3 is required to be $0 < \varepsilon_3 \ll \varepsilon_2 \ll 1$ since \dot{u}_r in (4.36), has the term $(1/\varepsilon_2)$.

Stability analysis starts from the fastest boundary layer system of the dynamic inversion in (4.36). The boundary layer system can be obtained setting $\varepsilon_3 = 0$ on the right-hand side of (4.36)

$$\varepsilon_3 \dot{s}_r = -\left(\frac{\partial F_{\Theta}}{\partial u_r}\right)^T F_{\Theta}(\Theta, e_{\chi} + \chi_r, s_t + u_t^*, s_r + u_r^*, \psi_r)$$
(4.37)

A Lyapunov function for the boundary layer system is $V_r = F_{\Theta}^T F_{\Theta}/2$. The derivatives of the Lyapunov function along trajectories in (4.37) and under Assumption 4. is

$$\dot{V}_{r} = -\left(\frac{1}{\varepsilon_{3}}\right) F_{\Theta}^{T} \left(\frac{\partial F_{\Theta}}{\partial u_{r}}\right) \left(\frac{\partial F_{\Theta}}{\partial u_{r}}\right)^{T} F_{\Theta}
+ F_{\Theta}^{T} \left[\left(\frac{\partial F_{\Theta}}{\partial \Theta}\right) \dot{\Theta} + \left(\frac{\partial F_{\Theta}}{\partial \chi}\right) \dot{\chi} - \left(\frac{1}{\varepsilon_{2}}\right) \left(\frac{\partial F_{\Theta}}{\partial u_{t}}\right) \left(\frac{\partial F_{\chi_{d}}}{\partial u_{t}}\right)^{T} F_{\chi_{d}}\right]$$
(4.38)

Then,

$$\dot{V}_r \le -\left(\frac{1}{2\varepsilon_3 \lambda_{\min}(P_r)}\right) V_r + \left(\frac{\delta_1}{\varepsilon_1} + \frac{\delta_2}{\varepsilon_2} + \delta_3\right) \tag{4.39}$$

where $P_r = (\partial F_{\Theta}/\partial u_r)(\partial F_{\Theta}/\partial u_r)^T$; and δ_1 , δ_2 , and δ_3 are positive constants related to the upper bounds for the terms $F_{\Theta}^T(\partial F_{\Theta}/\partial \Theta)\dot{\Theta}$, $F_{\Theta}^T(\partial F_{\Theta}/\partial u_t)(\partial F_{\chi}/\partial u_t)^T F_{\chi}$, and $F_{\Theta}^T(\partial F_{\Theta}/\partial \chi)\dot{\chi}$ and independent of ε_3 . With $\varepsilon_3 \ll \varepsilon_2 \ll \varepsilon_1 \ll 1$, \dot{V}_r is negative with $V_r \neq 0$.

Now the fastest variable u_r reached in the quasi-steady state, i.e. $u_r = u_r^*$ and the other subsystems (4.33), (4.34), and (4.35) are viewed as the reduced system with $\varepsilon_3 = 0$ and $s_r = 0$. The reduce system has a multi-time-scale structure in which (4.35) is fast and the other two, (4.33) and (4.34) are slow. By setting $\varepsilon_2 = 0$, and $s_r = 0$ (i.e., the fastest system reaches the quasi-steady state) on the right-hand side of (4.35), the boundary layer systems for the second fastest dynamic inversion is obtained by

$$\varepsilon_2 \dot{s}_t = -\left(\frac{\partial F_{\chi_d}}{\partial u_t}\right)^T F_{\chi_d}(\Theta, e_{\chi} + \chi_r, s_t + u_t^*, u_c) \tag{4.40}$$

A Lyapunov function $V_t = (F_{\chi_d}^T F_{\chi_d})/2$ is defined and the derivative of the Lyapunov functiono is

$$\dot{V}_{t} = -\left(\frac{1}{\varepsilon_{2}}\right) F_{\chi_{d}}^{T} \left(\frac{\partial F_{\chi_{d}}}{\partial u_{t}}\right) \left(\frac{\partial F_{\chi_{d}}}{\partial u_{t}}\right)^{T} F_{\chi_{d}}
+ F_{\chi_{d}}^{T} \left[\left(\frac{\partial F_{\chi_{d}}}{\partial \Theta}\right) \dot{\Theta} + \left(\frac{\partial F_{\chi_{d}}}{\partial \chi}\right) \dot{\chi} + \left(\frac{\partial F_{\chi_{d}}}{\partial u_{c}}\right) \dot{u}_{c}\right]$$
(4.41)

$$\dot{V}_t \le -\left(\frac{1}{2\varepsilon_2 \lambda_{\min}(P_t)}\right) V_t + \left(\frac{\delta_4}{\varepsilon_1} + \delta_5\right) \tag{4.42}$$

where $P_t = (\partial F_{\chi_d}/\partial u_t)(\partial F_{\chi_d}/\partial u_t)^T$, δ_4 and δ_5 are positive constants related to the upper bounds for the terms $F_{\chi_d}^T(\partial F_{\chi_d}/\partial \Theta)\dot{\Theta}$, $F_{\chi_d}^T(\partial F_{\chi_d}/\partial \chi)\dot{\chi}$, and $F_{\chi_d}^T(\partial F_{\chi_d}/\partial u_c)\dot{u}_c$, and independent of ε_2 . With $\varepsilon_2 \ll \varepsilon_1 \ll 1$, \dot{V}_t is negative with $V_t \neq 0$. Two fast variables u_r and u_t reach in the quasi-steady state, i.e., $u_r = u_r^*$ and $u_t = u_t^*$

$$s_{r} = u_{r} - u_{r}^{*} = \begin{bmatrix} T_{T} - T_{T}^{*} \\ a_{1s} - a_{1s}^{*} \\ b_{1s} - b_{1s}^{*} \end{bmatrix} = 0, \quad s_{t} = u_{t} - u_{t}^{*} = \begin{bmatrix} T_{M} - T_{M}^{*} \\ \phi_{d} - \phi_{r} \\ \theta_{d} - \theta_{r} \end{bmatrix} = 0$$
 (4.43)

With $\Theta_r = [\phi_d, \theta_d, \psi_r]^T$ and $\Theta_r = [\phi_r, \theta_r, \psi_r]^T$ given below (4.28) and (4.43), we obtain $(\Theta_d - \Theta_r) = 0$. Setting $\varepsilon_i = 0$ for $i = 1, 2, s_t = 0$, and $s_r = 0$ on the right-hand side of both (4.33) and (4.34), we obtain the reduce system

$$\dot{e}_{\chi} = A_{\chi} e_{\chi},\tag{4.44}$$

$$\varepsilon_1 \dot{e}_{\Theta} = A_{\Theta} e_{\Theta} - \varepsilon_1^2 \ddot{\Theta}_r - \varepsilon_1 k_2 \dot{\Theta}_r \tag{4.45}$$

Now, in the reduced system, (4.44) and (4.45), the rotational dynamics are faster than the translational dynamics. The boundary layer system for (4.45) is obtained setting $\varepsilon_1 = 0$ on the right-hand side of (4.45),

$$\varepsilon_1 \dot{e}_{\Theta} = A_{\Theta} e_{\Theta} \tag{4.46}$$

which has asymptotic stability at $e_{\Theta} = 0$. Setting $\varepsilon_1 = 0$ and $e_{\Theta} = 0$, the reduced system for (4.44) is

$$\dot{e}_{\chi} = A_{\chi} e_{\chi} \tag{4.47}$$

which is asymptotically stable at $e_{\chi} = 0$. By using a composite Lyapunov function, the effect of the interconnections for the closed-loop system (4.33), (4.34), (4.35), and (4.36), can be considered. The procedure for the effect of the interconnections are similar to the output feedback control stability analysis. So, we omit the procedure which will be shown

in Section 4.4.

4.4 Stability Analysis in the Presence of Disturbances

In this section, output feedback control will be designed using the extended high-gain observer to estimate unmeasured system states and external disturbances. Using the singular perturbation method, stability analysis for the closed-loop system will be conducted.

Let us consider the case where the helicopter dynamics in (4.11) and (4.16) have external disturbances as follows.

$$\dot{\chi} = A\chi + B[F_O(\Theta, u_t) + \sigma_{\chi}(t)]$$

$$y_{\chi} = C\chi$$

$$\dot{\Theta} = A\Theta + B[F_I(\Theta, u_t, u_r) + \sigma_{\Theta}(t)]$$

$$y_{\Theta} = C\Theta$$

$$(4.48)$$

where χ and $F_O(\Theta, u_t)$ for the translational dynamics and Θ and $F_I(\Theta, u_t, u_r)$ for the rotational dynamics are given right after below of (4.11) and (4.16), respectively; y_{χ} and y_{Θ} are measurements; and $C = \text{block diag}[C_1, C_1, C_1]$ is with $C_1 = [1, 0]$. It is assumed that the external disturbances, $\sigma_{\chi}(t) = [\sigma_x, \sigma_y, \sigma_z]^T$ and $\sigma_{\Theta}(t) = [\sigma_\phi, \sigma_\theta, \sigma_\psi]^T$ have the following properties.

Assumption 6. The functions $\sigma_{\chi}(t)$ and $\sigma_{\Theta}(t)$ are continuously differentiable.

4.4.1 Design of Extend High-Gain Observers (EHGOs)

Unknown external disturbances σ_{χ} and σ_{Θ} , and unmeasured states will be estimated using the EHGO

$$\dot{\hat{\chi}} = A\hat{\chi} + B[F_O(\hat{\Theta}, u_t) + \hat{\sigma}_{\chi}(t)] + H_{\chi}(\varepsilon_4)(y_{\chi} - C\hat{\chi})$$

$$\dot{\hat{\sigma}}_{\chi} = H_{\chi_e}(y_{\chi} - C\hat{\chi})$$

$$\dot{\hat{\Theta}} = A\hat{\Theta} + B[F_I(\hat{\Theta}, u_t, u_r) + \hat{\sigma}_{\Theta}(t)] + H_{\Theta}(\varepsilon_4)(y_{\Theta} - C\hat{\Theta})$$

$$\dot{\hat{\sigma}}_{\Theta} = H_{\Theta_e}(y_{\Theta} - C\hat{\Theta})$$
(4.49)

where the estimates of χ and Θ are $\hat{\chi} = [\hat{\chi}_x^T, \hat{\chi}_y^T, \hat{\chi}_z^T]^T$ and $\hat{\Theta} = [\hat{\Theta}_{\phi}^T, \hat{\Theta}_{\theta}^T, \hat{\Theta}_{\psi}^T]^T$, respectively, with

$$\hat{\chi}_x = [\hat{x}_1, \hat{x}_2]^T, \quad \hat{\chi}_y = [\hat{y}_1, \hat{y}_2]^T, \quad \hat{\chi}_z = [\hat{z}_1, \hat{z}_2]^T
\hat{\Theta}_{\phi} = [\hat{\phi}_1, \hat{\phi}_2]^T, \quad \hat{\Theta}_{\theta} = [\hat{\theta}_1, \hat{\theta}_2]^T, \quad \hat{\Theta}_{\psi} = [\hat{\psi}_1, \hat{\psi}_2]^T$$
(4.50)

and $\hat{\sigma}_{\chi} = [\hat{\sigma}_{x}, \hat{\sigma}_{y}, \hat{\sigma}_{z}]^{T}$ and $\hat{\sigma}_{\Theta} = [\hat{\sigma}_{\phi}, \hat{\sigma}_{\theta}, \hat{\sigma}_{\psi}]^{T}$ are estimates of $\sigma_{\chi}(t)$ and $\sigma_{\Theta}(t)$, respectively. The observer gains, H_{χ} , $H_{\chi_{e}}$, H_{Θ} and $H_{\Theta_{e}}$ are given by

$$\begin{split} H_{\chi} &= \operatorname{block} \, \operatorname{diag}[H_1, H_2, H_3], \quad H_{\Theta} = \operatorname{block} \, \operatorname{diag}[H_4, H_5, H_6] \\ H_i &= [h_{i1}/\varepsilon_4, h_{i2}/\varepsilon_4^2]^T, \quad \text{for} \ i = 1, \dots, 6 \\ H_{\chi_e} &= \operatorname{block} \, \operatorname{diag}[h_{13}/\varepsilon_4^3, h_{23}/\varepsilon_4^3, h_{33}/\varepsilon_4^3], \quad H_{\Theta_e} = \operatorname{block} \, \operatorname{diag}[h_{43}/\varepsilon_4^3, h_{53}/\varepsilon_4^3, h_{63}/\varepsilon_4^3] \end{split} \tag{4.51}$$

where the components h_{i1} , h_{i2} , and h_{i3} of the high gains are chosen such that the polynomials

$$\lambda^3 + h_{i,1}\lambda^2 + h_{i,2}\lambda + h_{i,3}$$
 for $i = 1, \dots, 6$ (4.52)

are Hurwitz and the control parameter $\varepsilon_4 > 0$ is small enough. The relation between ε_3 and ε_4 is $\varepsilon_4 \ll \varepsilon_3 \ll 1$ since the dynamic inversion uses estimates provided by the EHGO.

4.4.2 Output feedback control

With the EHGO in (4.49), the output feedback control, based on the dynamic inversion, is designed as

$$\varepsilon_{2}\dot{u}_{t} = -\left(\frac{\partial F_{\chi_{d}}}{\partial u_{t}}\right)^{T} F_{\chi_{s}}(\Theta_{s}, \chi_{s}, u_{t}, u_{c}, \hat{\sigma}_{\chi_{s}})$$

$$\varepsilon_{3}\dot{u}_{r} = -\left(\frac{\partial F_{\Theta}}{\partial u_{r}}\right)^{T} F_{\Theta_{s}}(\Theta_{s}, u_{t}, u_{r}, \psi_{r}, \hat{\sigma}_{\Theta_{s}})$$

$$(4.53)$$

where

$$\Theta_{s} = \left[\Theta_{\phi_{s}}^{T}, \Theta_{\theta_{s}}^{T}, \Theta_{\psi_{s}}^{T}\right]^{T} \quad \chi_{s} = \left[\chi_{x_{s}}^{T}, \chi_{y_{s}}^{T}, \chi_{z_{s}}^{T}\right]^{T} \\
\Theta_{\phi_{s}} = \begin{bmatrix} \phi_{1} \\ M_{\phi} \text{sat} \left(\frac{\hat{\phi}_{2}}{M_{\phi}}\right) \end{bmatrix}, \quad \Theta_{\theta_{s}} = \begin{bmatrix} \theta_{1} \\ M_{\theta} \text{sat} \left(\frac{\hat{\theta}_{2}}{M_{\theta}}\right) \end{bmatrix}, \quad \Theta_{\psi_{s}} = \begin{bmatrix} \psi_{1} \\ M_{\psi} \text{sat} \left(\frac{\hat{\psi}_{2}}{M_{\psi}}\right) \end{bmatrix} \\
\chi_{x_{s}} = \begin{bmatrix} x_{1} \\ M_{x} \text{sat} \left(\frac{\hat{x}_{2}}{M_{x}}\right) \end{bmatrix}, \quad \chi_{y_{s}} = \begin{bmatrix} y_{1} \\ M_{y} \text{sat} \left(\frac{\hat{y}_{2}}{M_{y}}\right) \end{bmatrix}, \quad \chi_{z_{s}} = \begin{bmatrix} z_{1} \\ M_{z} \text{sat} \left(\frac{\hat{z}_{2}}{M_{z}}\right) \end{bmatrix},$$

$$\hat{\sigma}_s = [\hat{\sigma}_{\chi_s}^T, \hat{\sigma}_{\Theta_s}^T]^T$$

$$\hat{\sigma}_{\chi_s} = \begin{bmatrix} M_1 \operatorname{sat}(\hat{\sigma}_x/M_1) \\ M_2 \operatorname{sat}(\hat{\sigma}_y/M_2) \\ M_3 \operatorname{sat}(\hat{\sigma}_z/M_3) \end{bmatrix}, \quad \hat{\sigma}_{\Theta_s} = \begin{bmatrix} M_4 \operatorname{sat}(\hat{\sigma}_\phi/M_4) \\ M_5 \operatorname{sat}(\hat{\sigma}_\theta/M_5) \\ M_6 \operatorname{sat}(\hat{\sigma}_\psi/M_6) \end{bmatrix}, \quad (4.55)$$

and F_{χ_s} and F_{Θ_s} are

$$F_{\chi_s} = \begin{bmatrix} f_x(\phi_d, \theta_d, \psi_1, T_M) + M_1 \operatorname{sat}(\hat{\sigma}_x/M_1) + k_{x_1}x_1 + k_{x_2}M_x \operatorname{sat}(\hat{x}_2/M_x) - r_x(t) \\ f_y(\phi_d, \theta_d, \psi_1, T_M) + M_2 \operatorname{sat}(\hat{\sigma}_y/M_2) + k_{y_1}y_1 + k_{y_2}M_y \operatorname{sat}(\hat{y}_2/M_y) - r_y(t) \\ f_z(\phi_d, \theta_d, \psi_1, T_M) + M_3 \operatorname{sat}(\hat{\sigma}_z/M_3) + k_{z_1}y_1 + k_{z_2}M_z \operatorname{sat}(\hat{z}_2/M_z) - r_z(t) \end{bmatrix}$$
(4.56)

$$F_{\Theta_s} = \begin{bmatrix} f_{\phi}(\Theta, u_t, u_r) + M_4 \operatorname{sat}(\hat{\sigma}_{\phi}/M_4) + k_{\phi_1}(\phi_1 - \phi_d) + k_{\phi_2} M_{\phi} \operatorname{sat}(\hat{\phi}_2/M_{\phi}) \\ f_{\theta}(\Theta, u_t, u_r) + M_5 \operatorname{sat}(\hat{\sigma}_{\theta}/M_5) + k_{\theta_1}(\theta_1 - \theta_d) + k_{\theta_2} M_{\theta} \operatorname{sat}(\hat{\theta}_2/M_{\theta}) \\ f_{\psi}(\Theta, u_t, u_r) + M_6 \operatorname{sat}(\hat{\sigma}_{\psi}/M_6) + k_{\psi_1}(\psi_1 - \psi_d) + k_{\psi_2} M_{\psi} \operatorname{sat}(\hat{\psi}_2/M_{\psi}) \end{bmatrix}$$

$$(4.57)$$

The saturation function, $sat(\cdot)$ is defined by

$$\operatorname{sat}(k) = \begin{cases} k & |k| \le 1\\ \operatorname{sign}(k) & |k| > 1 \end{cases}$$

$$(4.58)$$

The saturation levels M_j for $j = \phi, \theta, \psi, x, y, z, 1, 2, ..., 6$ are determined such that the saturation function will not be activated under the state feedback.

4.4.3 Stability analysis in the presence of disturbances

The fast error variables $\eta = [\eta_\chi^T, \eta_\Theta^T]^T$ for the EHGO are given by

$$\eta_{\chi} = [\eta_{x}^{T}, \eta_{y}^{T}, \eta_{z}^{T}]^{T}, \quad \eta_{\Theta} = [\eta_{\phi}^{T}, \eta_{\theta}^{T}, \eta_{\psi}^{T}]^{T}$$

$$\eta_{x} = [\eta_{x_{1}}, \eta_{x_{2}}, \eta_{x_{3}}]^{T}, \quad \eta_{y} = [\eta_{y_{1}}, \eta_{y_{2}}, \eta_{y_{3}}]^{T}, \quad \eta_{z} = [\eta_{z_{1}}, \eta_{z_{2}}, \eta_{z_{3}}]^{T}$$

$$\eta_{\phi} = [\eta_{\phi_{1}}, \eta_{\phi_{2}}, \eta_{\phi_{3}}]^{T}, \quad \eta_{\theta} = [\eta_{\theta_{1}}, \eta_{\theta_{2}}, \eta_{\theta_{3}}]^{T}, \quad \eta_{\psi} = [\eta_{\psi_{1}}, \eta_{\psi_{2}}, \eta_{\psi_{3}}]^{T}$$

$$(4.59)$$

where

$$\eta_{x_{1}} = \frac{x_{1} - \hat{x}_{1}}{\varepsilon_{4}^{2}}, \quad \eta_{x_{2}} = \frac{x_{2} - \hat{x}_{2}}{\varepsilon_{4}}, \quad \eta_{x_{3}} = \sigma_{x}(t) - \hat{\sigma}_{x}(t)
\eta_{y_{1}} = \frac{y_{1} - \hat{y}_{1}}{\varepsilon_{4}^{2}}, \quad \eta_{y_{2}} = \frac{y_{2} - \hat{y}_{2}}{\varepsilon_{4}}, \quad \eta_{y_{3}} = \sigma_{y}(t) - \hat{\sigma}_{y}(t)
\eta_{z_{1}} = \frac{z_{1} - \hat{z}_{1}}{\varepsilon_{4}^{2}}, \quad \eta_{z_{2}} = \frac{z_{2} - \hat{z}_{2}}{\varepsilon_{4}}, \quad \eta_{z_{3}} = \sigma_{z}(t) - \hat{\sigma}_{z}(t)$$
(4.60)

and

$$\eta_{\phi_1} = \frac{\phi_1 - \hat{\phi}_1}{\varepsilon_4^2}, \quad \eta_{\phi_2} = \frac{\phi_2 - \hat{\phi}_2}{\varepsilon_4}, \quad \eta_{\phi_3} = \sigma_{\phi}(t) - \hat{\sigma}_{\phi}(t)$$

$$\eta_{\theta_1} = \frac{\theta_1 - \hat{\theta}_1}{\varepsilon_4^2}, \quad \eta_{\theta_2} = \frac{\theta_2 - \hat{\theta}_2}{\varepsilon_4}, \quad \eta_{\theta_3} = \sigma_{\theta}(t) - \hat{\sigma}_{\theta}(t)$$

$$\eta_{\psi_1} = \frac{\psi_1 - \hat{\psi}_1}{\varepsilon_4^2}, \quad \eta_{\psi_2} = \frac{\psi_2 - \hat{\psi}_2}{\varepsilon_4}, \quad \eta_{\psi_3} = \sigma_{\psi}(t) - \hat{\sigma}_{\psi}(t)$$
(4.61)

Error dynamics for the EHGO are

$$\varepsilon_4 \dot{\eta} = \Lambda \eta + \varepsilon_4 [\bar{B}_1 \Delta_1 + \bar{B}_2 \Delta_2] \tag{4.62}$$

where $\Lambda = \text{block diag}[A, A] \in \mathbf{R}^{18 \times 18}$,

$$\bar{B}_1 = \text{block diag}[B_{e_1}, \dots, B_{e_1}] \in \mathbf{R}^{18 \times 6}, \quad B_{e_1} = [0, 1, 0]^T$$

$$\bar{B}_2 = \text{block diag}[B_{e_2}, \dots, B_{e_2}] \in \mathbf{R}^{18 \times 6}, \quad B_{e_2} = [0, 0, 1]^T$$
(4.63)

$$\Delta_{1} = \begin{bmatrix}
(f_{x}(\phi_{1}, \theta_{1}, \psi_{1}, T_{M}) - f_{x}(\hat{\phi}_{1}, \hat{\theta}_{1}, \hat{\psi}_{1}, T_{M}))/\varepsilon_{4} \\
(f_{y}(\phi_{1}, \theta_{1}, \psi_{1}, T_{M}) - f_{y}(\hat{\phi}_{1}, \hat{\theta}_{1}, \hat{\psi}_{1}, T_{M}))/\varepsilon_{4} \\
(f_{z}(\phi_{1}, \theta_{1}, T_{M}) - f_{z}(\hat{\phi}_{1}, \hat{\theta}_{1}, T_{M}))/\varepsilon_{4} \\
(f_{\phi}(\Theta, u) - f_{\phi}(\hat{\Theta}, u))/\varepsilon_{4} \\
(f_{\theta}(\Theta, u) - f_{\theta}(\hat{\Theta}, u))/\varepsilon_{4} \\
(f_{\psi}(\Theta, u) - f_{\psi}(\hat{\Theta}, u))/\varepsilon_{4}
\end{bmatrix}, \quad \Delta_{2} = \begin{bmatrix} \dot{\sigma}_{x} \\ \dot{\sigma}_{y} \\ \dot{\sigma}_{z} \\ \dot{\sigma}_{\phi} \\ \dot{\sigma}_{\theta} \\ \dot{\sigma}_{\theta} \\ \dot{\sigma}_{\theta} \end{bmatrix}$$

$$(4.64)$$

We note that the components of Δ_1 , i.e., $(f_i(\Theta, u) - f_i(\hat{\Theta}, u))$ for $i = x, y, z, \phi, \theta, \psi$, have the bound $||f_i(\Theta, u) - f_i(\hat{\Theta}, u)|| \le \varepsilon_4 ||\eta||$, and $||\Delta_2|| \le k_\delta$ with $k_\delta > 0$.

Using the target system of (4.14), the plant dynamics (4.48), and (4.53) with the error

variables e_{χ} , e_{Θ} , and s, the closed-loop system is presented in the singularly perturbed form

$$\dot{e}_{\chi} = A_{\chi} e_{\chi} + BF_{\chi}(\Theta, e_{\chi} + \chi_r, u_t, u_c, \sigma_{\chi}(t)) \tag{4.65}$$

$$\varepsilon_1 \dot{e}_{\Theta} = A_{\theta} e_{\Theta} + B[k_1(\Theta_d - \Theta_r) + \varepsilon_1^2 F_{\Theta}(\Theta, u_t, u_r, \psi_r, \sigma_{\Theta}(t)) - \varepsilon_1^2 \ddot{\Theta}_r - \varepsilon_1 k_2 \dot{\Theta}_r]$$
(4.66)

$$\varepsilon_2 \dot{s}_t = -\left(\frac{\partial F_{\chi_d}}{\partial u_t}\right)^T F_{\chi_d}(\Theta, e_\chi + \chi_r, s_t + u_t^*, u_c, \sigma_\chi) + \Delta_{\sigma_\chi} + \Delta_\chi - \varepsilon_2 \dot{u}_t^* \tag{4.67}$$

$$\varepsilon_{3}\dot{s}_{r} = -\left(\frac{\partial F_{\Theta}}{\partial u_{r}}\right)^{T} F_{\Theta}(\Theta, s_{t} + u_{t}^{*}, s_{r} + u_{r}^{*}, \psi_{r}, \sigma_{\Theta}) + \Delta_{\sigma_{\Theta}} + \Delta_{\Theta} - \varepsilon_{3}\dot{u}_{r}^{*}$$

$$(4.68)$$

$$\varepsilon_4 \dot{\eta} = \Lambda \eta + \varepsilon_4 [\bar{B}_1 \Delta_1 + \bar{B}_2 \Delta_2] \tag{4.69}$$

where F_{χ} and F_{Θ} are given in (4.26) and (4.21), respectively and u_t^* and u_r^* are satisfied with

$$F_{\chi}(\Theta, \chi, u_t^*, u_c, \sigma_{\chi}) = 0, \quad F_{\Theta}(\Theta, u_t, u_r^*, \psi_r, \sigma_{\Theta}) = 0, \tag{4.70}$$

$$\Delta_{\sigma_{\chi}} = \begin{bmatrix}
M_{1} \operatorname{sat} \left(\frac{\hat{\sigma}_{x}}{M_{1}}\right) - \sigma_{x} \\
M_{2} \operatorname{sat} \left(\frac{\hat{\sigma}_{y}}{M_{2}}\right) - \sigma_{y} \\
M_{3} \operatorname{sat} \left(\frac{\hat{\sigma}_{z}}{M_{3}}\right) - \sigma_{z}
\end{bmatrix}, \quad \Delta_{\sigma_{\Theta}} = \begin{bmatrix}
M_{4} \operatorname{sat} \left(\frac{\hat{\sigma}_{\phi}}{M_{4}}\right) - \sigma_{\phi} \\
M_{5} \operatorname{sat} \left(\frac{\hat{\sigma}_{y}}{M_{5}}\right) - \sigma_{\theta} \\
M_{6} \operatorname{sat} \left(\frac{\hat{\sigma}_{z}}{M_{6}}\right) - \sigma_{\psi}
\end{bmatrix}$$

$$(4.71)$$

$$\Delta_{\chi} = \begin{bmatrix} k_{x_2} \left(M_x \operatorname{sat} \left(\frac{\hat{x}_2}{M_x} \right) - x_2 \right) \\ k_{y_2} \left(M_y \operatorname{sat} \left(\frac{\hat{y}_2}{M_y} \right) - y_2 \right) \\ k_{z_2} \left(M_z \operatorname{sat} \left(\frac{\hat{z}_2}{M_z} \right) - z_2 \right) \end{bmatrix}, \quad \Delta_{\Theta} = \begin{bmatrix} k_{\phi_2} \left(M_\phi \operatorname{sat} \left(\frac{\hat{\phi}_2}{M_\phi} \right) - \phi_2 \right) \\ k_{\theta_2} \left(M_\phi \operatorname{sat} \left(\frac{\hat{\theta}_2}{M_\theta} \right) - \theta_2 \right) \\ k_{\psi_2} \left(M_\phi \operatorname{sat} \left(\frac{\hat{\psi}_2}{M_z} \right) - \psi_2 \right) \end{bmatrix} \tag{4.72}$$

Now, the next theorem states the stability analysis for the closed-loop system (4.65), (4.66), (4.67), (4.67), and (4.69).

Theorem 3. Consider the closed-loop system (4.65), (4.66), (4.67), (4.67), and (4.69) under

the Assumption 4, 5, and 6. There exists ε^* such that all

$$\varepsilon_1 < \varepsilon^*, \quad \varepsilon_2 < \varepsilon^*, \quad \varepsilon_3 < \varepsilon^*, \quad \varepsilon_4 < \varepsilon^*$$

$$(\varepsilon_2/\varepsilon_1) < \varepsilon^*, \quad (\varepsilon_3/\varepsilon_2) < \varepsilon^*, \quad (\varepsilon_4/\varepsilon_3) < \varepsilon^*$$
(4.73)

and for all initial states $(\chi(0), \Theta(0)) \in X_1$, $(u_t(0), u_r(0)) \in X_2$, and $(\hat{\chi}(0), \hat{\Theta}(0)) \in X_3$, where X_1 is a compact set of (χ, Θ) in the domain $D_{\chi} \times D_{\Theta}$, X_2 is any compact subset of \mathbb{R}^2 , and X_3 is any compact subset of \mathbb{R}^{18} , all trajectories are bounded and the size of the ultimate boundedness for error state variables in the error dynamics can be arbitrarily small with sufficiently small ε_i for $i = 1, \ldots, 4$ and $(\varepsilon_2/\varepsilon_1)$, $(\varepsilon_3/\varepsilon_2)$, $(\varepsilon_4/\varepsilon_3)$.

Proof. We consider Lyapunov functions $V_{\chi} = e_{\chi}^T P_{\chi} e_{\chi}$, $V_{\Theta} = e_{\Theta}^T P_{\chi} e_{\Theta}$, and $V_{\eta} = \eta^T P_{\eta} \eta$ where P_{χ} , P_{Θ} , and P_{η} are solutions of the Lyapunov equations, $A_{\chi}^T P_{\chi} + P_{\chi} A_{\chi} = -I$, $A_{\Theta}^T P_{\Theta} + P_{\Theta} A_{\Theta} = -I$, and $\Lambda^T P_{\eta} + P_{\eta} \Lambda = -I$. Since we are going to use a time-scale separation approach between subsystems, sets are defined by

$$\Omega_{a} = \{V_{\chi} \leq a_{1}\} \times \{V_{\Theta} \leq a_{2}\} \times \{V_{t} \leq a_{3}\} \times \{V_{r} \leq a_{4}\}$$

$$\Omega_{b} = \{V_{\chi} \leq b_{1}\} \times \{V_{\Theta} \leq b_{2}\} \times \{V_{t} \leq b_{3}\} \times \{V_{r} \leq b_{4}\}$$

$$\Omega_{c} = \{V_{\chi} \leq c_{1}\} \times \{V_{\Theta} \leq c_{2}\} \times \{V_{t} \leq c_{3}\}$$

$$\Omega_{d} = \{V_{\chi} \leq d_{1}\} \times \{V_{\Theta} \leq d_{2}\}$$

$$(4.74)$$

with

$$0 < a_1 < b_1 < c_1 < d_1, \quad 0 < a_2 < b_2 < c_2 < d_2, \quad 0 < a_3 < b_3 < c_3, \quad o < a_4 < b_4 \quad (4.75)$$

To consider relations between the trajectories χ and e_{χ} , and Θ and e_{Θ} , the constants m_1 and m_2 are chosen such that

$$(e_{\chi}, e_{\Theta}) \in \{V_{\chi} \le a_1\} \times \{V_{\Theta} \le a_2\} \Longrightarrow (\chi, \Theta) \in X_1 \tag{4.76}$$

Now, we briefly describe the process of the proof for the boundedness of trajectories using the next steps:

- initially, the trajectories $(e_{\chi}, e_{\Theta}, s_t, s_r)$ and η starting from $(e_{\chi}(0), e_{\Theta}(0), s_t(0), s_r(0)) \in \Omega_a$ and $\eta(0)$ from the outside of the set of $\{V_{\eta} \in \rho \varepsilon_4^2\}$, enter the set $\Omega_b \times \{V_{\eta} \leq \rho_1 \varepsilon_4^2\}$;
- secondly, the trajectories $(e_{\chi}, e_{\Theta}, s_t, s_r)$ and η starting from $\Omega_b \times \{V_{\eta} \leq \rho \varepsilon_4^2\}$ enter the set $\Omega_c \times \{V_r \leq \rho_2 \mu_1^2\} \times \{V_n \leq \rho_1 \varepsilon_4^2\}$ with $\mu_1 = (\varepsilon_3/\varepsilon_2)$;
- thirdly, the trajectories $(e_{\chi}, e_{\Theta}, s_t, s_r)$ and η starting from $\Omega_c \times \{V_r \leq \rho_2 \mu_1^2\} \times \{V_{\eta} \leq \rho_1 \varepsilon_4^2\}$ enter the set $\Omega_d \times \{V_t \leq \rho_3 \mu_2^2\} \times \{V_r \leq \rho_2 \mu_1^2\} \times \{V_{\eta} \leq \rho_1 \varepsilon_4^2\}$ with $\mu_2 = (\varepsilon_2/\varepsilon_1)$;
- lastly, the trajectories $(e_{\chi}, e_{\Theta}, s_t, s_r)$ and η starting from $\Omega_d \times \{V_t \leq \rho_3 \mu_2^2\} \times \{V_r \leq \rho_2 \mu_1^2\} \times \{V_{\eta} \leq \rho_1 \varepsilon_4^2\}$ enter the set $\{V_{\chi} \leq e_1\} \times \{V_{\Theta} \leq e_2 \varepsilon_1^2\} \times \{V_t \leq \rho_3 \mu_2^2\} \times \{V_r \leq \rho_2 \mu_1^2\} \times \{V_{\eta} \leq \rho_1 \varepsilon_4^2\}$, where e_1 and e_2 are positive constants.

Since these above four steps are similar, we are going to show only the first bullet and the others will be omitted. In the first step, initial trajectories $(e_{\chi}, e_{\Theta}, s_t, s_r)$ and η start from the set $(e_{\chi}(0), e_{\Theta}(0), s_t(0), s_r(0)) \in \Omega_a$ and $\eta \notin \{V_{\eta} \in \rho \varepsilon_4^2\}$ with $\|\eta(0)\| \leq (k/\varepsilon_4^2)$. The derivative of V_{η} along the trajectories (4.65), (4.66), (4.67), (4.68), and (4.69) is

$$\dot{V}_{\eta} = -\left(\frac{1}{\varepsilon_4}\right)\eta^T \eta + (\bar{B}_1 \Delta_1 + \bar{B}_2 \Delta_2)^T P_{\eta} \eta \tag{4.77}$$

Using the bound of the term $(\bar{B}_1\Delta_1 + \bar{B}_2\Delta_2)$ in (4.69) for all $(e_{\chi}, e_{\Theta}, s_t, s_r) \in \Omega_a$, i.e., $k_{o_1} ||\eta|| + k_{o_2}$ for some positive constants k_{o_1} and k_{o_2} , we obtain

$$\dot{V}_{\eta} \leq -\frac{1}{\varepsilon_4} \|\eta\|^2 + k_{o_3} \|\eta\|^2 + k_{o_4} \|\eta\|
\leq -\frac{1}{2\varepsilon_4} \|\eta\|^2 + k_{o_4} \|\eta\| \quad \text{for } \varepsilon_4 < \frac{1}{2k_{o_3}}$$
(4.78)

where k_{o_i} for i = 1, ..., 4 are positive constants. With $\varepsilon_4 < 1/(2k_{o_3})$,

$$\dot{V}_{\eta} \le -\left(\frac{\gamma_1}{\varepsilon_4}\right) V_{\eta}, \quad \text{for } V_{\eta} \ge \rho_1 \varepsilon_4^2$$
 (4.79)

where $\rho_1 = P_{\eta_m}^2 \gamma_2^2$, some $\gamma_1 > 0$, $\gamma_2 > 0$, and $P_{\eta_m} = \lambda_{\max}(P_{\eta})$. As previous works of the high-gain observers, the trajectory η starts from the outside of the set $\{V_{\eta} \leq \rho \varepsilon_4^2\}$ with $\|\eta(0)\| \leq (k/\varepsilon_4^2)$ and enters into the set $\Omega_b \times \{V_{\eta} \leq \rho_1 \varepsilon_4^2\}$ in a finite time $T(\varepsilon_4)$. As $\varepsilon_4 \to 0$, $T(\varepsilon_4) \to 0$. Since the proof of the finite time convergence is similar to previous Chapter 2 and 3, the proof is omitted.

For the second bullet, since the trajectory η cannot leave the set $\{V_{\eta} \leq \rho_1 \varepsilon_4^2\}$, η has the upper bound, $\|\eta\| \leq 4k_{o_4}\varepsilon_4$. With this upper bound, the similar procedure can be used to prove the second bullet so that the proof for the rest of them will be omitted. All trajectories enter the set, $\{V_{\chi} \leq e_1\} \times \{V_{\Theta} \leq e_2 \varepsilon_1^2\} \times \{V_t \leq \rho \mu_2^2\} \times \{V_r \leq \rho \mu_1^2\} \times \{V_{\eta} \leq \rho_1 \varepsilon_4^2\}$, which can be taken as a positively invariant set.

We are going to show that the size of the ultimate boundedness can be arbitrarily small with sufficient small control parameters, $0 < \varepsilon_4 \ll \varepsilon_3 \ll \varepsilon_2 \ll \varepsilon_1 \ll 1$. Consider the derivative of the Lyapunov function V_{χ} along the trajectories (4.65), (4.66), (4.67), (4.68), and (4.69) is

$$\dot{V}_{\chi} = -e_{\chi}^{T} e_{\chi} + 2F_{\chi}^{T}(\Theta, e_{\chi} + \chi_{r}, u_{t}, u_{c}, \sigma_{\chi})_{\chi} B^{T} P_{\chi} e_{\chi}
\leq -\|e_{\chi}\|^{2} + 2P_{\chi_{m}}(k_{\chi_{1}} \|e_{\Theta}\| + k_{\chi_{2}} \|s_{t}\|) \|e_{\chi}\|$$
(4.80)

where $||P_{\chi}|| \leq P_{\chi_m}$ and some positive constants $k_{\chi_1} > 0$ and $k_{\chi_2} > 0$. The derivative of the Lyapunov function V_{Θ} along the trajectories (4.65), (4.66), (4.67), (4.68), and (4.69), is

$$\dot{V}_{\Theta} = -\left(\frac{1}{\varepsilon_{1}}\right) e_{\Theta}^{T} e_{\Theta} + 2\left[\varepsilon_{1} (F_{\Theta}^{T} - \ddot{\Theta}_{r}^{T}) - k_{2} \dot{\Theta}_{r}^{T} + \left(\frac{2k_{1}}{\varepsilon_{1}}\right) (\Theta_{d} - \Theta_{r})^{T}\right] B^{T} P_{\Theta} e_{\Theta}
\leq -\left(\frac{1}{\varepsilon_{1}}\right) \|e_{\Theta}\|^{2} + \left[\varepsilon_{1} k_{\Theta_{1}} (\|F_{\Theta}\| + \Theta_{r_{1}}) + k_{\Theta_{2}} \Theta_{r_{2}} + \left(\frac{k_{\Theta_{3}}}{\varepsilon_{1}}\right) \|s_{t}\|\right] \|e_{\Theta}\|$$
(4.81)

where k_{Θ_i} for i = 1, 2, 3 are positive constants. The derivative of the Lyapunov function V_t along the trajectories (4.65), (4.66), (4.67), (4.68), and (4.69), is

$$\dot{V}_{t} = -\left(\frac{1}{\varepsilon_{2}}\right) F_{\chi_{d}}^{T} \left(\frac{\partial F_{\chi_{d}}}{\partial u_{t}}\right) \left(\frac{\partial F_{\chi_{d}}}{\partial u_{t}}\right)^{T} F_{\chi_{d}} - \left(\frac{1}{\varepsilon_{2}}\right) F_{\chi_{d}}^{T} \left(\frac{\partial F_{\chi_{d}}}{\partial u_{t}}\right) \left(\frac{\partial F_{\chi_{d}}}{\partial u_{t}}\right)^{T} \left(F_{\chi_{s}} - F_{\chi_{d}}\right)
+ F_{\chi_{d}}^{T} \left(\frac{\partial F_{\chi_{d}}}{\partial \Theta}\right) \left\{ \left(\frac{1}{\varepsilon_{1}}\right) \left[A_{\Theta}e_{\Theta} + k_{1}B(\Theta_{d} - \Theta_{r})\right] + \left[\varepsilon_{1}(F_{\Theta} - \ddot{\Theta}_{r}) + \dot{\Theta}_{r} + \ddot{\Theta}_{r}(t)\right] \right\}
+ F_{\chi_{d}}^{T} \left(\frac{\partial F_{\chi_{d}}}{\partial \chi}\right) \left[A_{\chi}e_{\chi} + F_{\chi} + \chi_{r}\right] + F_{\chi_{d}}^{T} \left\{ \left(\frac{\partial F_{\chi_{d}}}{\partial u_{c}}\right) \dot{u}_{c} + \left(\frac{\partial F_{\chi_{d}}}{\partial \sigma_{\chi}}\right) \dot{\sigma}_{\chi} \right\},$$

$$(4.82)$$

Using the bounds, \dot{V}_t is

$$\dot{V}_{t} \leq -\left(\frac{k_{t_{1}}}{\varepsilon_{2}}\right) \|F_{\chi_{d}}\|^{2} + \left(\frac{k_{t_{2}}}{\varepsilon_{2}}\right) \|F_{\chi_{d}}\| (\Delta_{\sigma_{\chi}} + \Delta_{\chi})
+ \left[\left(\frac{1}{\varepsilon_{1}}\right) (k_{t_{3}} \|e_{\Theta}\| + k_{t_{4}} \|s_{t}\|) + \varepsilon_{1} k_{t_{5}} (\|F_{\Theta}\| + \Theta_{r_{1}}(t)) + k_{t_{6}} \bar{\Theta}_{1}(t)\right] \|F_{\chi_{d}}\|
+ \left[k_{t_{7}} \|e_{\chi}\| + k_{t_{8}} (k_{\chi_{1}} \|e_{\Theta}\| + k_{\chi_{2}} \|s_{t}\|)\right] \|F_{\chi_{d}}\| + k_{t_{9}} \Delta_{t}(t) \|F_{\chi_{d}}\|$$
(4.83)

where k_{t_i} for i = 1, ..., 9 are positive constants, the bounds for $\Delta_{\sigma_{\chi}}$ and Δ_{χ} are $\Delta_{\sigma_{\chi}} \leq k_{t_{10}} \|\eta\|$ with $k_{t_{10}} > 0$ and $\Delta_{\chi} \leq \varepsilon_3 \|\eta\|$ after the saturation active period for the EHGO. The derivative of the Lyapunov function V_r along the trajectories (4.65), (4.66), (4.67), (4.68), and (4.69), is

$$\dot{V}_{r} = -\left(\frac{1}{\varepsilon_{3}}\right) F_{\Theta}^{T} \left(\frac{\partial F_{\Theta}}{\partial u_{r}}\right) \left(\frac{\partial F_{\Theta}}{\partial u_{r}}\right)^{T} F_{\Theta} - \left(\frac{1}{\varepsilon_{3}}\right) F_{\Theta}^{T} \left(\frac{\partial F_{\Theta}}{\partial u_{r}}\right) \left(\frac{\partial F_{\Theta}}{\partial u_{r}}\right)^{T} \left[F_{\Theta_{s}} - F_{\Theta}\right]
- \left(\frac{1}{\varepsilon_{2}}\right) F_{\Theta}^{T} \left(\frac{\partial F_{\Theta}}{\partial u_{t}}\right) \left(\frac{\partial F_{\chi_{d}}}{\partial u_{t}}\right)^{T} F_{\chi_{d}} + F_{\Theta}^{T} \left[\left(\frac{\partial F_{\Theta}}{\partial \psi_{r}}\right) \dot{\psi}_{r} + \left(\frac{\partial F_{\Theta}}{\partial \sigma_{\Theta}}\right) \dot{\sigma}_{\Theta}\right]
+ F_{\Theta}^{T} \left(\frac{\partial F_{\Theta}}{\partial \Theta}\right) \left\{\left(\frac{1}{\varepsilon_{1}}\right) \left[A_{\Theta} e_{\Theta} + k_{1} B(\Theta_{d} - \Theta_{r})\right] + \left[\varepsilon_{1} (F_{\Theta} - \ddot{\Theta}_{r}) + \dot{\Theta}_{r} + \ddot{\Theta}_{r}(t)\right]\right\}$$

$$(4.84)$$

Then, inequality for \dot{V}_r is

$$\dot{V}_{r} \leq -\left(\frac{k_{r_{1}}}{\varepsilon_{3}}\right) \|F_{\Theta}\|^{2} + \left(\frac{k_{r_{2}}}{\varepsilon_{3}}\right) \|F_{\Theta}\| (\Delta_{\sigma_{\Theta}} + \Delta_{\Theta}) + \left(\frac{k_{r_{3}}}{\varepsilon_{2}}\right) \|F_{\Theta}\| \|F_{\chi_{d}}\|
+ \left[\left(\frac{1}{\varepsilon_{1}}\right) (k_{r_{4}} \|e_{\Theta}\| + k_{r_{5}} \|s_{t}\|) + \varepsilon_{1} k_{r_{6}} (\|F_{\Theta}\| + k_{r_{7}} \Theta_{r_{1}})\right] \|F_{\Theta}\| + \bar{\Theta}_{2}(t) \|F_{\Theta}\|$$
(4.85)

where k_{r_i} for $i=1,\ldots,7$ are positive constants, $\Delta_{\sigma_{\Theta}}$ and Δ_{Θ} become $\Delta_{\sigma_{\Theta}} \leq k_{\Theta_8} \|\eta\|$ and $\Delta_{\Theta} \leq \varepsilon_4 k_{\Theta_9} \|\eta\|$ after passing the transient period for the EHGOs. Using the method in Section 9.3 of in [33] with (4.78), (4.80), (4.81), (4.83), (4.85) and choosing $W_1 = \sqrt{V_{\chi}}$, $W_2 = \sqrt{V_{\Theta}}$, $W_3 = \sqrt{V_t}$, $W_4 = \sqrt{V_r}$, and $W_5 = \sqrt{V_{\eta}}$, we obtain

$$D^{+}W_{1} \leq -\bar{k}_{a_{1}}W_{1} + \bar{k}_{a_{2}}W_{2} + \bar{k}_{a_{3}}W_{3}$$

$$D^{+}W_{2} \leq -\left(\frac{\bar{k}_{b_{1}}}{\varepsilon_{1}}\right)W_{2} + \varepsilon_{1}\bar{k}_{b_{2}}W_{4} + \left(\frac{\bar{k}_{b_{3}}}{\varepsilon_{1}}\right)W_{3} + \varepsilon_{1}\bar{k}_{b_{4}}\bar{\delta}_{1}(t) + \bar{k}_{b_{5}}\bar{\delta}_{2}(t)$$

$$D^{+}W_{3} \leq -\left(\frac{\bar{k}_{c_{1}}}{\varepsilon_{2}} - \frac{\bar{k}_{c_{2}}}{\varepsilon_{1}} - \bar{k}_{c_{3}}\right)W_{3} + \left(\frac{\bar{k}_{c_{4}} + \varepsilon_{4}\bar{k}_{c_{5}}}{\varepsilon_{2}}\right)W_{5} + \varepsilon_{1}\bar{k}_{c_{6}}W_{4}$$

$$+\left(\frac{\bar{k}_{c_{7}}}{\varepsilon_{1}} + \bar{k}_{c_{8}}\right)W_{2} + \bar{k}_{c_{9}}W_{1} + \varepsilon_{1}\bar{k}_{c_{10}}\bar{\delta}_{3}(t) + \bar{k}_{c_{11}}\bar{\delta}_{4}(t)$$

$$D^{+}W_{4} \leq -\left(\frac{\bar{k}_{d_{1}}}{\varepsilon_{3}} - \varepsilon_{1}\bar{k}_{d_{2}}\right)W_{4} + \left(\frac{\bar{k}_{d_{3}} + \bar{k}_{d_{4}}\varepsilon_{4}}{\varepsilon_{3}}\right)W_{5} + \left(\frac{\bar{k}_{d_{5}}}{\varepsilon_{2}} + \frac{\bar{k}_{d_{6}}}{\varepsilon_{1}}\right)W_{3} + \left(\frac{\bar{k}_{d_{7}}}{\varepsilon_{1}}\right)W_{2}$$

$$+ \varepsilon_{1}\bar{k}_{d_{8}}\bar{\delta}_{5}(t) + \bar{k}_{d_{9}}\bar{\delta}_{6}(t)$$

$$D^{+}W_{5} \leq -\left(\frac{\bar{k}_{e_{1}}}{\varepsilon_{4}}\right)W_{5} + \bar{k}_{e_{2}}W_{5} + \bar{k}_{e_{3}}\bar{\delta}_{7}(t)$$

$$(4.86)$$

where $D^+W(\cdot)$ denotes the upper right-hand derivative; the notation related to \bar{k}_{p_i} for p=a,b,c,d,e and $i=1,2,\ldots,11$, denotes the positive constants independent on $\varepsilon_1, \varepsilon_2, \varepsilon_3$, and ε_4 ; and $\bar{\delta}_i$ for $i=1,\ldots,7$ are nonvanishing perturbations. The matrix form of (4.86) is

$$D^+W \le -HW + \varepsilon_1 \Gamma_1 + \Gamma_2 \tag{4.87}$$

where $D^+W=[D^+W_1,D^+W_2,D^+W_3,D^+W_4,D^+W_5]^T,~W=[W_1,W_2,W_3,W_4,W_5]^T;~\Gamma_1$ and

 Γ_2 are

$$\Gamma_1 = [0, \bar{k}_{b_4}\bar{\delta}_1(t), \bar{k}_{c_{10}}\bar{\delta}_3(t), \bar{k}_{d_8}\bar{\delta}_5(t), 0]^T, \quad \Gamma_2 = [0, \bar{k}_{b_5}\bar{\delta}_2(t), \bar{k}_{c_{11}}\bar{\delta}_4(t), \bar{k}_{d_9}\bar{\delta}_6(t), \bar{k}_{e_3}\bar{\delta}_7(t)]^T \quad (4.88)$$

Since the off-diagonal components of H are positive, H is quasi-monotone increasing [58] with the condition $0 < \varepsilon_4 \ll \varepsilon_3 \ll \varepsilon_2 \ll \varepsilon_1 \ll 1$ and is given in Appendix Appendix B. Consider the differential equation

$$\dot{U} = -HU + \varepsilon_1 \Gamma_1 + \Gamma_2 \tag{4.89}$$

with $U = [U_1, U_2, U_3, U_4]^T$ and the same initial conditions U(0) = W(0). Using the vectorial comparison method in Chapter IX of [58], it is concluded that $W \leq U$ for all $t \geq 0$ and the steady state of U(t) is $H^{-1}(\varepsilon_1\Gamma_1 + \Gamma_2)$. The computation of the size of the ultimate boundedness is given in Appendix Appendix B. Since the size of ultimate boundedness is dependent on ε_i for i = 1, ..., 4, i.e., as $\varepsilon_i \to 0$ for i = 1, ..., 4 with $0 < \varepsilon_4 \ll \varepsilon_3 \ll \varepsilon_2 \ll \varepsilon_1 \ll 1$, the size of the ultimate boundedness can be made arbitrarily small.

4.5 Simulation Results

The performances of the proposed controller are illustrated through dynamics of a helicopter. The inertial, geometric, and aerodynamic parameters from [37] are listed below

$$\begin{split} I_x &= 0.142413 & I_y = 0.271256 & Iz = 0.271492 \\ l_M &= -0.015 & y_M = 0 & h_M = 0.2943 \\ C_M^Q &= 0.004452 & D_M^Q = 0.6304 & (\partial R_M/\partial b_{1s}) = 25.23 \\ C_T^Q &= 0.005066 & D_T^Q = 0.008488 & (\partial M_M/\partial a_{1s}) = 25.23. \end{split}$$

With full dynamics of a helicopter, results from the state feedback are compared to results from the output feedback to show the important role and benefit of the EHGO in presence of uncertainties. The translational and rotational dynamics of a helicopter given in (4.7) and (4.1), respectively, were considered in presence of disturbances, $\sigma_{\chi} = [3 \sin t, 3 \sin t, 3 \sin t]^T$ and $\sigma_{\Theta} = [\cos t, \cos t, \cos t]^T$ like wind gusts. The control objective is to track the reference $u(t) = [r_x, r_y, r_z]^T = [5 \sin t, 5 \cos t, 5 \sin t]^T$ and $\psi_r = 0.1$ rad in the presence of the external disturbances σ_{χ} and σ_{Θ} . In numerical simulations, we used a helicopter model in (4.1) and (4.7) without approximations.

For the state feedback controller in (4.18) and (4.20), and the output feedback controller (4.53), the common control parameters are given by

$$k_p = 8, \quad k_v = 4, \quad k_1 = 2 \quad k_2 = 4,$$

 $\varepsilon_1 = 0.1, \quad \varepsilon_2 = 0.001, \quad \varepsilon_3 = 0.0007$

$$(4.90)$$

For the EHGO, the observer gains of H_i , H_{χ_e} , and H_{Θ_e} in (4.49), are

$$\varepsilon_4 = 0.0001, \quad h_{i1} = 3, \quad h_{i2} = 3, \quad h_{i3} = 1, \quad \text{for } i = 1, \dots, 6$$
 (4.91)

The saturation levels for the estimates by the EHGO are chosen not to be activated under the state feedback. For both the state feedback and output feedback, the initial states for the plant and reference dynamics were chosen as

$$\chi = [1, 0.2, 1, -0.1, 1, 0.1]^T, \quad \Theta = [0, 0, 0, 0, 0, 0]^T, \quad \chi_r = [0.1, 1, 0, 0, 1]^T$$
(4.92)

The initial conditions for the dynamic inversion controllers and the EHGO were

$$u_t(0) = [T_M(0), \phi_d(0), \theta_d(0)]^T = [48, 0.5, 0.5]^T,$$

$$u_r(0) = [T_T(0), a_{1s}(0), b_{1s}(0)]^T = [3, 0, 0]^T$$

$$\hat{\chi}(0) = [0, 0, 0, 0, 0, 0]^T, \quad \hat{\Theta}(0) = [1, 0, 1, 1, 1, 0]^T,$$

$$\hat{\sigma}_{\chi} = [0, 0, 0]^T, \quad \hat{\sigma}_{\Theta} = [0, 1, 0]^T$$

$$(4.93)$$

For the comparison with the output feedback, the state feedback controllers (4.18) and (4.20)

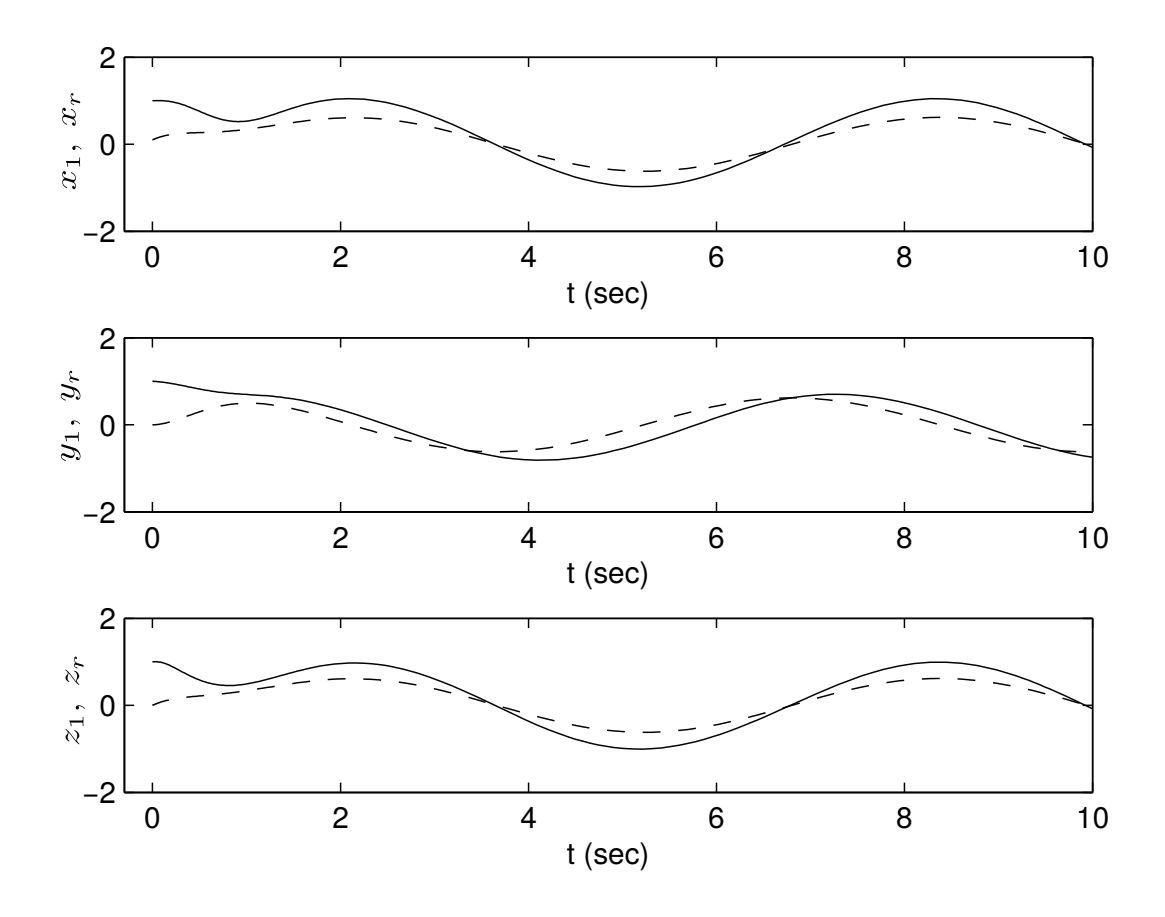


Figure 4.3: Trajectories x_1 , y_1 , and z_1 (solid-lines) under the state feedback in the presence of disturbances and reference states x_r , y_r , and z_r (dished-lines)

with the control parameters (4.90) and the initial conditions in (4.93), was simulated, which is shown in Fig. 4.3. In Fig. 4.3, we can see tracking errors between trajectories x_1 , y_1 , and z_1 driven by the state feedback controller and the reference states x_r , y_r , and z_r due to the effects of external disturbances. In Fig. 4.4 and 4.5, under the proposed output feedback, system states, χ and Θ and the references x_r , y_r , z_r , and ψ_r are almost indistinguishable. In Fig. 4.5, the references are ϕ_d and ψ_d which are provided by the dynamic inversion. In Fig. 4.6 and 4.7, the system states x_i , y_i , and z_i for i = 1, 2 are plotted with solid-lines. The estimates \hat{x}_i , \hat{y}_i , and \hat{z}_i for i = 1, 2 are dashed-lines. At begin of the simulations, the peaking due to high gains and the difference of initial conditions, is saturated to prevent

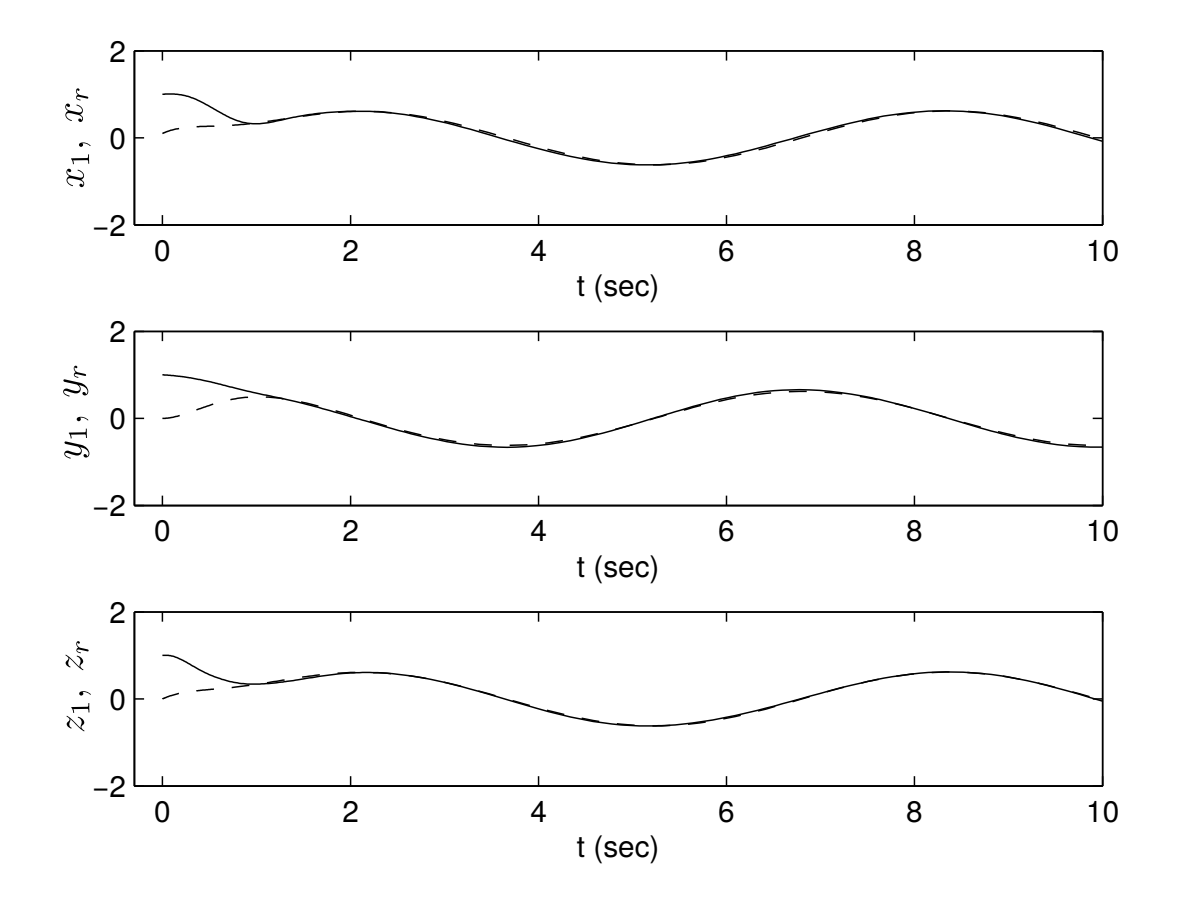


Figure 4.4: Trajectories of x_1 , y_1 , and z_1 (solid-lines) under the output feedback in (4.53) in the presence of disturbances, and references x_r , y_r , and z_r (dashed-lines) for $r_x(t) = 5 \sin t$, $r_y(t) = 5 \cos t$, and $r_z(t) = 5 \sin t$ in (4.14)

from degrading the system performance. In Fig. 4.8 and 4.9, trajectories of the state states ϕ_i , θ_i , and ψ_i , and the estimate $\hat{\phi}_i$, $\hat{\theta}_i$, and $\hat{\psi}_i$ for i=1,2 are shown. At the beginning of the simulation, peaking is saturated. Expect at the beginning of the simulation, the systems states and estimates are indistinguishable. In Fig. 4.10, the components of sum of F_p in (4.7) and σ_{χ} are plotted with solid-lines and the components of sum of F_O in (4.11) and $\hat{\sigma}_{\chi}$ are plotted with dashed-lines. At the first part of simulations, the peaking is saturated. In Fig. 4.11, the external disturbance σ_{Θ} (solid lines) and tis estimate $\hat{\sigma}_{\Theta}$ (dashed-lines) are shown. At the first part of simulations, the peaking is saturated. The actual helicopter control inputs T_M , T_T , a_{1s} , and b_{1s} are shown in Fig. 4.12.

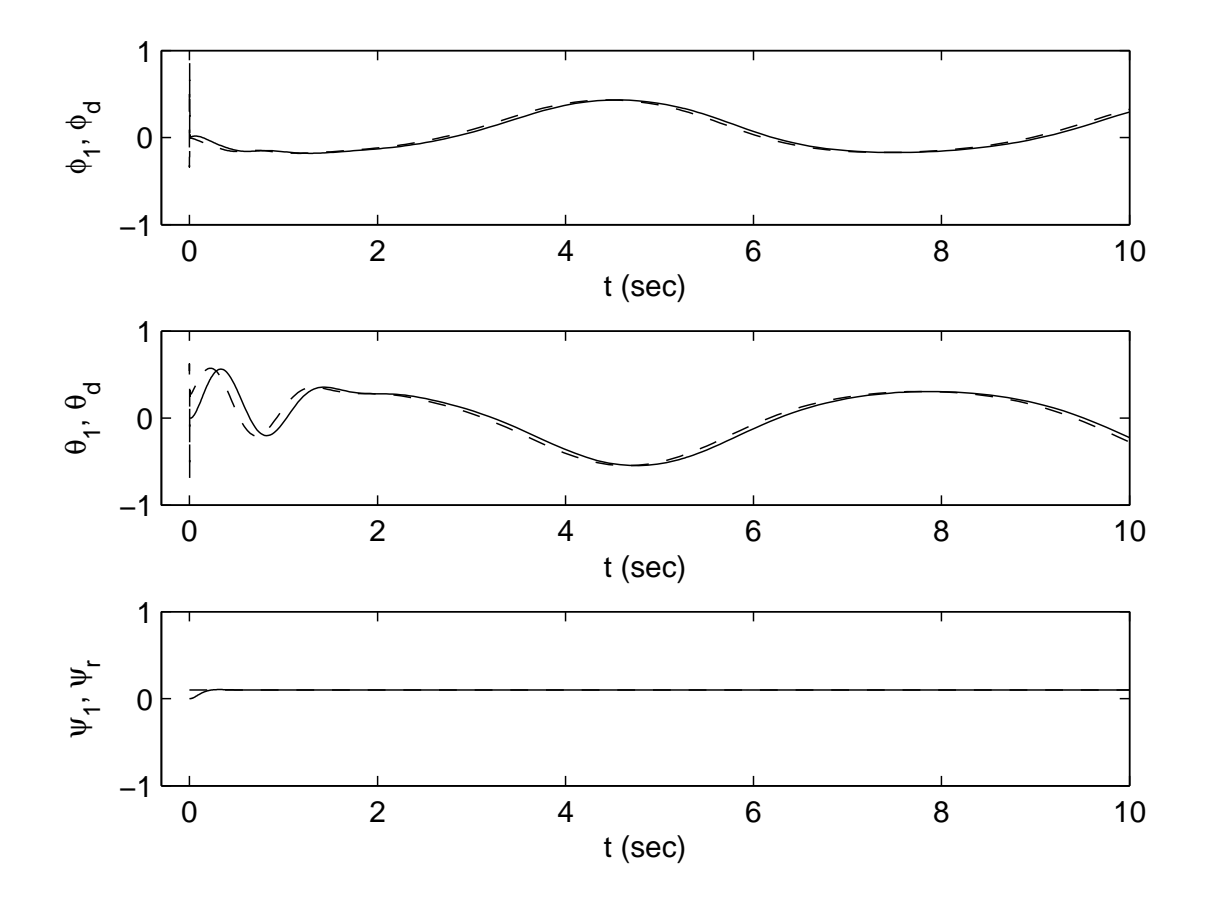


Figure 4.5: Trajectories ϕ_d , θ_d , and ψ_r (dashed-lines) are references for the states ϕ_1 , θ_1 , ψ_1 of the rotational dynamics in the presence of disturbances.

4.6 Conclusions

An output feedback controller for a helicopter system was presented. In the presence of uncertainties, the output feedback controller is able to track the given reference trajectories x_r , y_r , z_r , and ψ_r . The states and uncertainties in the helicopter dynamics were estimated using the EHGO and dynamic inversion was subsequently used for design of the controller to deal with nonaffine control inputs. In the time-scale structure the EHGO estimated unmeasurable system states and uncertain system parameters and external disturbances and the estimates were utilized in the two dynamic inversion controllers. There is also a time-scale structure between the two dynamic inversion controllers, in which the rotational

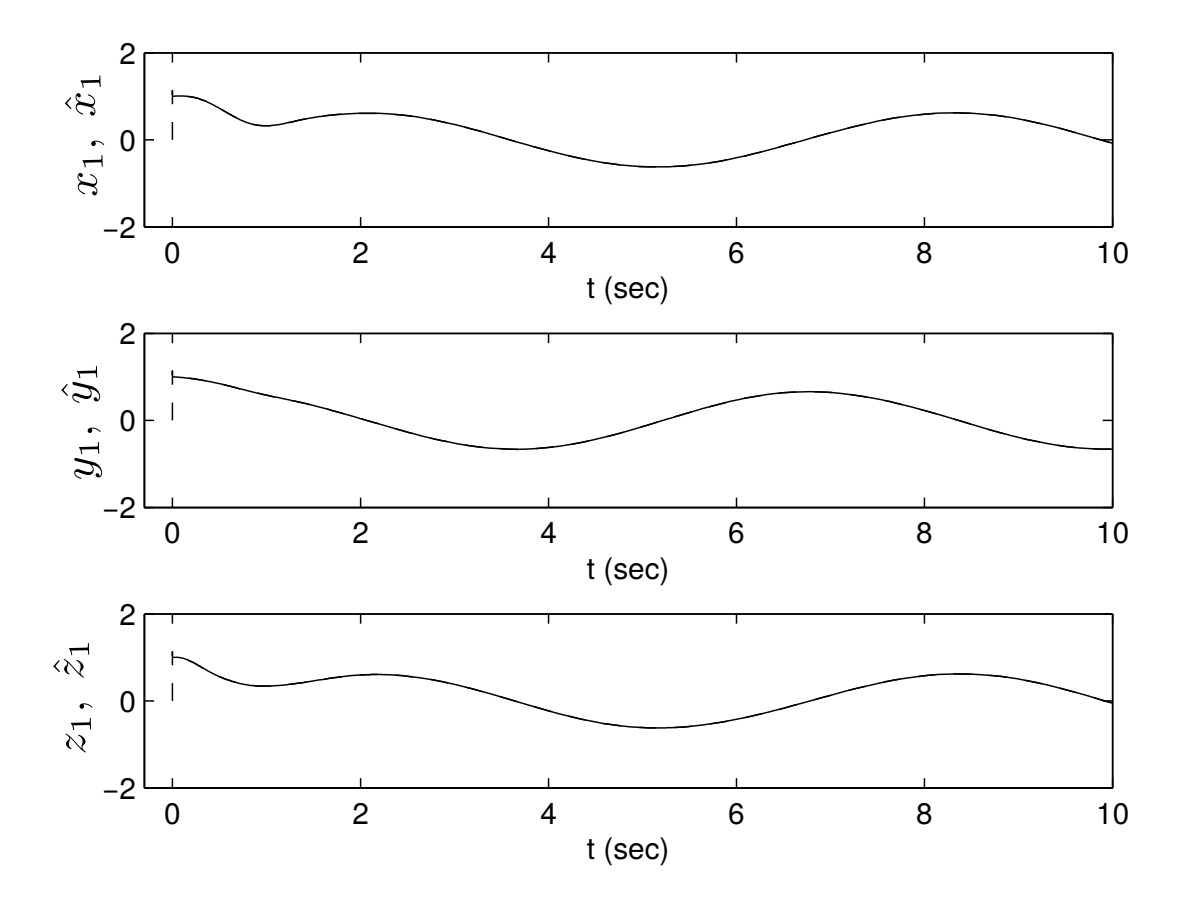


Figure 4.6: Trajectories x_1 , y_1 and z_1 (solid-lines) and the estimates \hat{x}_1 , \hat{y}_1 , and \hat{z}_1 (dashed-lines) by the EHGO

dynamic inversion controller is faster than the translational dynamic inversion controller. By using a time scale between the two dynamic inversion controller, we were able to design an efficient controller with less dimensions than one dynamic inversion without a time scale. The dynamic inversion controllers were designed to render the rotational dynamics faster than the translational dynamics to overcome underactuated system structures. Using the multi-time-scale separation approach, the proposed controller was able to control the full degree of freedom (i.e. 6 degrees of freedom) for an unmanned helicopter. The singular perturbation method was used to design controllers and analyze the multi-time-scale structure. This is confirmed through numerical simulations.

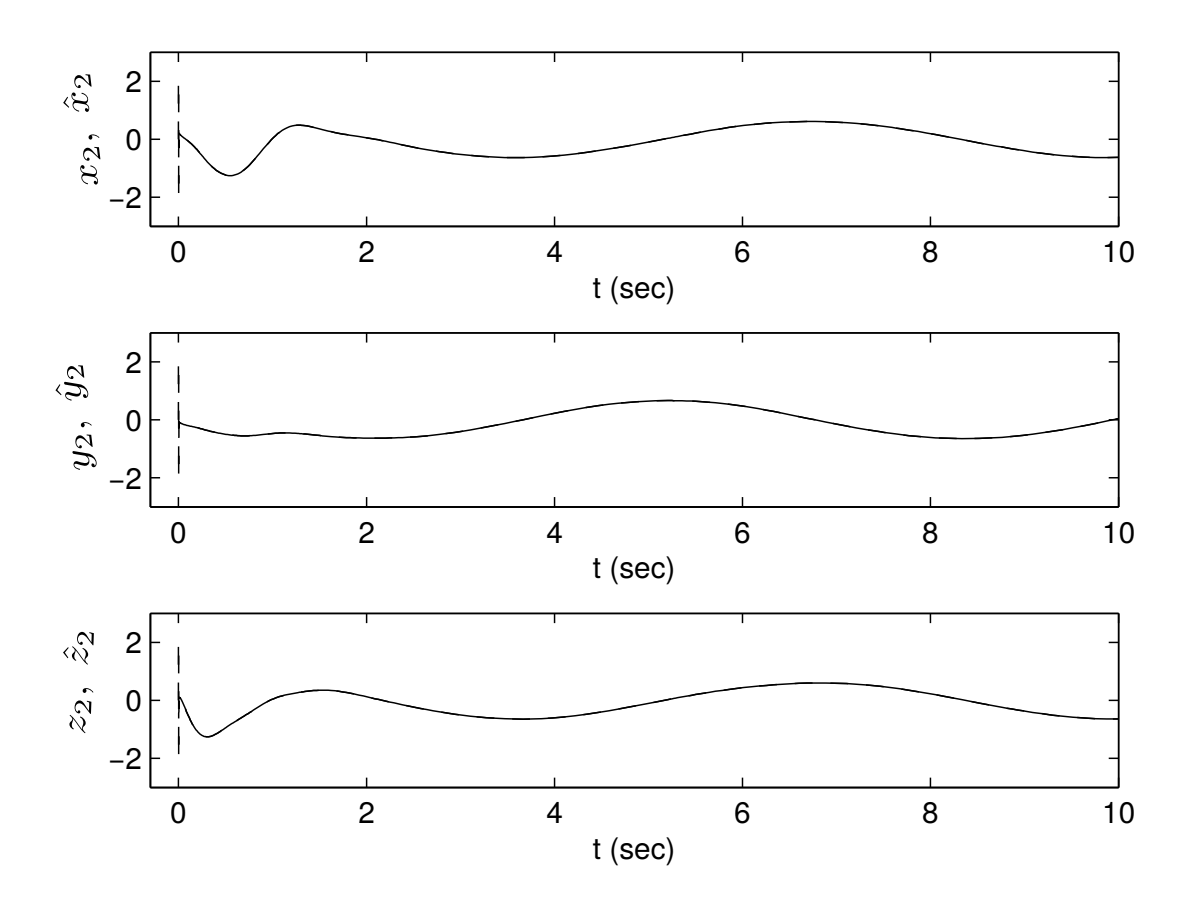


Figure 4.7: Trajectories x_2 , y_2 and z_2 (solid-lines) and the estimates \hat{x}_2 , \hat{y}_2 , and \hat{z}_2 (dashed-lines) by the EHGO

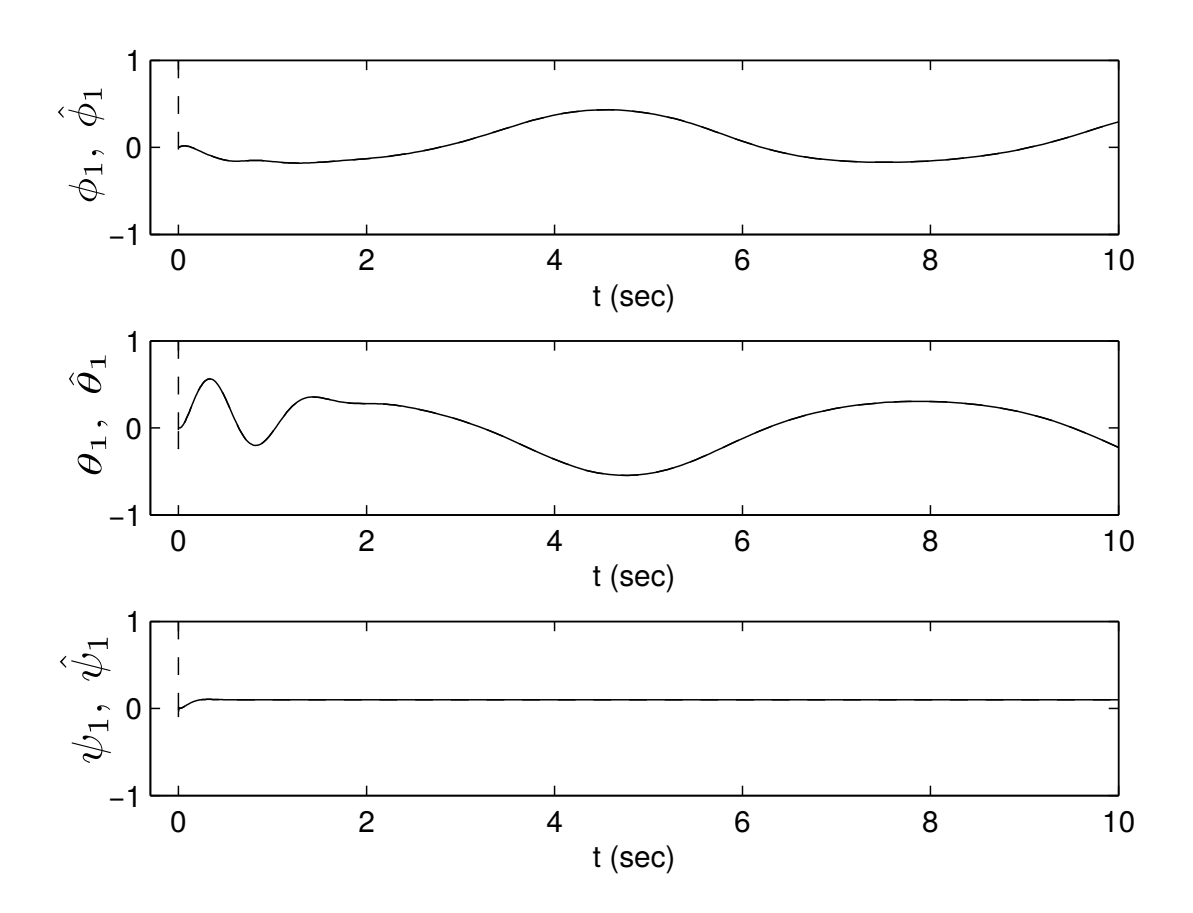


Figure 4.8: Trajectories ϕ_1 , θ_1 and ψ_1 (solid-lines) and the estimates $\hat{\phi}_1$, $\hat{\theta}_1$, and $\hat{\psi}_1$ (dashed-lines) by the EHGO

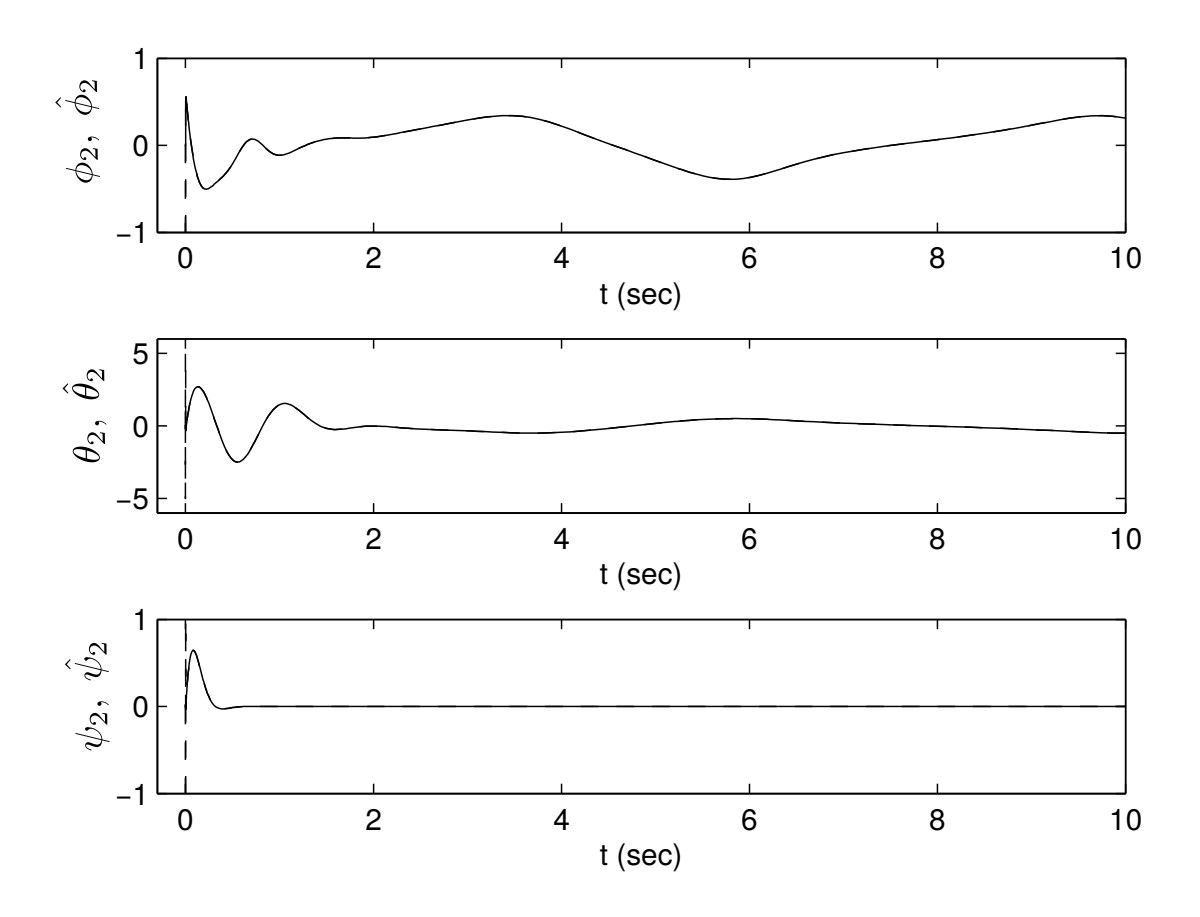


Figure 4.9: Trajectories ϕ_2 , θ_2 and ψ_2 (solid-lines) and the estimates $\hat{\phi}_2$, $\hat{\theta}_2$, and $\hat{\psi}_2$ (dashed-lines) by the EHGO

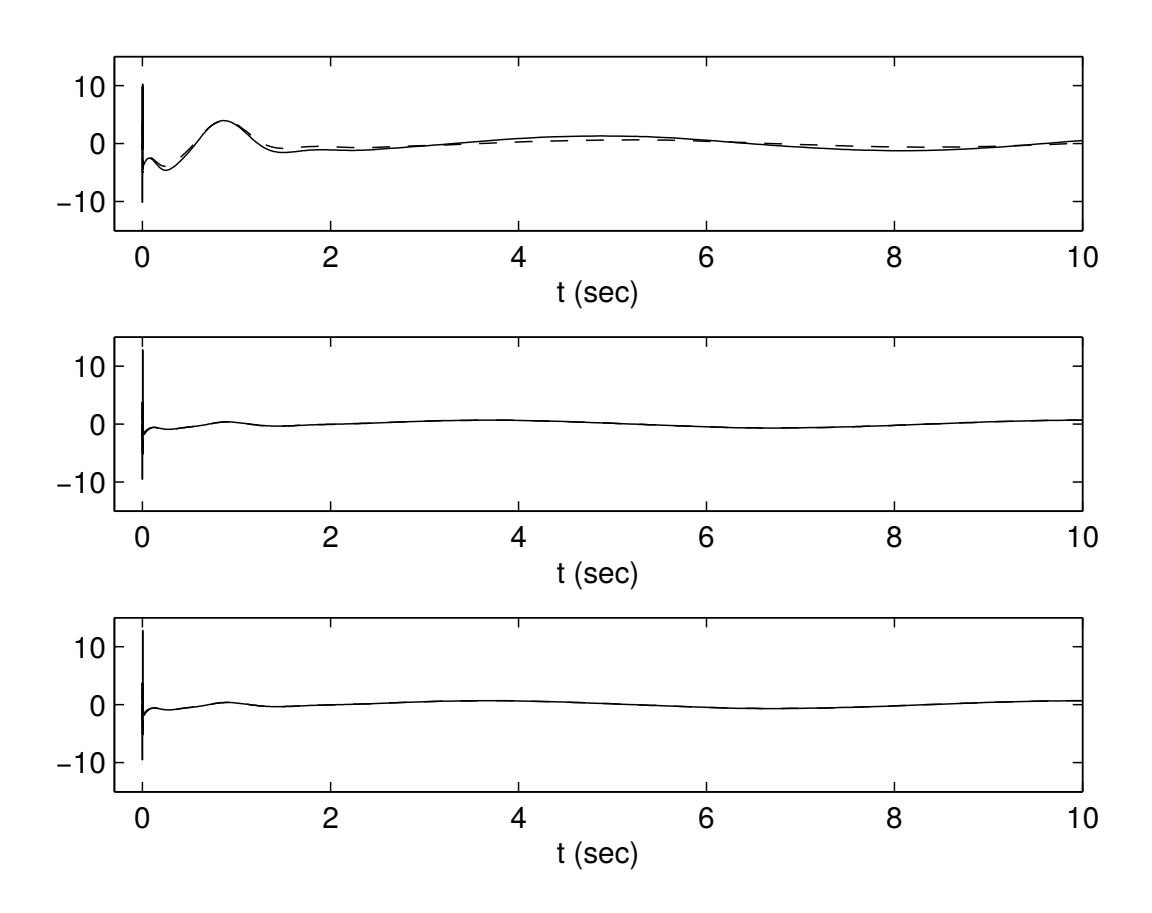


Figure 4.10: Plots for sum of the actual terms of acceleration (without approximation in model, F_p in (4.7)) and external disturbances σ_{Θ} : dashed-lines and plots for sum of nominal terms of acceleration (i.e., F_O in (4.11)) the estimate of external disturbances σ_{χ} by the EHGO: solid-lines

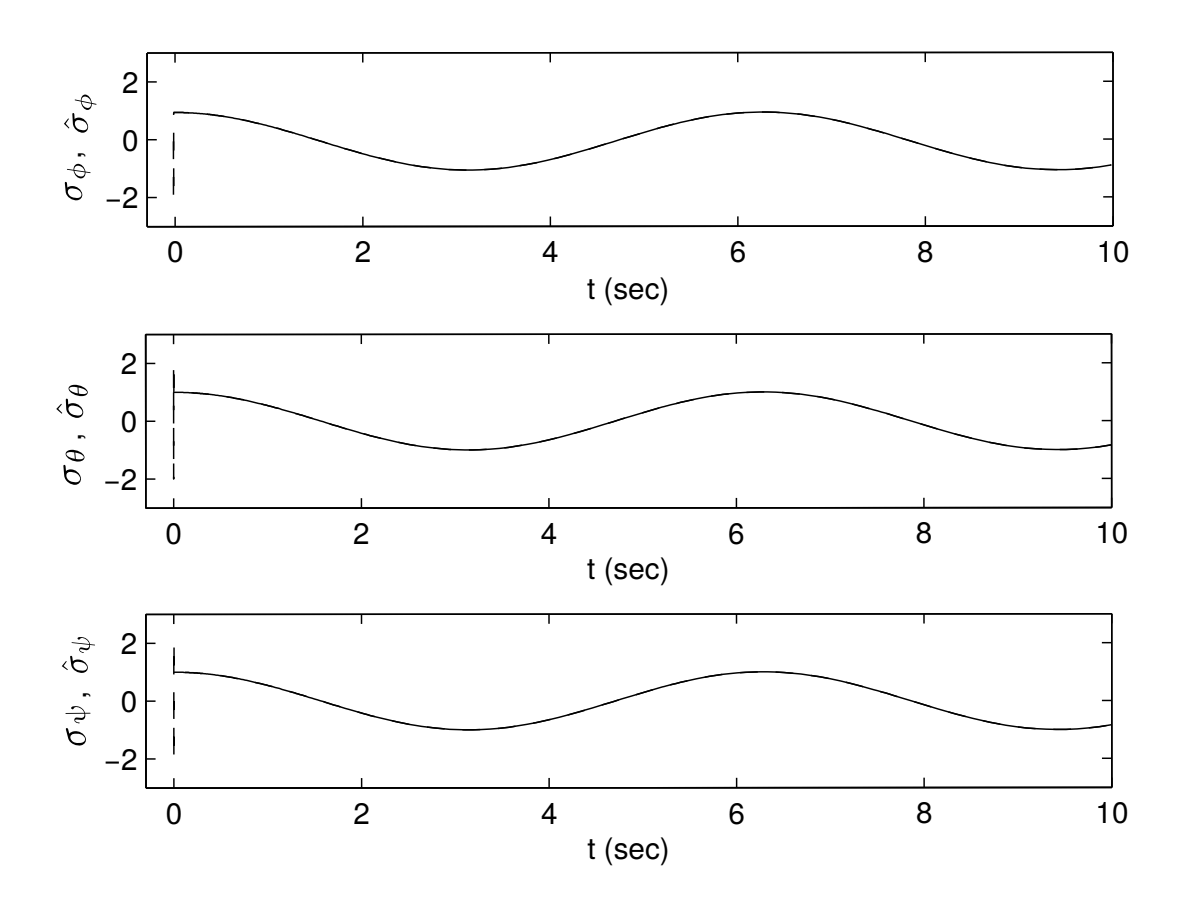


Figure 4.11: Plots for the external disturbances σ_{Θ} (solid-lines) and plots for the estimates $\hat{\sigma}_{\Theta}$ (dashed-lines)

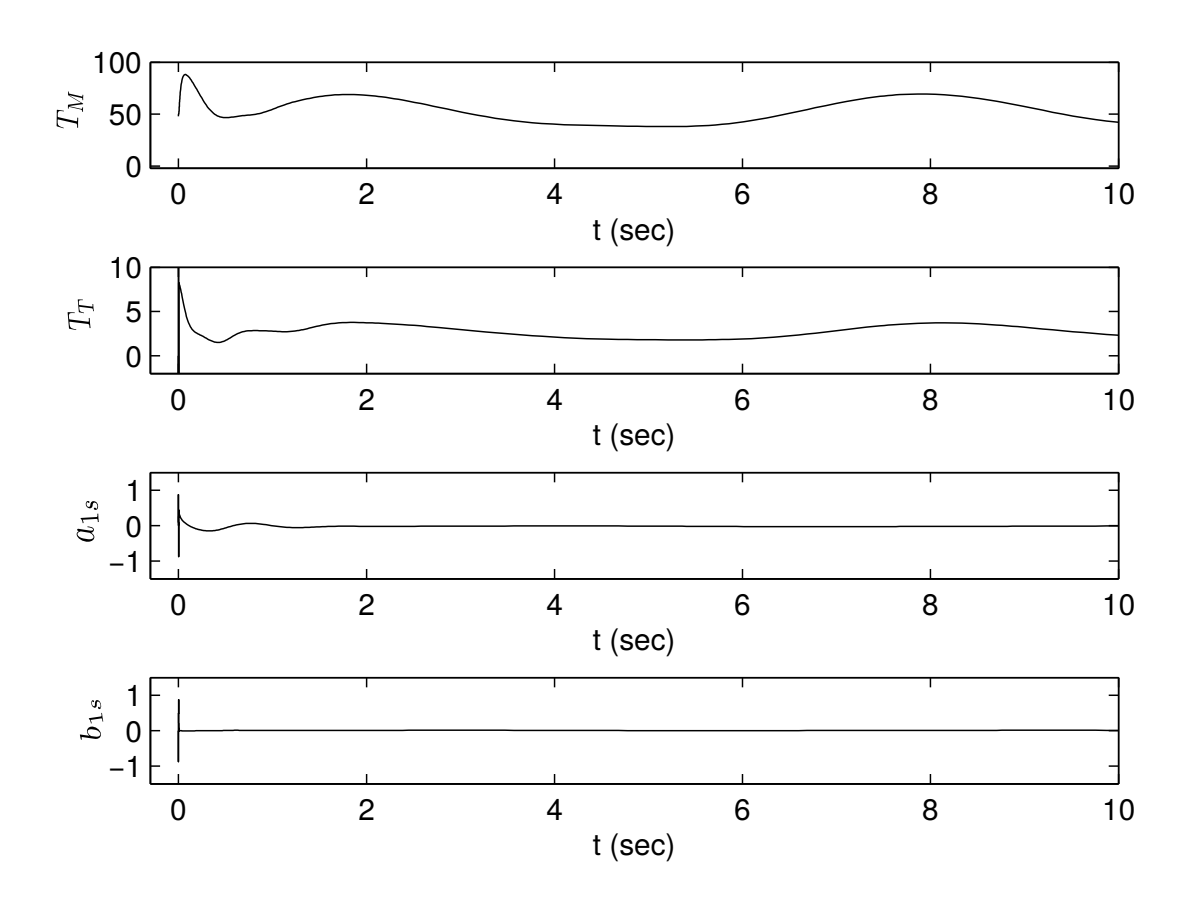


Figure 4.12: Plots for the helicopter actual control inputs, T_M , T_T , a_{1s} , and b_{1s} under the output feedback

Chapter 5

Conclusions and Future Works

5.1 Concluding Remarks

This dissertation is considering a class of uncertain nonlinear systems which have the form of a chain of integrators focusing on output feedback. The uncertain nonlinear systems were governed by a multi-time-scale structure control design. In the output feedback design, the Extended High-Gain Observers were used to estimate unmeasured systems states, uncertain system parameters, and external disturbances as well. Using the Extended High-Gain Observers, the uncertain factors were eliminated in the uncertain nonlinear systems. The estimates were provided to the dynamic inversion. The dynamic inversion was able to deal with nonaffine control inputs, system parameter uncertainties, and disturbances using the estimates. The proposed control design created a multi-time-scale structure in the uncertain nonlinear systems, in which the plant dynamics were forced to have a time-scale structure by the controller.

The time-scale structure was well-suited to underactuated mechanical systems where the number of inputs are less than the number of the degrees of freedom since the fast dynamics in the plant are considered as virtual inputs to the slow dynamics. This time-scale structure approach were verified using two examples of underactuated mechanical systems: the

inverted pendulum on a cart and the autonomous helicopter.

The multi-time scale structures were analyzed through the singular perturbation method. Moreover, the stability for the close-loop systems was guaranteed by the proposed control schemes. The proposed controllers were verified through the numerical simulations and experimental tests.

5.1.1 Main contributions

The main contributions of this dissertation are as follow as.

1. In Chapter 2,

- this dissertation provided a novel way to deal with nonlinear systems which have the form of chains of integrators, nonaffine control inputs, unmeasured system states, and uncertainties;
- to deal with the uncertain, nonaffine, nonlinear systems, the extended high-gain observer and the dynamic inversion were combined using a multi-time-scale separation approach;
- the time-scale approach control design was devised and the stability of the proposed controller was conducted using the singular perturbation method.

2. In Chapter 3,

- the output feedback stabilization control design for the inverted pendulum on a car in the presence of uncertainties was proposed through a multi-time-scale approach;
- the combination of the Extended High-Gain Observer and the dynamic inversion provided a new way to deal with unmeasured systems states and uncertain system parameters;

- the stability analysis for the closed-loop system of the inverted pendulum on a cart was conducted using the singular perturbation method;
- the proposed control design was verified through both numerical simulations and experimental tests.

3. In Chapter 4,

- output feedback control design for tracking given reference of the autonomous helicopter in the presence of uncertainties was proposed through a multi-timescale separation approach;
- Using the extended high-gain observers and two dynamic inversion controllers with a multi-time-scale separation, the nonaffine control inputs and uncertainties were considered and a time-scale structure between the translational and rotational dynamics were constructed;
- The stability analysis for the multi-time-scale structure in the closed-loop system was conducted through the singular perturbation method;
- the proposed controller was verified through numerical simulations.

5.2 Future Works

Extensions of this dissertation as future works are given as follows.

- In Chapter 2, the future work will consider extension of our approach to non-minimum phase systems. The main issue of this work would be how to deal with unstable zero dynamics in the absence of measurements in the zero dynamics;
- in Chapter 3, our future work will focus on extending our approach to output feedback stabilization of other underactuated mechanical systems with two degrees of freedom. Expected difficulties would be how to create a time-scale structure in the underacuated mechanical systems with the two degrees of freedom;

• in Chapter 4, extension of our work will be implementing the proposed control algorithm into miniature helicopters and develop new control algorithms for the other types of unmanned vehicles.

APPENDICES

Appendix A Appendix for Chapter 2

In this section, we are going to derive the standard singularly perturbed systems (3.32), (3.33), (3.34), and (3.35) with time-scaled variables.

Error dynamics of the EHGOs

With the fast variables for EHGOs are

$$\eta_{x_1} = \frac{x_1 - \hat{x}_1}{\varepsilon_3^2}, \ \eta_{x_2} = \frac{x_2 - \hat{x}_2}{\varepsilon_3},
\eta_{x_3} = \sigma_x(\theta_1 + \alpha_r, \theta_2, F) - \hat{\sigma}_x
\eta_{\alpha_1} = \frac{\alpha_1 - \hat{\alpha}_1}{\varepsilon_3^2}, \ \eta_{\alpha_2} = \frac{\alpha_2 - \hat{\alpha}_2}{\varepsilon_3},
\eta_{\alpha_3} = \sigma_\alpha(\theta_1 + \alpha_r, \theta_2, F) - \hat{\sigma}_\alpha,$$
(1)

with $\theta_1 = \alpha_1 - \alpha_r$, $\theta_2 = \alpha_2$, where \hat{x}_i and $\hat{\alpha}_i$ for i = 1, 2, and $\hat{\sigma}_x$ and $\hat{\sigma}_\alpha$, are given in (3.25). The derivatives of η_{x_1} and η_{α_1} along the trajectories of (3.2) and (3.25) are

$$\varepsilon_3 \dot{\eta}_{x_1} = -h_{11} \eta_{x_1} + \eta_{x_2}$$

$$\varepsilon_3 \dot{\eta}_{\alpha_1} = -h_{21} \eta_{\alpha_1} + \eta_{\alpha_2}$$
(2)

The derivatives of η_{x_2} and η_{α_2} along the trajectories of (3.2) and (3.25) are

$$\varepsilon_{3}\dot{\eta}_{x_{2}} = -h_{12}\eta_{x_{1}} + \sigma_{x}(\alpha_{1}, \alpha_{2}, F) - \hat{\sigma}_{x}(t)
+ \bar{f}_{x}(\alpha_{1}, \alpha_{2}, F) - \bar{f}_{x}(\hat{\alpha}_{1}, \hat{\alpha}_{2}, F)
= -h_{12}\eta_{x_{1}} + \eta_{x_{3}} + \bar{f}_{x}(\alpha_{1}, \alpha_{2}, F) - \bar{f}_{x}(\hat{\alpha}_{1}, \hat{\alpha}_{2}, F)
\varepsilon_{3}\dot{\eta}_{\alpha_{2}} = -h_{22}\eta_{\alpha_{1}} + \sigma_{\alpha}(\alpha_{1}, \alpha_{2}, F) - \hat{\sigma}_{\alpha}(t)
+ \bar{f}_{\alpha}(\alpha_{1}, \alpha_{2}, F) - \bar{f}_{\alpha}(\hat{\alpha}_{1}, \hat{\alpha}_{2}, F)
= -h_{22}\eta_{\alpha_{1}} + \eta_{\alpha_{3}} + \bar{f}_{\alpha}(\alpha_{1}, \alpha_{2}, F) - \bar{f}_{\alpha}(\hat{\alpha}_{1}, \hat{\alpha}_{2}, F)$$
(3)

The derivatives of η_{x_3} and η_{α_3} along the trajectories of (3.2), (3.25) and (3.26) are

$$\varepsilon_{3}\dot{\eta}_{x_{3}} = -h_{13}\eta_{x_{1}} + \varepsilon_{3}\dot{\sigma}_{x}(\alpha_{1}, \alpha_{2}, F)
= -h_{13}\eta_{x_{1}} + \varepsilon_{3} \left\{ \left(\frac{\partial \sigma_{x}}{\partial \alpha_{1}} \right) \alpha_{2} + \left(\frac{\partial \sigma_{x}}{\partial \alpha_{2}} \right) \dot{\alpha}_{2} \right.
\left. - \frac{1}{\varepsilon_{2}} \cdot \left(\frac{\partial \sigma_{x}}{\partial F} \right) \left[\bar{f}_{x}(\alpha_{1}, M_{\theta} \operatorname{sat}(\frac{\hat{\alpha}_{2}}{M_{\theta}}), F) \right.
\left. + M_{x} \operatorname{sat}(\hat{\sigma}_{x}/M_{x}) - u \right] \right\}
\left. \varepsilon_{3}\dot{\eta}_{\alpha_{3}} = -h_{23}\eta_{\alpha_{1}} + \varepsilon_{3}\dot{\sigma}_{\alpha}(\alpha_{1}, \alpha_{2}, F) \right.
\left. = -h_{23}\eta_{\alpha_{1}} + \varepsilon_{3} \left\{ \left(\frac{\partial \sigma_{\alpha}}{\partial \alpha_{1}} \right) \alpha_{2} + \left(\frac{\partial \sigma_{\alpha}}{\partial \alpha_{2}} \right) \dot{\alpha}_{2} \right.
\left. - \frac{1}{\varepsilon_{2}} \cdot \left(\frac{\partial \sigma_{\alpha}}{\partial F} \right) \left[\bar{f}_{x}(\alpha_{1}, M_{\theta} \operatorname{sat}(\frac{\hat{\alpha}_{2}}{M_{\theta}}), F) \right.
\left. + M_{x} \operatorname{sat}(\hat{\sigma}_{x}/M_{x}) - u \right] \right\}$$

$$(4)$$

The error dynamics for the EHGOs are

$$\varepsilon_3 \dot{\eta} = A_\eta \eta + \varepsilon_3 [\bar{B}_1 \Delta_1 + \bar{B}_2 \Delta_2 + \left(\frac{1}{\varepsilon_2}\right) \bar{B}_2 \Delta_3] \tag{5}$$

where $\eta = [\eta_x^T, \eta_\alpha^T]^T$ with $\eta_x = [\eta_{x_1}, \eta_{x_2}, \eta_{x_3}]^T$ and $\eta_\alpha = [\eta_{\alpha_1}, \eta_{\alpha_2}, \eta_{\alpha_3}]^T$; the matrices $A_\eta = \begin{bmatrix} A_{\eta_1} & 0_{3\times 3} \\ 0_{3\times 3} & A_{\eta_2} \end{bmatrix}$, \bar{B}_1 and \bar{B}_2 are given by

$$A_{\eta_1} = \begin{bmatrix} -h_{11} & 1 & 0 \\ -h_{12} & 0 & 1 \\ -h_{13} & 0 & 0 \end{bmatrix}, A_{\eta_2} = \begin{bmatrix} -h_{21} & 1 & 0 \\ -h_{22} & 0 & 1 \\ -h_{23} & 0 & 0 \end{bmatrix},$$

$$\bar{B}_j = \begin{bmatrix} B_j & 0_{3\times 1} \\ 0_{3\times 1} & B_j \end{bmatrix}, \text{ for } j = 1, 2$$

$$B_1 = [0, 1, 0]^T, B_2 = [0, 0, 1]^T$$

with the zero matrix $0_{i\times j}\in\mathbf{R}^{i\times j}$, $B=[0,1]^T$; and Δ_i for i=1,2,3 are

$$\Delta_{1} = \begin{bmatrix} \frac{\bar{f}_{x}(\alpha_{1}, \alpha_{2}, F) - \bar{f}_{x}(\hat{\alpha}_{1}, \hat{\alpha}_{2}, F)}{\varepsilon_{3}} \\ \frac{\bar{f}_{\alpha}(\alpha_{1}, \alpha_{2}, F) - \bar{f}_{\alpha}(\hat{\alpha}_{1}, \hat{\alpha}_{2}, F)}{\varepsilon_{3}} \end{bmatrix}$$

$$\Delta_{2} = \begin{bmatrix} \left(\frac{\partial \sigma_{x}}{\partial \alpha_{1}}\right) \alpha_{2} + \left(\frac{\partial \sigma_{x}}{\partial \alpha_{2}}\right) f_{\alpha}(\alpha_{1}, \alpha_{2}, F) \\ \left(\frac{\partial \sigma_{\alpha}}{\partial \alpha_{1}}\right) \alpha_{2} + \left(\frac{\partial \sigma_{\alpha}}{\partial \alpha_{2}}\right) f_{\alpha}(\alpha_{1}, \alpha_{2}, F) \end{bmatrix}$$

$$\Delta_{3} = \begin{bmatrix} \left(\frac{\partial \sigma_{x}}{\partial F}\right) [\bar{f}_{x}(\alpha_{1}, M_{\theta} \text{sat}(\frac{\hat{\alpha}_{2}}{M_{\theta}}), F) + M_{x} \text{sat}(\frac{\hat{\sigma}_{x}}{M_{x}}) - u] \\ \left(\frac{\partial \sigma_{\alpha}}{\partial F}\right) [\bar{f}_{x}(\alpha_{1}, M_{\theta} \text{sat}(\frac{\hat{\alpha}_{2}}{M_{\theta}}), F) + M_{x} \text{sat}(\frac{\hat{\sigma}_{x}}{M_{x}}) - u] \end{bmatrix}$$

where $\|\Delta_1\| \leq k_{\Delta} \|\eta\|$ with a positive constant k_{Δ} due to the Lipschitz conditions $\|\bar{f}_x(\alpha_1, \alpha_2, F) - \bar{f}_x(\hat{\alpha}_1, \hat{\alpha}_2, F)\| \leq \varepsilon_3 k_{\Delta_x} \|\eta\|$ and $\|\bar{f}_\alpha(\alpha_1, \alpha_2, F) - \bar{f}_\alpha(\hat{\alpha}_1, \hat{\alpha}_2, F)\| \leq \varepsilon_3 k_{\Delta_\alpha} \|\eta\|$ with positive constants k_{Δ_x} and k_{Δ_α} .

Error dynamics of the dynamic inversion

With the change of variables for the dynamic inversion,

$$z_F = F - F^*, \quad z_u = u - u^*$$
 (6)

the derivative of z_F along the trajectories of (3.2), (3.25), and (3.26) with multiplication of ε_2 , is

$$\varepsilon_{2}\dot{z}_{F} = \varepsilon_{2}\dot{F} - \varepsilon_{2}\dot{F}^{*}
= -\bar{f}_{x}\left(\alpha_{1}, M_{\theta}\operatorname{sat}(\frac{\hat{\alpha}_{2}}{M_{\theta}}), F\right) - M_{x}\operatorname{sat}\left(\frac{\hat{\sigma}_{x}}{M_{x}}\right) + u - \varepsilon_{2}\dot{F}^{*} \tag{7}$$

By adding and subtracting $\bar{f}_x(\alpha_1, \alpha_2, F) + \sigma_x(\alpha_1, \alpha_2, F)$ and adding $\bar{f}_x(\alpha_1, \alpha_2, F^*) + \sigma_x(\alpha_1, \alpha_2, F^*) - u^*$ (i.e., $\bar{f}_x(\alpha_1, \alpha_2, F^*) + \sigma_x(\alpha_1, \alpha_2, F^*) - u^* = 0$) to the right-hand side

of $\varepsilon_2 \dot{z}_F$, we obtain

$$\varepsilon_{2}\dot{z}_{F} = -\bar{f}_{x}(\alpha_{1}, \alpha_{2}, F) - \sigma_{x}(\alpha_{1}, \alpha_{2}, F)
+ \bar{f}_{x}(\alpha_{1}, \alpha_{2}, F^{*}) + \sigma_{x}(\alpha_{1}, \alpha_{2}, F^{*})
+ \bar{f}_{x}(\alpha_{1}, \alpha_{2}, F) - \bar{f}_{x}\left(\alpha_{1}, M_{\theta} \operatorname{sat}\left(\frac{\hat{\alpha}_{2}}{M_{\theta}}\right), F\right)
+ \sigma_{x}(\alpha_{1}, \alpha_{2}, F) - M_{x} \operatorname{sat}\left(\frac{\hat{\sigma}_{x}}{M_{x}}\right) + u - u^{*} - \varepsilon_{2}\dot{F}^{*}$$
(8)

Since

$$\bar{f}_x(\alpha_1, \alpha_2, F^*) + \sigma_x(\alpha_1, \alpha_2, F^*)
- \bar{f}_x(\alpha_1, \alpha_2, F) - \sigma_x(\alpha_1, \alpha_2, F) = -c_x z_F,$$
(9)

it is simplified to

$$\varepsilon_{2}\dot{z}_{F} = -c_{x}z_{F} + z_{u}
+ \bar{f}_{x}(\alpha_{1}, \alpha_{2}, F) - \bar{f}_{x}\left(\alpha_{1}, M_{\theta} \operatorname{sat}\left(\frac{\hat{\alpha}_{2}}{M_{\theta}}\right), F\right)
+ \sigma_{x}(\alpha_{1}, \alpha_{2}, F) - M_{x} \operatorname{sat}\left(\frac{\hat{\sigma}_{x}}{M_{x}}\right) - \varepsilon_{2}\dot{F}^{*}$$
(10)

Since $F^* = F^*(\alpha_1, \alpha_2, \nu_d)$ is

$$F^* = \frac{[u^* - G_x]}{c_x}, \quad u^* = g \tan \alpha_1 - \left(\frac{\ell}{\cos \alpha_1}\right) \nu_d, \tag{11}$$

with c_x in (3.22), G_x in (3.3), and ν_d in (3.12), \dot{F}^* is

$$\dot{F}^* = \left(\frac{\partial F^*}{\partial \alpha_1}\right) \dot{\alpha}_1 + \left(\frac{\partial F^*}{\partial \alpha_2}\right) \dot{\alpha}_2 + \left(\frac{\partial F^*}{\partial \nu_d}\right) \dot{\nu}_d
= F_1(\theta_1 + \alpha_r, \theta_2, F^*) + \varepsilon_1 F_2(\theta_1 + \alpha_r, \theta_2, y, F^*)$$
(12)

where F_1 and F_2 are

$$F_{1} = \left(\frac{\partial F^{*}}{\partial \alpha_{1}} - \beta_{1} \frac{\partial F^{*}}{\partial \nu_{d}}\right) \alpha_{2} + \left(\frac{\partial F^{*}}{\partial \alpha_{2}} - \beta_{2} \frac{\partial F^{*}}{\partial \nu_{d}}\right) f_{\alpha}(\cdot)$$

$$F_{2} = -\beta_{1} \left(\frac{\partial F^{*}}{\partial \nu_{d}}\right) \left(\frac{g}{g^{2} + \nu_{ext}^{2}}\right) \left[k_{1}y_{2} + k_{2}f_{x}(\cdot)\right]$$
(13)

By differentiating z_u and multiplying \dot{z}_u by ε_2 , we obtain

$$\varepsilon_{2}\dot{z}_{u} = \varepsilon_{2}\dot{u} - \varepsilon_{2}\dot{u}^{*}
= \bar{f}_{\alpha}\left(\alpha_{1}, M_{\mathcal{E}}\operatorname{at}\left(\frac{\hat{\alpha}_{2}}{M_{\theta}}\right), F\right) + M_{\alpha}\operatorname{sat}\left(\frac{\sigma_{\alpha}}{M_{\alpha}}\right) - \hat{\nu}_{d} - \varepsilon_{2}\dot{u}^{*} \tag{14}$$

With the similar procedure of the derivation for $\varepsilon_2 \dot{z}_F$, adding and subtracting $\bar{f}_{\alpha}(\alpha_1, \alpha_2, F) + \sigma_{\alpha}(\alpha_1, \alpha_2, F)$ and subtracting $\bar{f}_{\alpha}(\alpha_1, \alpha_2, F^*) + \sigma_{\alpha}(\alpha_1, \alpha_2, F^*) - \nu_d$ (i.e., $\bar{f}_{\alpha}(\alpha_1, \alpha_2, F^*) + \sigma_{\alpha}(\alpha_1, \alpha_2, F^*) - \nu_d = 0$), we obtain

$$\varepsilon_{3}\dot{z}_{u} = -c_{\alpha}z_{F} + \bar{f}_{\alpha}\left(\alpha_{1}, M_{e}\operatorname{sat}\left(\frac{\hat{\alpha}_{2}}{M_{\theta}}\right), F\right) - \bar{f}_{\alpha}(\alpha_{1}, \alpha_{2}, F)
+ M_{\alpha}\operatorname{sat}\left(\frac{\hat{\sigma}_{\alpha}}{M_{\alpha}}\right) - \sigma_{\alpha}(\alpha_{1}, \alpha_{2}, F) + \nu_{d} - \hat{\nu}_{d} - \varepsilon_{2}\dot{u}^{*} \tag{15}$$

where

$$\nu_d - \hat{\nu}_d = -\beta_1 (\alpha_r - \hat{\alpha}_r) - \beta_2 \left[M_\theta \operatorname{sat} \left(\frac{\hat{\alpha}_2}{M_\theta} \right) - \alpha_2 \right]$$
(16)

with $\hat{\alpha}_r$ in (3.27) and $u^* = u^*(\alpha_1, \nu_d)$ in (11), \dot{u}^* is

$$\dot{u}^* = \left(\frac{\partial u^*}{\partial \alpha_1}\right) \dot{\alpha}_1 + \left(\frac{\partial u^*}{\partial \nu_d}\right) \dot{\nu}_d
= u_1(\theta_1 + \alpha_r, \theta_2, F) + \varepsilon_1 u_2(\theta_1 + \alpha_r, \theta_2, y, F)$$
(17)

$$u_{1} = \left(\frac{\partial u^{*}}{\partial \alpha_{1}} - \beta_{1} \frac{\partial u^{*}}{\partial \nu_{d}}\right) \alpha_{2} - \beta_{2} \left(\frac{\partial u^{*}}{\partial \nu_{d}}\right) f_{\alpha}(\cdot)$$

$$u_{2} = -\beta_{1} \left(\frac{\partial u^{*}}{\partial \nu_{d}}\right) \left(\frac{g}{g^{2} + v_{ext}^{2}}\right) \left[k_{1} y_{2} + k_{2} f_{x}(\cdot)\right]$$
(18)

With (10) and (15), we obtain

$$\varepsilon_2 \dot{z} = A_z z + \psi(\cdot) - \varepsilon_2 \phi(\cdot) \tag{19}$$

where A_z is given in (3.24), $z = [z_F, z_u]^T$, $\phi = [\dot{F}^*, \dot{u}^*]^T$, $\psi = [\psi_1, \psi_2 + \nu_d - \hat{\nu}_d]^T$ is

$$\psi_{1} = \bar{f}_{x}(\alpha_{1}, \alpha_{2}, F) - \bar{f}_{x}\left(\alpha_{1}, M_{\theta} \operatorname{sat}\left(\frac{\hat{\alpha}_{2}}{M_{\theta}}\right), F\right)
+ \sigma_{x}(\alpha_{1}, \alpha_{2}, F) - M_{x} \operatorname{sat}\left(\frac{\hat{\sigma}_{x}}{M_{x}}\right)
\psi_{2} = \bar{f}_{\alpha}\left(\alpha_{1}, M_{\theta} \operatorname{sat}\left(\frac{\hat{\alpha}_{2}}{M_{\theta}}\right), F\right) - \bar{f}_{\alpha}(\alpha_{1}, \alpha_{2}, F)
+ M_{\alpha} \operatorname{sat}\left(\frac{\hat{\sigma}_{\alpha}}{M_{\alpha}}\right) - \sigma_{\alpha}(\alpha_{1}, \alpha_{2}, F)$$
(20)

and $\psi(\cdot)|_{\eta=0}=0$ and when saturation is not effective $\|\psi\| \leq k_{\psi} \|\eta\|$ with a positive constant k_{ψ} .

Error dynamics of the plant

The change of variables $\theta_1 = \alpha_1 - \alpha_r$ with α_r in (3.11) and $\theta_2 = \alpha_2$ for the pendulum dynamics, and $y_1 = \varepsilon_1^2 x_1$ and $y_2 = \varepsilon_1 x_2$ for the cart dynamics, is used. The derivative of θ_1 along the trajectories of (3.2), (3.25), and (3.26) is

$$\dot{\theta}_1 = \dot{\alpha}_1 - \dot{\alpha}_r = \theta_2 + \varepsilon_1 h_\alpha \tag{21}$$

with h_{α} in (3.18) and the derivative of θ_2 is

$$\dot{\theta}_2 = f_\alpha(\alpha_1, \alpha_2, F) = -c_\alpha F + G_\alpha \tag{22}$$

with c_{α} in (3.22) and G_{α} in (3.3). Adding and subtracting $f_{\alpha}(\alpha_1, \alpha_2, F^*) = -c_{\alpha}F^* + G_{\alpha}$ with F^* and u^* in (11), we obtain

$$\dot{\theta}_{2} = f_{\alpha}(\alpha_{1}, \alpha_{2}, F^{*}) + f_{\alpha}(\alpha_{1}, \alpha_{2}, F) - f_{\alpha}(\alpha_{1}, \alpha_{2}, F^{*})$$

$$= -c_{\alpha}F^{*} + G_{\alpha} + f_{\alpha}(\alpha_{1}, \alpha_{2}, F) - f_{\alpha}(\alpha_{1}, \alpha_{2}, F^{*})$$

$$= -\beta_{1}\theta_{1} - \beta_{2}\theta_{2} - c_{\alpha}z_{F}$$
(23)

With (21) and (23), the pendulum dynamics is

$$\dot{\theta} = A_{\theta}\theta + \varepsilon_1 E h_{\alpha}(y, \theta, \alpha_r, F) - B c_{\alpha} z_F \tag{24}$$

where A_{θ} is given in (3.19), $\theta = [\theta_1, \theta_2]^T$, $E = [1, 0]^T$, and $B = [0, 1]^T$. With the slow variables of $y_1 = \varepsilon_1^2 x_1$ and $y_2 = \varepsilon_1 x_2$ for the cart dynamics, the derivatives of y_1 and y_2 along the trajectories of (3.2), (3.25), and (3.26) are

$$\dot{y}_1 = \varepsilon_1 y_2
\dot{y}_2 = \varepsilon_1 f_x(\alpha_1, \alpha_2, F)$$
(25)

With F^* and u^* in (11), adding and subtracting $\varepsilon_1 f_x(\alpha_1, \alpha_2, F^*) = \varepsilon_1 [c_x F^* + G_x]$ to \dot{y}_2 , it is obtained

$$\dot{y}_{2} = \varepsilon_{1}[f_{x}(\alpha_{1}, \alpha_{2}, F^{*}) + f_{x}(\alpha_{1}, \alpha_{2}, F) - (\alpha_{1}, \alpha_{2}, F^{*})]
= \varepsilon_{1}[c_{x}F^{*} + G_{x} + c_{x}z_{F}]
= \varepsilon_{1}[-k_{1}y_{1} - k_{2}y_{2} + h_{x} + c_{x}z_{F}]$$
(26)

with $h_x(\theta, \alpha_r)$ in (3.18) and $h_x(0, \alpha_r) = 0$. With (25) and (26), we obtain

$$\dot{y} = \varepsilon_1 \left[A_y y + B \left(h_x(\theta, \alpha_r) + c_x z_F \right) \right] \tag{27}$$

where A_y is given in (3.20) and $y = [y_1, y_2]^T$.

Appendix B Appendix for Chapter 4

Jacobian matrix

Jacobian matrix for the translational dynamics

The Jacobian for the translational dynamics $(\partial F_{\chi_d}/\partial u_t)$ is given by $(\partial F_{\chi}/\partial u_t)$ is

$$\frac{\partial F_{\chi}}{\partial u_{t}} = \begin{bmatrix}
\frac{\partial f_{x}}{\partial T_{M}} & \frac{\partial f_{x}}{\partial \phi_{d}} & \frac{\partial f_{x}}{\partial \theta_{d}} \\
\frac{\partial f_{y}}{\partial T_{M}} & \frac{\partial f_{y}}{\partial \phi_{d}} & \frac{\partial f_{y}}{\partial \theta_{d}} \\
\frac{\partial f_{z}}{\partial T_{M}} & \frac{\partial f_{z}}{\partial \phi_{d}} & \frac{\partial f_{z}}{\partial \theta_{d}}
\end{bmatrix}$$
(28)

The components of the matrix are as follows.

$$\frac{\partial f_x}{\partial T_M} = -\left(\frac{1}{m}\right) \left(\cos\phi_d \sin\theta_d \cos\psi_1 + \sin\phi_d \sin\psi_1\right)
\frac{\partial f_x}{\partial \phi_d} = \left(\frac{1}{m}\right) \left(\sin\phi_d \sin\theta_d \cos\psi_1 - \cos\phi_d \sin\psi_1\right) T_M
\frac{\partial f_x}{\partial \theta} = -\left(\frac{1}{m}\right) \left(\cos\phi_d \cos\theta_d \cos\psi_1\right) T_M$$
(29)

$$\frac{\partial f_y}{\partial T_M} = -\left(\frac{1}{m}\right) \left(\cos\phi_d \sin\theta_d \sin\psi_1 - \sin\phi_d \cos\psi_1\right)
\frac{\partial f_y}{\partial \phi_d} = \left(\frac{1}{m}\right) \left(\sin\phi_d \sin\theta_d \sin\psi_1 + \cos\phi_d \cos\psi_1\right) T_M
\frac{\partial f_y}{\partial \theta_d} = -\left(\frac{1}{m}\right) \left(\cos\phi_d \cos\theta_d \sin\psi_1\right) T_M$$
(30)

$$\frac{\partial f_z}{\partial T_M} = -\left(\frac{1}{m}\right) (\cos \phi_d \cos \theta_d)
\frac{\partial f_z}{\partial \phi_d} = \left(\frac{1}{m}\right) (\sin \phi_d \cos \theta_d) T_M
\frac{\partial f_z}{\partial \theta_d} = \left(\frac{1}{m}\right) (\cos \phi_d \sin \theta_d) T_M$$
(31)

Jacobian matrix for the rotational dynamics

The Jacobian matrix $(\partial F_{\Theta}/\partial u_r)$ is

$$\frac{\partial F_{\Theta}}{\partial u_r} = \begin{bmatrix}
\frac{\partial f_{\phi}}{\partial T_T} & \frac{\partial f_{\phi}}{\partial a_{1s}} & \frac{\partial f_{\phi}}{\partial b_{1s}} \\
\frac{\partial f_{\theta}}{\partial T_T} & \frac{\partial f_{\theta}}{\partial a_{1s}} & \frac{\partial f_{\theta}}{\partial b_{1s}} \\
\frac{\partial f_{\psi}}{\partial T_T} & \frac{\partial f_{\psi}}{\partial a_{1s}} & \frac{\partial f_{\psi}}{\partial b_{1s}}
\end{bmatrix}$$
(32)

The components of the matrix are as follows.

$$\frac{\partial f_{\phi}}{\partial T_{T}} = \left(\frac{1}{I_{xx}}\right) \left(\frac{\partial \tau_{1}^{b}}{\partial T_{T}}\right) + \left(\frac{\sin \phi_{1} \tan \theta_{1}}{I_{yy}}\right) \left(\frac{\partial \tau_{2}^{b}}{\partial T_{T}}\right) + \left(\frac{\cos \phi_{1} \tan \theta_{1}}{I_{zz}}\right) \left(\frac{\partial \tau_{3}^{b}}{\partial T_{T}}\right) \\
\frac{\partial f_{\phi}}{\partial a_{1s}} = \left(\frac{1}{I_{xx}}\right) \left(\frac{\partial \tau_{1}^{b}}{\partial a_{1s}}\right) + \left(\frac{\sin \phi_{1} \tan \theta_{1}}{I_{yy}}\right) \left(\frac{\partial \tau_{2}^{b}}{\partial a_{1s}}\right) + \left(\frac{\cos \phi_{1} \tan \theta_{1}}{I_{zz}}\right) \left(\frac{\partial \tau_{3}^{b}}{\partial a_{1s}}\right) \\
\frac{\partial f_{\phi}}{\partial b_{1s}} = \left(\frac{1}{I_{xx}}\right) \left(\frac{\partial \tau_{1}^{b}}{\partial b_{1s}}\right) + \left(\frac{\sin \phi_{1} \tan \theta_{1}}{I_{yy}}\right) \left(\frac{\partial \tau_{2}^{b}}{\partial b_{1s}}\right) + \left(\frac{\cos \phi_{1} \tan \theta_{1}}{I_{zz}}\right) \left(\frac{\partial \tau_{3}^{b}}{\partial b_{1s}}\right) \\
(33)$$

$$\frac{\partial f_{\theta}}{\partial T_{T}} = \left(\frac{\cos \phi_{1}}{I_{yy}}\right) \left(\frac{\partial \tau_{2}^{b}}{\partial T_{T}}\right) - \left(\frac{\sin \phi_{1}}{I_{zz}}\right) \left(\frac{\partial \tau_{3}^{b}}{\partial T_{T}}\right)
\frac{\partial f_{\theta}}{\partial a_{1s}} = \left(\frac{\cos \phi_{1}}{I_{yy}}\right) \left(\frac{\partial \tau_{2}^{b}}{\partial a_{1s}}\right) - \left(\frac{\sin \phi_{1}}{I_{zz}}\right) \left(\frac{\partial \tau_{3}^{b}}{\partial a_{1s}}\right)
\frac{\partial f_{\theta}}{\partial b_{1s}} = \left(\frac{\cos \phi_{1}}{I_{yy}}\right) \left(\frac{\partial \tau_{2}^{b}}{\partial b_{1s}}\right) - \left(\frac{\sin \phi_{1}}{I_{zz}}\right) \left(\frac{\partial \tau_{3}^{b}}{\partial b_{1s}}\right)$$
(34)

$$\frac{\partial f_{\psi}}{\partial T_{T}} = \left(\frac{\sec \theta_{1} \sin \phi_{1}}{I_{yy}}\right) \left(\frac{\partial \tau_{2}^{b}}{\partial T_{T}}\right) + \left(\frac{\cos \phi_{1} \sec \theta_{1}}{I_{zz}}\right) \left(\frac{\partial \tau_{3}^{b}}{\partial T_{T}}\right)
\frac{\partial f_{\psi}}{\partial a_{1s}} = \left(\frac{\sec \theta_{1} \sin \phi_{1}}{I_{yy}}\right) \left(\frac{\partial \tau_{2}^{b}}{\partial a_{1s}}\right) + \left(\frac{\cos \phi_{1} \sec \theta_{1}}{I_{zz}}\right) \left(\frac{\partial \tau_{3}^{b}}{\partial a_{1s}}\right)
\frac{\partial f_{\psi}}{\partial b_{1s}} = \left(\frac{\sec \theta_{1} \sin \phi_{1}}{I_{yy}}\right) \left(\frac{\partial \tau_{2}^{b}}{\partial b_{1s}}\right) + \left(\frac{\cos \phi_{1} \sec \theta_{1}}{I_{zz}}\right) \left(\frac{\partial \tau_{3}^{b}}{\partial b_{1s}}\right)$$
(35)

$$\frac{\partial \tau_1^b}{\partial T_T} = -h_T, \quad \frac{\partial \tau_1^b}{\partial a_{1s}} = -Q_M \cos a_{1s} + T_M \sin a_{1s} \cos b_{1s} y_M,
\frac{\partial \tau_1^b}{\partial b_{1s}} = \frac{\partial R_M}{\partial b_{1s}} + T_M h_M \cos b_{1s} + T_M y_M \cos a_{1s} \sin b_{1s},
\frac{\partial \tau_2^b}{\partial T_T} = -1.5 C_T^Q T_T^{0.5}, \quad \frac{\partial \tau_2^b}{\partial a_{1s}} = \frac{\partial M_M}{\partial a_{1s}} + T_M h_M \cos(a_{1s}) + T_M \sin(a_{1s}) \cos(b_{1s}) l_M,
\frac{\partial \tau_2^b}{\partial b_{1s}} = Q_M \cos(b_{1s}) + T_M \cos(a_{1s}) \sin(b_{1s}) l_M,
\frac{\partial \tau_3^b}{\partial T_T} = l_T, \quad \frac{\partial \tau_3^b}{\partial a_{1s}} = Q_M \sin(a_{1s}) \cos(b_{1s}),
\frac{\partial \tau_3^b}{\partial b_{1s}} = Q_M \cos(a_{1s}) \sin(b_{1s}) - T_M \cos(b_{1s}) l_M.$$
(36)

Computation for the size of ultimate boundedness

The matrix H

The matrix H is given by

$$H = \begin{bmatrix} H_4 & H_{51} \\ \mathbf{0}_{1\times 4} & \overline{k_{e_1}} - \overline{k_{e_2}} \end{bmatrix}, \quad H_{51} = \begin{bmatrix} 0 \\ 0 \\ -\left(\frac{\overline{k_{d_3}} + \overline{k_{d_4}\varepsilon_4}}{\varepsilon_3}\right) \\ -\left(\frac{\overline{k_{c_4}} + \varepsilon_4 \overline{k_{c_5}}}{\varepsilon_2}\right) \end{bmatrix}$$
(37)

$$H_{4} = \begin{bmatrix} H_{3} & H_{41} \\ H_{42} & (\frac{\bar{k}_{d_{1}}}{\varepsilon_{3}} - \varepsilon_{1}\bar{k}_{d_{2}}) \end{bmatrix}, H_{41} = \begin{bmatrix} 0 \\ -\varepsilon_{1}\bar{k}_{b_{2}} \\ -\varepsilon_{1}\bar{k}_{c_{6}} \end{bmatrix}, H_{42} = \begin{bmatrix} 0 \\ -\frac{\bar{k}_{d_{7}}}{\varepsilon_{1}} \\ -(\frac{\bar{k}_{d_{5}}}{\varepsilon_{2}} + \frac{\bar{k}_{d_{6}}}{\varepsilon_{1}}) \end{bmatrix}^{T}$$
(38)

$$H_{3} = \begin{bmatrix} \bar{k}_{a_{1}} & -\bar{k}_{a_{2}} & -\bar{k}_{a_{3}} \\ 0 & \frac{\bar{k}_{b_{1}}}{\varepsilon_{1}} & -\frac{\bar{k}_{b_{3}}}{\varepsilon_{1}} \\ -\bar{k}_{c_{9}} & -\left(\frac{\bar{k}_{c_{7}}}{\varepsilon_{1}} + \bar{k}_{c_{8}}\right) & \left(\frac{\bar{k}_{c_{1}}}{\varepsilon_{2}} - \frac{\bar{k}_{c_{2}}}{\varepsilon_{1}} - \bar{k}_{c_{3}}\right) \end{bmatrix}$$
(39)

The size of ultimate boundedness

By multiplying ε_4 by both left-hand and right-hand sides of the last inequality, D^+W_5 in (4.86), the size of the upper bound W_5 is approximated to

$$||W_5|| \le \bar{k}_{e_3}\bar{\delta}_7(t)/(\bar{k}_{e_1} + \varepsilon_4\bar{k}_{e_2})$$
 (40)

The sizes of the boundedness for W_i for i = 1, ..., 4, are computed by using the inverse of block matrices in Appendix A.20 of [32] as follows.

$$H_4^{-1} = \begin{bmatrix} H_3 & H_{41} \\ H_{42} & (\frac{\bar{k}_{d_1}}{\varepsilon_3} - \varepsilon_1 \bar{k}_{d_2}) \end{bmatrix}^{-1} = \begin{bmatrix} H_3^{-1} + E_4 \Delta_4^{-1} F_4 & -E_4 \Delta_4^{-1} \\ -\Delta_4^{-1} F_4 & \Delta_4^{-1} \end{bmatrix}$$
(41)

where $\Delta_4 = (\bar{k}_{d_1} - \varepsilon_3 \varepsilon_1 \bar{k}_{d_2})/\varepsilon_3 - H_{42}H_3^{-1}H_{41}$, $E_4 = H_3^{-1}H_{41}$ and $F_4 = H_{42}H_3^{-1}$. The matrix H_4^{-1} is rewritten as

$$H_4^{-1} = \begin{bmatrix} H_3^{-1} + O(\varepsilon_3)H_{41} & O(\varepsilon_3)\bar{H}_{42} \\ O(\varepsilon_3)\bar{H}_{43} & O(\varepsilon_3) \end{bmatrix}$$
(42)

where $0 < O(\varepsilon_p) \le k_p \varepsilon_p$ with positive numbers k_p , ε_p , $0 < \varepsilon_p \ll k_p$. The matrix H_3^{-1} can be computed as

$$H_3^{-1} = \begin{bmatrix} H_2 & H_{31} \\ H_{32} & \left(\frac{k_{c_1}}{\varepsilon_2} - \frac{k_{c_2}}{\varepsilon_1} - \bar{k}_{c_3}\right) \end{bmatrix}^{-1} = \begin{bmatrix} H_2^{-1} + E_3 \Delta_3^{-1} F_3 & -E_3 \Delta_3^{-1} \\ -\Delta_3^{-1} F_3 & \Delta_3^{-1} \end{bmatrix}$$
(43)

where

$$H_{2} = \begin{bmatrix} \bar{k}_{a_{1}} & -\bar{k}_{a_{2}} \\ 0 & \frac{\bar{k}_{b_{1}}}{\varepsilon_{1}} \end{bmatrix}, \quad H_{31} = \begin{bmatrix} -\bar{k}_{a_{3}} \\ -\frac{\bar{k}_{b_{3}}}{\varepsilon_{1}} \end{bmatrix}, \quad H_{32} = \begin{bmatrix} -\bar{k}_{c_{9}} \\ -\left(\frac{\bar{k}_{c_{7}}}{\varepsilon_{1}} + \bar{k}_{c_{8}}\right) \end{bmatrix}^{T}$$
(44)

$$\Delta_3 = \left(\frac{1}{\varepsilon_2}\right) \left(\bar{k}_{c_1} - \frac{\varepsilon_2 \bar{k}_{a_2}}{\varepsilon_1} - \varepsilon_2 \bar{k}_{c_3}\right) - H_{32} H_2^{-1} H_{31} \tag{45}$$

 $E_3 = H_2^{-1} H_{31}$ and $F_3 = H_{32} H_2^{-1}$. The matrix H_3^{-1} is rewritten as

$$H_3^{-1} = \begin{bmatrix} H_2^{-1} + O(\varepsilon_2)H_{31} & O(\varepsilon_2)\bar{H}_{32} \\ O(\varepsilon_2)\bar{H}_{33} & O(\varepsilon_2) \end{bmatrix}$$
(46)

With (42), (46), and (44), the upper bounds of W_i for i = 1, 2, 3, 4 can be computed by using

$$H_4^{-1}(\varepsilon_1 \Gamma_3 + \Gamma_4) = \Gamma = [\Gamma_{11}, \Gamma_{22}, \Gamma_{33}, \Gamma_{44}]^T$$

$$\Gamma_3 = [0, \bar{k}_{b_4} \bar{\delta}_1(t), \bar{k}_{c_{10}} \bar{\delta}_3(t), \bar{k}_{d_8} \bar{\delta}_5(t)]^T, \quad \Gamma_4 = [0, \bar{k}_{b_5} \bar{\delta}_2(t), \bar{k}_{c_{11}} \bar{\delta}_4(t), \bar{k}_{d_9} \bar{\delta}_6(t)]^T$$

$$(47)$$

Then the upper bounds for each component of Γ is

$$\|\Gamma_{11}\| \leq [\varepsilon_{1}k_{f_{1}} + O(\varepsilon_{2})][\varepsilon_{1}\bar{k}_{b_{4}}\bar{\delta}_{1}(t) + \bar{k}_{b_{5}}\bar{\delta}_{2}(t)] + O(\varepsilon_{2})[\varepsilon_{1}\bar{k}_{c_{10}}\bar{\delta}_{3}(t) + \bar{k}_{c_{11}}\bar{\delta}_{4}(t)]$$

$$+ O(\varepsilon_{3})[\varepsilon_{1}\bar{k}_{d_{8}}\bar{\delta}_{5}(t) + \bar{k}_{d_{9}}\bar{\delta}_{6}(t)]$$

$$\|\Gamma_{22}\| \leq O(\varepsilon_{2})[\varepsilon_{1}\bar{k}_{b_{4}}\bar{\delta}_{1}(t) + \bar{k}_{b_{5}}\bar{\delta}_{2}(t)] + [\varepsilon_{1}k_{f_{2}} + O(\varepsilon_{2})][\varepsilon_{1}\bar{k}_{c_{10}}\bar{\delta}_{3}(t) + \bar{k}_{c_{11}}\bar{\delta}_{4}(t)]$$

$$+ O(\varepsilon_{3})[\varepsilon_{1}\bar{k}_{d_{8}}\bar{\delta}_{5}(t) + \bar{k}_{d_{9}}\bar{\delta}_{6}(t)]$$

$$\|\Gamma_{33}\| \leq O(\varepsilon_{2})[\varepsilon_{1}\bar{k}_{b_{4}}\bar{\delta}_{1}(t) + \bar{k}_{b_{5}}\bar{\delta}_{2}(t)] + O(\varepsilon_{2})[\varepsilon_{1}\bar{k}_{c_{10}}\bar{\delta}_{3}(t) + \bar{k}_{c_{11}}\bar{\delta}_{4}(t)]$$

$$+ O(\varepsilon_{3})[\varepsilon_{1}\bar{k}_{d_{8}}\bar{\delta}_{5}(t) + \bar{k}_{d_{9}}\bar{\delta}_{6}(t)]$$

$$\|\Gamma_{44}\| \leq O(\varepsilon_{2})O(\varepsilon_{3})[\varepsilon_{1}\bar{k}_{b_{4}}\bar{\delta}_{1}(t) + \bar{k}_{b_{5}}\bar{\delta}_{2}(t)] + O(\varepsilon_{2})O(\varepsilon_{3})[\varepsilon_{1}\bar{k}_{c_{10}}\bar{\delta}_{3}(t) + \bar{k}_{c_{11}}\bar{\delta}_{4}(t)]$$

$$+ O(\varepsilon_{3})[\varepsilon_{1}\bar{k}_{d_{8}}\bar{\delta}_{5}(t) + \bar{k}_{d_{9}}\bar{\delta}_{6}(t)]$$

with $\bar{k}_{f_1} > 0$ and $\bar{k}_{f_2} > 0$. Using the upper bounds $\|\Gamma_{11}\|$, $\|\Gamma_{22}\|$, and $\|\Gamma_{33}\|$ in (48) and $\|w_5\|$ in (40), the ultimate boundedness is $\sqrt{\|\Gamma_{11}\|^2 + \|\Gamma_{22}\|^2 + \|\Gamma_{33}\|^2 + \|W_5\|^2}$.

BIBLIOGRAPHY

BIBLIOGRAPHY

- [1] http://www.quanser.com/Products/linear_servo_IP02.
- [2] N. Adhikary and C. Mahanta. Integral backstepping sliding mode control for underactuated systems: Swing-up and stabilization of the cart-pendulum system. *ISA Transactions*, 58:870 880, 2013.
- [3] B. Ahmed, H. R. Pota, and M. Garratt. Flight control of rotary wing uav a practical approach. in *IEEE Conference on Decision and Control*, pages 5042 5047, 2008.
- [4] D. Angeli. Almost global stabilization of the inverted pendulum via continuous state feedback. *Automatica*, 37:1103 1108, 2001.
- [5] A. Astolfi, D. Karagiannis, and R. Ortega. Nonlinear and adaptive control design and applications. *London:Springer-Verlag*, 2007.
- [6] K. J. Astrom and K. Furuta. Swining up a pendulum by energy control. *Automatica*, 36:287 295, 2000.
- [7] A. N. Atassi and H. K. Khalil. A separation principle for the stabilization of a class of nonlinear systems. *IEEE Transactions Automatic Control*, 44(9):1672 1687, 1999.
- [8] D. Auckly, L. Kapitanski, and W. White. Control of nonlinear underactuated systems. Communications on Pure Applied Mathematics, 53:354 – 369, 2000.
- [9] J. Back and H. Shim. Adding robustness to nominal output-feedback controllers for uncertain nonlinear systems: A nonlinear version of disturbance observer. *Automatica*, 44:2528 2537, 2008.
- [10] J. Back and H. Shim. An inner-loop controller guaranteeing robust transient performance for uncertain mimo nonlinear systems. *IEEE Transactions on Automatic Control*, 54:1601 1607, 2009.
- [11] A. M. Bloch, D. E. Chang, and J. E. Marsden N. E. Leonard, and. Controlled Lagrangians and the stabilization of mechanical systems II: Potential shaping. *IEEE Transactions Automatic Control*, 46(10):1556 1571, 2001.
- [12] A. M. Bloch and J. E. Marsden N. E. Leonard, and. Controlled Lagrangians and the stabilization of mechanical systems I: The first matching theorem. *IEEE Transactions Automatic Control*, 45(12):2253 2270, 2000.
- [13] A. M. A. Boker and H. K. Khalil. Nonlinear observers comprising high-gain observers and extended kalman filters.
- [14] A. J. Calise, B. S. Kim, J. Leitner, and J. V. R. Prasad. Helicopter adaptive flight control using neural networks. *in IEEE Conference on Decision and Control*, pages 3336 3341, 1994.

- [15] W. Cao and J. Xu. Nonlinear integral-type sliding surface for both matched and unmatched uncertain systems. *IEEE Transactions on Automatic Control*, 49:1355 1360, 2004.
- [16] A. Chakrabortty and M. Arcak. Robust stabilization and performance recovery of nonlinear systems with unmodeled dynamics. *IEEE Transactions on Automatic Control*, 54:1351 1356, 2009.
- [17] A. Chakrabortty and M. Arcak. Time-sacle separation redesigns for stabilization and performance recovery of uncertain nonlinear systems. *Automatica*, 45:34 44, 2009.
- [18] M. Chen, S. S. Ge, and B. V. E. How. Robust adaptive neural network control for a class of uncertain mimo nonlinear systems with input nonlinearities. *IEEE Transactions on Neural Networks*, 21:796 812, 2010.
- [19] M. Chen, S.S. Ge, and B. Ren. Robust attitude control of helicopters with actuator dynamics using neural networks.
- [20] T. Cheviron, F. Plestan, and A. Chriette. A robust guidance and control scheme of an autonoumous scale helicopter in presence of wind gusts. *International Journal of Control*, 82:2206 22220, 2009.
- [21] F. Esfandiari and H. K. Khalil. Output feedback stabilization of fully linearizable systems. *International Journal of Control*, 56:1712 1725, 1992.
- [22] A. L. Fradkov. Swinging control of nonlinear oscillations. *International Journal of Control*, 64:1189 1202, 1996.
- [23] L. Freidovich and H. K. Khalil. Performance recovery of feedback-linearization-based designs. *IEEE Transactions on automatic control*, 53(10):2324 2334, November 2008.
- [24] S. S. Ge and J. Zhang. Neural-network control of nonaffine nonlinear system with zero dynamics by state and output feedback. *IEEE Transactions on Neural Networks*, 14:900 – 918, 2003.
- [25] N. H. Getz. Dynamic Inversion of Nonlinear Maps with Applications to Nonlinear Control and Robotics. PhD thesis, university of California at Berkeley, 1995.
- [26] N. H. Getz and J. K. Hedrick. An internal equilibrium manfold method of tracking for nonlinear nonminimum phase systems. *IEEE American Control Conference*, pages 2241 – 2245, June 1995.
- [27] N. Hovakimyan, E. Lavretsky, and C. Cao. Adaptive dynamic inversion via time-scale separation. *IEEE Transactions on Neural Networks*, 19:1702 1711, 2008.
- [28] N. Hovakimyan, E. Lavretsky, and C. Cao. Dynamic inversion for multivariable non-affine-in-control system via time-scale separation. *International Journal of Control*, 81(12):1960 1967, December 2008.

- [29] N. Hovakimyan, E. Lavretsky, and A. J. Sasane. Dynamic inversion for nonaffine-in-control systems via time-scale separation: Part 1. In Proc. IEEE int. American Control Conference, 2005.
- [30] A. Isidori. Nonlinear control systems. Springer, 1995.
- [31] A. Isidori, L. Marconi, and A. Serrani. Robust nonlinear motion control of a helicopter. *IEEE Transactions on Automatic Control*, 48:413 425, 2003.
- [32] T. Kailath. Linear systems. Printice Hall, 1980.
- [33] H. K. Khalil. Nonlinear systems. Printice Hall, 2002.
- [34] H. K. Khalil. Nonlinear control. Pearson, 2015.
- [35] H. K. Khalil and L. Praly. High-gain observers in nonlinear feedback control. *International Journal of Robust and Nonlinear Control*, 24:993 1015, 2014.
- [36] P. Kokotovic, H. K. Khalil, and J. O'Reilly. Singular perturbation methods in control analysis and design. SIAM, 1986.
- [37] T. J. Koo, Y. Ma, and S. S. Sastry. Nonlinear control of a helicopter based unmanned aerial vehicle model. *IEEE Transactions on Control Systems Technology*, 2001.
- [38] T. J. Koo and S. S. Sastry. Output tracking control design of a helicopter model based on approximation linearization. *In Proc. IEEE int. Conf. Decision, Control*, pages 3635 3640, 1998.
- [39] T. J. Koo and S. S. Sastry. Differential flatness based full authority helicopter control design. *In Proc. IEEE int. Conf. Decision, Control*, pages 1982 1987, 1999.
- [40] A. Lavant. Robust exact differentiation via sliding mode technique. *Automatica*, 34:379 384, 1998.
- [41] J. Lee, R. Mukherjee, and H. Khalil. Control design for a helicopter using dynamic inversion and extended high gain observers. *ASME Dynamic Systems and Control Conference*, October 2012.
- [42] J. Lee, R. Mukherjee, and H. Khalil. Performance recovery under output feedback for input nonaffine nonlinear systems. *IEEE Conference on Decision and Control*, December 2012.
- [43] J. Lee, R. Mukherjee, and H. K. Khalil. Output feedback performance recovery in the presence of uncertainties. *submitted to Systems and Control Letters*.
- [44] J. Lee, R. Mukherjee, and H. K. Khalil. Prformance recovery under output feedback for input nonaffine nonlinear systems. *submitted for publication*, pages 326 331, 2012.
- [45] C. Liu, W. Chen, and J. Andrew. Tracking control of small-scale helicopters using explicit nonlinear mpc augmented with disturbance observers.

- [46] R. Lozano, I. Fantoni, and D. J. Block. Stabilization of the inverted pendulum around its homoclinic orbit. System and Control Letters, 40:197 204, 2000.
- [47] L. Marconi and R. Naldi. Aggressive control of helicopters in presence of parameter and dynamical uncertainties.
- [48] L. Marconi and R. Naldi. Robust full degree-of-freedom tracking control of a helicopter. Automatica, 43:1909 1920, 2007.
- [49] F. Mazenc and L. Praly. Adding integrations, saturated controls, and stabilization for feedforward systems. *IEEE Transactions on Automatic Control*, 41:1559 1578, 1996.
- [50] V. Muralidharan, M. T. Ravichandran, and A. D. Mahindrakar. Extending interconnection and damping assignment passivity-based control (ida-pbc) to underactuated mechanical systems with nonholonomic pfaffian constraints: The mobile inverted pendulum robot. IEEE Conference on Decision and Control and 28th Chinese Control Conference, pages 6305 6310, 2009.
- [51] M. S. Nazrulla and H. K. Khalil. Robust stabilization of non-minimum phase nonlinear systems using extended high gain observers.
- [52] S. Nicosia, A. Tornambe, and P. Valigi. A solution to the generalized problem of nonlinear map inversion. *System and Control Letters*, 17:383 394, 1991.
- [53] S. Nicosia, A. Tornambe, and P. Valigi. Use of observers for the inversion of nonlinear maps. *System and Control Letters*, 16:447 455, 1991.
- [54] R. Olfati-Saber. Normal forms for underactuated mechanical systems with symmetry. *IEEE Transactions on Automatic Control*, 47:305 308, 2002.
- [55] R. Ortega, M. Spong, F. Gomez-Estern, and G. Blankenstein. Stabilization of class of underactuated mechanical systems via interconnection and damping assignment. *IEEE Transactions Automatic Control*, 47(10):1218 1233, 2002.
- [56] M. Park and D. Chwa. Swing-up and stabilization control of inverted-pendulum systems via coupled sliding-mode control method. *IEEE Transactions Industrial Electronics*, 56:3541 3555, 2009.
- [57] M. T. Ravichandran and A. D. Mahindrakar. Robust stabilization of a class of underactuated mechanical systems using time scaling and lyapunov redesign. *IEEE Transactions on Industrial Electronics*, 58:4299 4313, 2011.
- [58] D. Rouche, P. Habets, and M. Laloy. Stability theory by Lyapunov's direct method. Springer-Verlag:New York, 1977.
- [59] I. Sarras, J. A. Acosta, R. Ortega, and A. D. Mahindrakar. Constructive immersion and invariance stabilization for a class of underactuated mechanical systems. *Automatica*, 49:1442 – 14448, 2013.

- [60] D. H. Shim, H. Chung, and S. S. Sastry. Autonomous exploration in unknown urban environments for unmanned aerial vehicles. *American Institute of Aeronautics and Astronautics*, pages 1 8, 2005.
- [61] A. S. Shiriaev, O. Egeland, H. Ludvigsen, and A. L. Fradkov. Vss-version of energy-based control for swinging up a pendulum. *System and Control Letters*, 44:45 56, 2001.
- [62] M. W. Spong and L. Praly. Control of underactuated mechanical systems using switching and saturation. *Proceedings of the Block Island Workshop on Control Using Logic Based Switching*, 1996.
- [63] B. Srinivasan, P. Huguenin, and D. Bonvin. Global stabilization of an inverted pendulum-control strategy and experimental verification. *Automatica*, 45:265 269, 2009.
- [64] M. Tanelli, E. Punta, and A. Ferrara. A switched second-order sliding mode control algorithm for non-affine systems with saturations. Proceedings of Conference on Decision and Control, pages 5488 5459, 2012.
- [65] K. P. Tee, S.S. Ge, and F. E. H. Tay. Adaptive neural network control for helicopters in vertical flight.
- [66] A. Teel. A nonlinear small gain theorem for the analysis of control system with saturation. *IEEE Transactions on Automatic Control*, 41:1256 1270, 1996.
- [67] R. Vidal, S. Rashid, C. Sharp, O. Shakernia, J. Kim, and S. S. Sastry. Pursuit-evansion games with unmanned ground and aerial vehicles. *International Conference on Robotics and Automation*, pages 2948 2955, 2001.
- [68] J. Xu, Z. Guo, and T. H. Lee. Design and implementation of integral sliding-mode control on an underactuated two-wheeled mobile robot. *ISA Transactions*, 58:870 – 880, 2013.